DECODING THE YEAST STRESS ADAPTATION CIRCUIT

Justin Gregory English

A dissertation submitted to the faculty of the University of North Carolina at Chapel Hill
in partial fulfillment of the requirements for the degree
of Doctor of Philosophy in the Department of Pharmacology.

Chapel Hill
2014

Approved by:

Timothy Elston

Henrik Dohlman

Channing Der

Klaus Hahn

Gary Johnson

ABSTRACT

JUSTIN ENGLISH: Decoding the Yeast Stress Adaptation Circuit
(Under the direction of Henrik Dohlman)

Cells must adapt to survive. To mount an appropriate adaptive response the cell must relay information from its surroundings to its adaptive machinery. This process, termed information transmission, is a universal property of biology. Determining how this information is transmitted, amplified, and interpreted throughout the cell is of paramount importance. By establishing how information is transmitted in biological systems we can identify new routes for intervention in disease progression. To this end, this thesis aims to resolve the information transmission mechanisms associated with the oft studied stress adaptation circuit of the yeast *S. cerevisiae*. The work herein considers two distinct properties of this stress circuit. First, a determination of the methods and mechanisms by which environmental information is conveyed. Second, an assessment of the consequences of this information on the reprogramming of cellular metabolism and protein expression. Combined, these two investigations uncover how yeast have engineered a dynamic system for responding to a broad range of cellular stress conditions.

To my wife, my partner in all things

ACKNOWLEDGEMENTS

First and foremost I wish to thank Henrik G. Dohlman. As my advisor and mentor he has supported me through all of the work contained in this document, and a substantial amount that is not. His capacity to remain level headed, guide me in the right direction, and help me when no one else is able are just some of the few reasons I was able to accomplish what I have during my time at UNC. Henrik has demonstrated an infinite amount of patience; as the several hundred manuscript edits and several thousand email correspondences between us will attest. I sincerely and truly thank you, for everything.

Second, I'd like to thank the Department of Pharmacology. All of the students, professors, and staff have been outstanding to work with each day. There are few places I have enjoyed doing and discussing science more, or likely will again. It has been a unique and wonderful experience to be instructed and educated by leaders of the cell signaling field. In addition, all these lessons were learned alongside bright peers who have challenged me every day to do better and push further than at times I thought I was capable. Thank you, to all of you.

I'd also like to thank the Dohlman lab, both past and present. Much like a family, lab mates see all of your worst moments, frustrations, and challenges. They keep you humble. But they are also always there to help you improve yourself, so you can show your best face to those on the outside. Thank you.

Lastly, I thank my family. They have endured from me what I can only describe as a constant haze of emotions, ranging from exhilaration to crushing frustration. Thank you to my Father, who has with near perfect regularity come to visit every 3 months since my wife and I moved to North Carolina. Your visits, support, and love have helped stabilize me through this long journey. Thank you to my Mother, who I'm not sure ever got away with a phone call that didn't run past an hour in length or a late night conversation at home that didn't drag on in to morning. You've always been there for me. Finally, thank you to my wife, Michelle. You must be exhausted. My constant stream of thoughts, ideas, complaints, and jubilations you've shouldered with an amazing degree of patience, love, and endurance. Far from being a sounding board and shoulder to cry on, you truly listen, understand, and talk me through every obstacle. I can also happily report that you are able to, with surprising eloquence, inform anyone who might ask what a "MAPK" is or how yeast research is important. You have on multiple occasions informed someone as to what I am researching - frequently when I myself didn't have the foggiest clue as to what I was doing. For all these reasons and so many more, I thank, and I love you.

TABLE OF CONTENTS

LIST OF TABLES

LIST OF FIGURES

LIST OF ABBREVIATIONS

Ala or A	Alanine
α	Alpha
Arg or R	Arginine
AMP	Adenosine monophosphate
ATP	Adenosine Triphosphate
β	Beta
CCD	Charge Coupled Device
CRE-LacZ or CLZ	cAMP Regulated Elemental fused to the β-Galactosidase Gene
Cys or C	Cysteine
Δ	Deletion
DNA	Deoxyribonucleic acid
EC50	Half Maximal Effective Concentration
E. coli	*Escherichia coli*
ERK	Extracellular Signal-Related Kinase
FMO	Fluorescence Minus One
FSC-A	Forward Scatter Area
γ	Gamma
GAP	GTPase Activating Protein
GDP	Guanosine Diphosphate

GEF	Guanine Nucleotide Exchange Factor
Gly or G	Glycine
GO	Gene Ontology
GFP	Green Fluorescent Protein
GTP	Guanosine Triphosphate
His or H	Histidine
HOG	High Osmolarity Glycerol
H_n	Hill slope
JNK	c-Jun N-Terminal Kinases
KanMX4	Kanamycin Resistance Gene
KCl	Potassium Chloride
Ile or I	Isoleucine
Leu or L	Leucine
Lys or K	Lysine
MAPK	Mitogen Activated Protein Kinase
MAP2K	Mitogen Activated Protein Kinase Kinase
MAP3K	Mitogen Activated Protein Kinase Kinase Kinase
Med.	Median
Min.	Minutes
mRNA	Messenger RNA
nm	Nanometer
PAGE	Polyacrylamide Gel Electrophoresis
PAK	p21 Activated Kinase

rCV	Robust Coefficient of Variation
S. cerevisiae	*Saccharomyces cerevisiae*
Ser or S	Serine
SCD	Synthetic Complete Dextrose
SDS	Sodium Dodecyl Sulfate
SEM	Standard Error of the Mean
SSC-A	Side Scatter Area
TCA	Trichloroacetic Acid
TF	Transcription Factor
Val or V	Valine
WGA	Wheat Germ Agglutinin
WT	Wild Type
YPD	Yeast Peptone Dextrose

CHAPTER I

INTRODUCTION[1]

Organisms respond to changes in their environment to maintain balance or homeostasis. This process is known as adaptation. Adaptation is essential for the survival of all organisms, as their internal and external environments are in a constant state of flux. For example, every day we consume a wide variety of foods whose content and concentration are a diverse mix of chemical signals. A healthy individual is able to digest, absorb, and use these materials with no ill effect. This is possible as a result of adaptation. Our bodies can detect the presence of food, or rising concentrations of nutrients in our blood stream, and generate suitable responses to those stimuli. Such responses may include an increased production of saliva, bile, or insulin. Eating is an example of adaptation to an acute signal of external origin; we also adapt to the inverse, a chronic signal of internal origin. An example would be body heat. We generate heat as we convert the raw materials from food in to energy. Regulating this heat, our body temperature, is a continuous adaptive process that engages a multitude of complex systems including blood flow, sweat glands, and air intake. The number of systems that function through adaptive response is innumerable. From our immune system to social interactions our bodies are engaged in a continuous adaptive cycle; receiving chemical and physical stimuli and responding to them in an appropriate fashion.

[1] All Figures Contributed by Justin English

Adaptation, with respect to the long-term health of an organism, is not always beneficial. Stress occurs when an organism adapts to a challenge, but ultimately deteriorates its health in the process. For example, atherosclerotic lesions are caused by inflammation of blood vessel epithelium[1,2]. Inflammation is an adaptive response of the epithelial cell to the accumulation of lipids, macrophages, and shear forces against its extracellular matrix. This inflammation is a stressful adaptation that can eventually result in various diseases, from high blood pressure to a stroke or heart attack if the lesion becomes unstable and ruptures. The adaptive response mounted by the epithelial cell is not a disease, it is the best effort of this cell to respond to and survive in a changing environment. The cell is attempting to maintain balance, but this process results in a stress, both for the cell and the organism.

While adaptation influences whole organisms, these adaptations originate from single cells. In the atherosclerosis example above, a handful of epithelial cells mount an adaptive response, resulting in a detriment to the organism. This example is just one of many instances where stressful cellular adaptations beget disease. We see the same patterns recur in diabetes[3], immune dysfunction[4], wound necrosis[5], arthritis[6], and ischemia[7]- just to name a few among many. The cells in these diseased tissues attempt to adapt to their environment and in turn generate a stress that develops in to the disease. To preempt or remedy disease progression it is vital that we understand how, when, and under what conditions cells make adaptive decisions.

To adapt, a cell must transmit information dictating the changes in its environment to its adaptation machinery. New mechanisms of cellular information transmission are being discovered all the time[8–10]. The work of this thesis focuses on understanding mitogen activated protein kinase (MAPK) signaling pathways, one of the most pervasive and

conserved cellular information transmission mechanisms. MAPK pathways receive input information as signals from extracellular receptors and convert these signals in to adaptive output through activation of downstream substrates. Our understanding of these information transmission processes has allowed the development of many disease interventions. These successes are based primarily on traditional pharmacological approaches that focus on intervening at the input, or receptor, level. However, MAPK pathways process these simple signal inputs in to complex system outputs. While interference at the input level can modulate MAPK activity, a fine-tuned therapeutic approach can be developed by modulating single aspects of MAPK signaling pathways[11–15]. A current limitation for designing these interventions is our narrow understanding of how MAPK pathways process input information. In the following I will expand on these principles and then introduce new insights from my graduate research, delineating new mechanisms of MAPK information processing that regulate stressful adaptations.

Cellular Information Theory and Transmission

To adapt a cell must detect and transmit the presence of an extracellular cue to its internal adaptive machinery. This process is termed information transmission[16,17]. Information transmission occurs any time an input is delivered from its origin to a receiver to generate a related output. Information transmission is a fundamental principle of the natural world. An entire branch of physics is based on the process of information transmission, since at its core, information transmission is a fight against entropy. In 1877 Ludwig Boltzmann, during his studies of the molecular properties of gas, inadvertently birthed the field of information theory by establishing that entropy is a measure of the number of ways that

energy can be configured in a system. The background noise in any system is a sampling of these many configurations. A signal, or information, is the amplification of a meaningful subset of these configurations. Claude E. Shannon, during his time at Bell Labs in 1948, published "A Mathematical Theory of Communication"[18], a seminal work in the field that expanded on the principles brought forth by Boltzmann to establish how a signal could be distinguished and transmitted in a system.

Shannon's work derived two key principles that have formed the foundation for all modern communication systems. First, he deduced that all information is encoded as interpretable symbols. Our alphabet is a suitable example as each letter is a symbol. Our alphabet, however, is a poor vehicle for rapidly transmitting information as no individual symbol conveys information in isolation. The word "no" is the smallest symbol combination possessing an isolated meaning. Shannon developed similar (though more complex) deductions to derive his second principle, that information has a specific symbol density. The rate at which information of a particular density can be conveyed in a system represents that systems bandwidth. Further details of Shannon's work falls outside the scope of this dissertation, but the core principles established above have shaped how we view information communication in biological systems[19–22]. For example, deoxyribonucleic acid (DNA) is frequently cited to explain how the principles of information theory pertain to biology. Information is written in to DNA using a four symbol code; A, T, G, and C. This code is delivered to ribosomes to inform protein synthesis and each symbol is read in groups of 3, the codon. The codon represents the density of DNA communication in this system. The bandwidth of translation is thus the number of codons the ribosome can read per unit time. This example highlights a paradigm that defines all biological systems; specifically an input

containing some density of information is delivered and transformed to generate a related output at a particular rate. Adaptation, including stress and disease progression, depend on this paradigm. In the following I will address how cells leverage this information transmission paradigm to convert simple signal inputs in to complex system outputs through MAPK signaling pathways.

Information Transmission in MAPK Signaling Pathways

Cells use protein networks to transmit information. For environmental adaptation this process can be summarized in to 3 stages; an environmental cue is internalized as a cytoplasmic signal, that signal is converted into information of a given density, and that information is communicated to adaptive machinery to encode a response. This generalization applies to a multitude of specific signaling mechanisms. The cue can be internalized as a signal through receptor transduction, active transport, or changes in membrane energy potential. This signal can then be converted to communicable information by a host of second messengers and signaling pathways ranging from classic signals such as cyclic AMP, phosphotidyl inositol, and calcium influx to more recent discoveries such as proton influx[23] and scaffold recruitment[24–26]. Each second messenger ultimately conveys signaling information to a signaling cascade that processes and stores this information for later communication to the cells adaptive machinery. There are many classes of signaling cascades, each of which perform crucial biological functions. Of these, mitogen activated protein kinase (MAPK) cascades are a canonical and widely studied example – and are the primary consideration of this thesis.

A kinase, the active unit of a MAPK cascade, is a simple enzyme that binds adenosine triphosphate (ATP) and liberates its y-phosphate using a coordinated charge re-distribution mechanism. Where kinases shine, from an information transmission point of view, is in their capacity to append this freed phosphate to specific residues of a bound protein substrate; a process referred to as phosphorylation. In so doing, kinases organize raw cellular energy in to an array of chemical signals. This organized phosphorylation represents a unique signature within the cell. However, as noted by Shannon and Boltzmann, for a signature to convey information it must be amplified above the stochastic noise of the system. To meet these signal propagation demands organisms utilize a startlingly elegant solution, MAPK cascades.

The core architecture of a MAPK cascade is the same in all eukaryotes[27,28], from yeast to humans. Each cascade is comprised of 3 kinases, which confer information to one another in series. The MAPK kinase kinase (MAP3K) is the first in the series. The MAP3K is the gatekeeper of activation for the cascade, and is activated by mediators of second messenger signals. Upon activation the MAP3K activates the MAPK kinase (MAP2K) by appending two phosphates on two distinct residues of the enzymes activation loop. Once activated the MAP2K repeats this process, phosphorylating and thereby activating the MAPK – the terminal signal integration point in the cascade.

The sequential signal transduction mechanism of MAPK cascades serves two important information transmission functions. First, the cascade converts the disparate chemical signals input at the MAP3K level in to a single phosphorylation-based language carried through the cascade. Second, the cascade exponentially amplifies input information through basic enzyme kinetics. If a single MAP3K molecule is activated by an upstream

signal it will subsequently act upon multiple MAP2K molecules, which will then act on an even greater proportion of MAPK molecules. This process is referred to as ultrasensitive signal propagation[29,30]. Ultrasensitive MAPK signals, without external regulation, result in exponential signal amplification. Studies of synthetic, unregulated MAPK cascades corroborate these conclusions[31]. Thus, nature has devised a simple signal converter and amplifier for communicating extracellular signals.

MAPK activation is essential for adaptation. The MAPK conveys the converted and amplified information of the upstream cascade to hundreds of downstream substrates[32–34]. This transmission step is what enables adaptive behavior. The MAPK conveys this information via substrate phosphorylation. Phosphorylation has been observed to amplify or weaken enzymatic activity, queue the substrate to be localized or degraded, and increase or decrease the affinity of the substrate to binding partners. Thus, by converting extracellular cues in to a universal phosphorylation signal and amplifying that signal, the MAPK cascade is able to reprogram molecular activity across the cell. This reprogramming impinges upon fundamental cellular processes such as transcription[35], translation[36], and metabolism[37] to augment cellular behaviors.

Ultimately, reprogramming causes the cell to either redefine or re-establish homeostasis. For example, the mammalian extracellular signal-regulated kinase (ERK) cascade is activated by numerous growth hormones, resulting in cell division or differentiation[38]. Thus, ERK signaling redefines homeostasis and pushes the cell toward a definitive state change. Conversely, the mammalian p38 MAPK cascade is activated by numerous cytotoxic agents, resulting in cell repair and ameliorative mechanisms[39]. Thus, p38 signaling re-establishes homeostasis by restoring balance in the face of an environmental

challenge. Notably, the cell is able to delineate these vastly different adaptive programs using the same general information transmission system, the MAPK cascade. By determining how MAPKs transmit adaptive information we can identify ideal means for modulating these processes in the interest of therapeutic intervention.

Two mechanisms dictate how MAPKs transmit adaptive information. The first is the substrate specificity of the MAPK. Each MAPK binds to and phosphorylates a specific panel of downstream substrates. Thus, the substrate interaction space for the kinase represents the adaptive machinery with which it can communicate. However, transient activation of the MAPK may only result in phosphorylation of the highest affinity substrates; whereas prolonged activation may result in saturation of the interaction space. Following the same kinetic logic, activation of a small number of MAPK molecules may minimally phosphorylate the substrate pool; whereas activation of all MAPK molecules may saturate the substrate pool. This potential for alternative outputs as a function of MAPK amplitude and duration was recently highlighted in a study of ERK activity[40]. By increasing ERK activity duration researchers were able to induce cell differentiation upon application of a proliferative stimulus. Therefore, the second mechanism mediating distribution of MAPK cascade information is the kinetics with which the MAPK is activated. The amplitude, duration, and frequency of MAPK activation represents its signaling profile[41]. Thus, much like telephone cables, the kinase-substrate affinities establish the connections in the communication network[32]; but the signaling profile of the kinase establishes the message transmitted on these cables.

The Computational Architecture of MAPK Signaling Pathways

MAPK substrate interaction networks have been generated under a plethora of signaling conditions, however in most instances the message originating at the nexus of these networks remains to be elucidated. To understand this message we must consider how it is generated; specifically by determining how the originating extracellular signal is converted, amplified, and applied to the MAPK. A suitable analogy for addressing this problem comes from mathematics. Specifically, an environmental input "x" is converted to a related output "y" through computation within the MAPK cascade "f(x)". This computation is performed over time, generating a signaling profile curve representing the relationship between input and MAPK activity.

From a strictly biochemical point of view the computational depth of a 3 kinase cascade is minimal (**Figure 1.1**). Each active kinase can have 3 variables that dictate the functional form of the pathway; abundance in the cell, binding rate, and catalytic rate. Over time, with ample ATP and a low rate of intrinsic dephosphorylation, all the kinase molecules in the cascade will arrive at a phosphorylated steady state. Thus, the system would truly only communicate one of two messages, on or off, a binary switch. A binary signal produces the lowest density of encoded information, and could never produce the flexible permutations of signal transduction necessary for life. For example, knowing that a hormone or cytotoxin is present in the environment is informative, but to mount an appropriate adaptive response the cell must also know the quantity of these cues. To this end, the cell utilizes numerous regulatory mechanisms to modulate MAPK cascade signals; tuning and controlling MAPK activity.

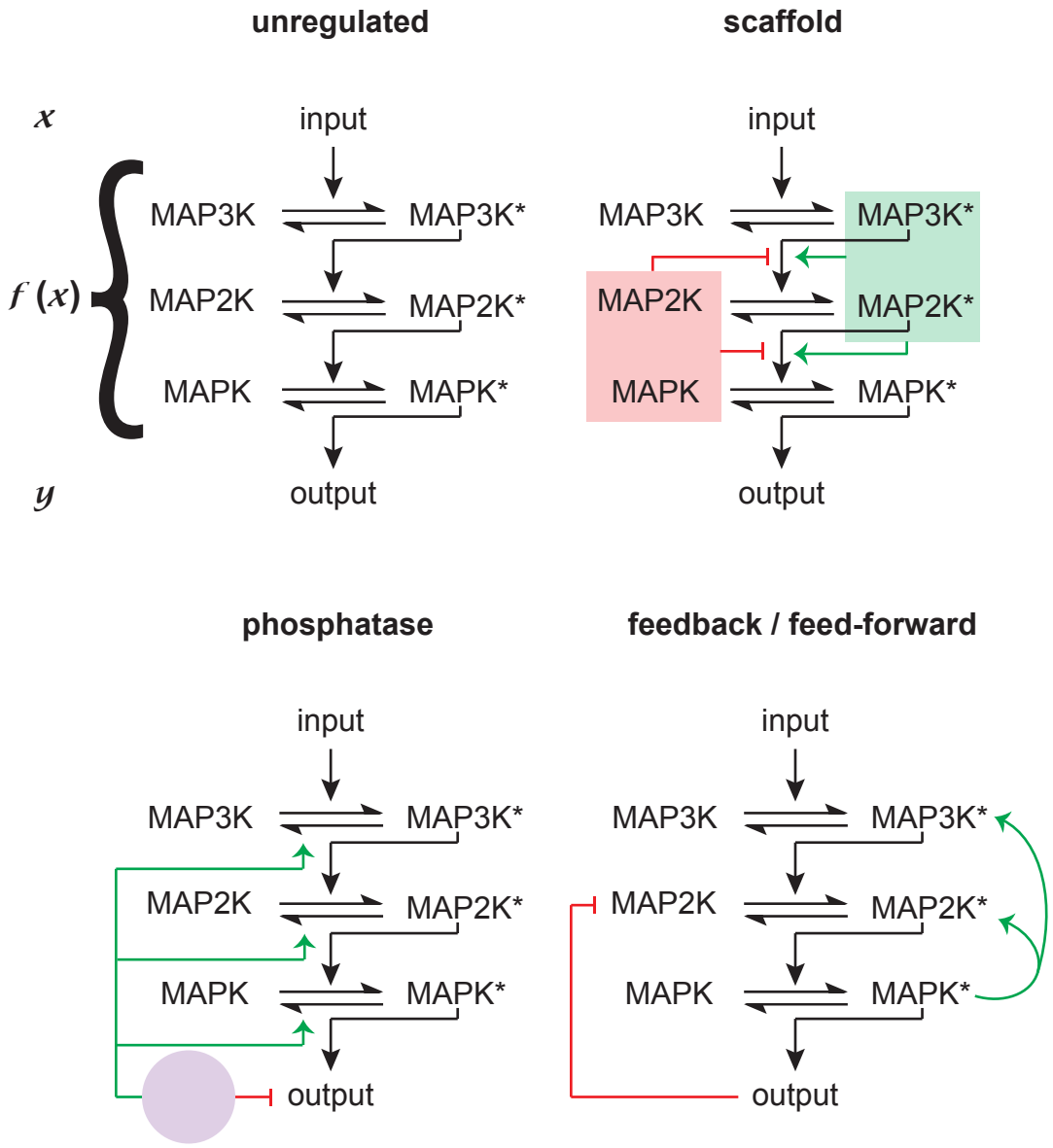

Figure 1.1. MAPK cascades convert and amplify input information in to adaptive outputs. An unregulated cascade represents the lowest order of computational complexity for this system. Through addition of single regulatory mechanisms, as illustrated for scaffolds, phosphatases, or feedback / feed-forward loops the dynamic range of these cascades can be greatly enhanced. It is not uncommon for a single cascade to possess several of these regulatory mechansisms in combination.

Regulatory mechanisms act as additional variables in our mathematical analogy. Addition of variables increases the dynamic range of the binary cascade, creating greater computational depth (**Figure 1.1**). This increase in computational depth is necessary for generating complex adaptive processes. A MAPK cascade and all its constituent regulatory mechanisms are referred to as a MAPK pathway. Numerous MAPK pathway components have been identified. For example, scaffolds are catalytically inactive proteins that simultaneously bind multiple pathway components[42]. In so doing, scaffolds can increase or decrease information transmission kinetics. Phosphatases also regulate MAPK cascade activity[43–46]. Phosphatases strip phosphates from peptides. If the rate with which a kinase phosphorylates a peptide is significantly lower than the dephosphorylation rate of a competing phosphatase the signal extinguishes. Thus, phosphatases can edit information transmission directly within the pathway or at the level of MAPK substrates. In this way, phosphatases filter low amplitude signaling events while increasing the dynamic range of the cascade. Lastly, feedback phosphorylation has been attributed to large increases in MAPK pathway computational complexity[47–51]. Through feedback MAPK pathways can exert differential computations on an input with respect to time, with early activation of the MAPK impinging on the computational equation to dynamically edit information transmission. A multitude of MAPK pathway regulators have been identified, each with unique activities and dose or time dependent behaviors[43,47,48]. Each serves to modulate the information transmission process, culminating in the controlled activation of just one protein, the MAPK.

Through kinase cascades, cells have developed a mechanism to convert and amplify extracellular signals in to transmittable information. Through modulation of these cascades cells dynamically regulate the information transmission process to tune their adaptive

response. This behavior can be captured in the above f(x) = y analogy, however this analogy remains a dramatic over-simplification of the complexities of biological activity. It does however, provide a reasonable platform for approaching a difficult question. Namely, how do MAPK pathways encode environmental information in a way that is both dynamic and meaningful for adaptation? To answer this question one must begin carefully measuring "y" for all "x" values. In this way, a relationship can be established and a signaling profile for the system elucidated. Using this simple approach, several researchers have recently uncovered a wealth of information regarding how information transmission informs cell fate[41,52]. To repeat an above example, the duration of ERK activity dictates whether a cell will proliferate or differentiate to the same stimulus[40]. Further, the sum of total active ERK molecules functions as a signal integrator capable of establishing a threshold for cell proliferation[53]. Like-wise, signaling profiles of p53 have demonstrated that the frequency of signaling, either pulsed or steady, can result in entirely different cell fate and recovery mechanisms to the same DNA damage stimulus[54]. These experiments highlight the importance of elucidating total signaling profiles for a given information transmission circuit. It is no longer sufficient to simply assess whether a signal is on or off.

The above examples of ERK activity represent a canonical signaling mechanism. Specifically, a graded signal dictates a switch-like cell fate decision. This rheostat to switch system is a logical process for determining if a change in cell fate is necessary. For example, the decision to divide is a major and irreversible decision. Thus, integrating environmental information as ERK activity duration can allow the cell to establish a decision making threshold[48,55]. This rheostat to switch decision making process exists for numerous biological systems. However, in the face of strong cytotoxic events, decision making prior to action

may not be an affordable luxury. Under these circumstances the cell should commit to adapting as soon as possible to mitigate damage, and tune its response thereafter. This system would represent a switch that tunes a biological rheostat. No MAPK signaling profiles have yet been identified that possess this switch-to-rheostat characteristic. However, recent observations of the high osmolarity glycerol (HOG) MAPK pathway in *S. cerevisiae* have hinted at just this possible ordering of operations.

HOG1: an Ancestral MAPK Pathway for Decoding Stress Adaptation

The bakers yeast *S. cerevisiae* has been a workhorse of stress signaling research for decades[56–60]. Central to the capacity of yeast to respond to extracellular stress is the HOG MAPK pathway. The HOG pathway is activated by hyperosmotic stress through the independent activation of two receptors; Sln1 and Sho1. The Sln1 branch is comprised of a histidine kinase cascade conserved from bacteria. The Sho1 branch is a canonical MAPK signaling cascade. The HOG pathway is among the best defined in biology[58]. In the Sln1 branch the receptor, Sln1, and two histidine kinases, Ypd1 and Ssk1, are coupled together at the membrane. During normal cellular conditions this complex is autophosphorylated via phosphorelay from Sln1 through Ypd1 to Ssk1. Upon osmotic shock autophosphorylation ceases and Ssk1 is activated. Upon activation Ssk1 phosphorylates Ssk2 and Ssk22, two downstream histidine kinases. Ssk2/22 phosphorylate and activate Pbs2, the MAP2K of the Hog1 cascade, which in turn phosphorylates and activates Hog1. In the Sho1 branch the receptor, Sho1, binds to two transmembrane mucin proteins Hkr1 and Msb2. Upon osmostress these mucins recruit a Rho GTPase (Cdc42) along with the GTPase activator Cdc24, a guanine nucleotide exchange factor, and a scaffold that brings Cdc42 and Cdc24 together (Bem1)[61]. While this is occurring the p21-activated protein kinase (PAK) Ste20 is

likely to associate with the Bem1/Cdc42/Cdc24 complex. Cdc24 activates Cdc42, which in turn activates Ste20. The MAP3K Ste11 is then chaperoned to the cell surface by the scaffold Ste50, which contacts Cdc42 and brings Ste11 in to proximity with active Ste20. Ste20 activates Ste11, and active Ste11 phosphorylates the MAP2K Pbs2, which again phosphorylates of the MAPK Hog1. Both branches have been described as having alternative mechanisms of regulation and activation kinetics. It is currently unclear whether this 2-branch system acts synergistically or competitively for Pbs2, however each branch is capable of activating Hog1 in isolation.

The Leading Edge of Hog1 Information Transmission

As mentioned, the Hog1 pathway and the entire osmostress response circuit have been studied extensively. The diversity of these studies has lent to formation of multiple context specific conflicts, however the core sequence of events culminating in adaptation from this pathway have been consistently observed. Namely, activation of the pathway results in the rapid localization of Hog1 to the nucleus[62–64]. This process depends on phosphorylation of Hog1, but occurs for numerous doses of osmostress within minutes of activation and nearly all Hog1 molecules are transported. This accumulation suggests that phosphorylation of Hog1 is switch-like. Indeed several recent studies have demonstrated a switch-like accumulation of phosphorylated Hog1[65]. This switch-like activation mechanism also results in the immediate blockade of the cell cycle, another switch-like event[66]. However, both the duration Hog1 remains in the nucleus and the quantity of transcriptional products produced during this time are dose-dependent[62]. Thus, the HOG pathway seems to function as a switch-to-rheostat information transmission system. As mentioned above, this is

an uncommonly observed organization of signal types. Thus far, a mechanism for how Hog1 achieves this unlikely ordering of operations, and the biological consequences of such actions, have remained elusive. The goal of this thesis is to resolve the mechanisms underlying these observations and elucidate the biological consequences of the information conveyed by the Hog1 stress adaptive circuit.

CHAPTER II

MAPK FEEDBACK SETS A SWITCH AND TIMER FOR TUNABLE STRESS ADAPTATION IN YEAST[1, 2]

Signaling pathways can behave as switches or rheostats, generating binary or graded responses to a given cell stimulus. Osmotic stress activates the MAPK Hog1 resulting in switch-like nuclear translocation and cell division arrest, but graded transcription and recovery. Here we consider how this pathway can simultaneously encode a switch and a rheostat. We demonstrate that Hog1 facilitates a bifurcated cellular response wherein Hog1 activation and commitment to adaptation are switch-like, while protein induction and the resolution of this commitment are graded. We demonstrate that graded recovery is encoded through feedback phosphorylation and a gene induction program that is both temporally staggered and variable across the population. This switch-to-rheostat signaling mechanism represents an ideal stress adaptation system; with a broad range of inputs generating an all-in response that is later tuned to allow graded recovery of individual cells over time.

[1] Elements of the work referenced in this chapter have been published in: PENDING

[2] Figures contributed by:

Justin G. English; 2.1, 2.2, 2.3, 2.4, 2.5, 2.6, 2.7, 2.8, 2.9, 2.10

James P. Shellhammer; 2.2c-d

Michael Malahe; 2.7b

Introduction

Mitogen activated protein kinase (MAPK) pathways are dynamic signaling modules present in all eukaryotic cells. These modules are activated by an environmental input such as the introduction of a hormone or cytotoxic stress, which generates a signal that is transmitted by sequential phosphorylation of a protein kinase cascade to a terminal MAPK. Once activated, the MAPK phosphorylates numerous protein substrates throughout the cell—effectively transmitting the input signal as a distinct pattern of protein phosphorylations. This phosphorylation-encoded information confers a symphony of changes in protein activity, localization, and abundance – a process that ultimately decodes the input information into adaptive behavior. For example, human growth factors activate the ERK MAPK module, which initiates cell division[38]. Cytotoxic agents activate the p38 and JNK MAPK modules, resulting in apoptosis, inflammation, or autophagy[67,68]. By deciphering how the cell encodes and decodes information via MAPK modules, we can begin to understand the molecular mechanisms driving animal development, behavior, homeostasis, and disease.

The high osmolarity glycerol (HOG) pathway of *S. cerevisiae* (yeast) has long been used to investigate how cells encode and decode environmental information into appropriate adaptive responses[56,69]. The HOG pathway has two distinct branches, each activated by osmotic stress. The first (Sln1 branch) is comprised of a 2-component system evolutionarily conserved in bacteria and yeast. The second (Sho1 branch) is activated by an integral membrane scaffold similar to numerous mammalian systems. These two branches converge on a shared MAPK kinase (MAP2K) Pbs2 and the MAPK Hog1. Hog1 activation triggers a cascade of signaling and transcription events that promote stress adaptation through osmolyte synthesis and other responses[58]. Notably, Hog1 was central in the discovery of the

mammalian stress adaptation MAPK JNK, demonstrating for the first time a conservation of MAPK function from yeast to humans[70].

MAPK signaling is a dynamic process with complexity that extends beyond mere activation and inactivation. Rather, MAPK modules are tunable communicators of information wherein the onset, amplitude, and duration of MAPK activation combine to generate a unique signaling profile[41]. These profiles directly affect how input information is encoded and ultimately decoded to change cellular behavior. For example, increasing the duration of ERK MAPK signaling causes the input normally used to encode cell division to instead initiate differentiation[40]. Appropriate responses to stress, mitogens, and other stimuli also hinge upon producing distinct signaling profiles[52,54,71]. However, it remains unclear how these signaling profiles are generated. Identifying the mechanisms that coordinate the onset, amplitude, and duration of MAPK activation will allow us to interpret, predict, and intervene in the information transmission processes of the cell. Such interventions may eventually include drugs that restore the MAPK signaling profile in disease states.

The terms switch and rheostat are traditionally used to describe the relationship between input and output in signaling systems. A switch produces a binary, on or off, fate decision with no intermediary responses. A rheostat generates a graded output. Cell division uses switches to threshold checkpoints at the level of MAPK signaling[72] and cell cycle progression[48]. Chemotaxis uses rheostats to flexibly track and dynamically adjust to signal amplitude and direction. In some cases a rheostat can beget a switch[53]. For example, activation of the MAPK Fus3 occurs in a dose-dependent manner, but leads to switch-like arrest of cell division and cell-cell fusion[42,66,73,74]. Conversely, several investigators have demonstrated that activation of Hog1 is switch-like, but ultimately leads to graded

outputs[62,65,66]. Unresolved are the direct biochemical mechanisms that can encode this unusual ordering of response types.

Here we define the mechanisms encoding the Hog1 response and its consequences on downstream output. Our strategy employs a new method to ratiometrically quantify phosphorylation at multiple levels of the Hog1 signaling cascade over time and in response to a wide range of input concentrations. In so doing, we define a linear function that relates the stimulus dose to Hog1 activity duration, a profile we had previously characterized as dose-to-duration signaling[75]. Dose-to-duration signaling can account for the ability of some cells to detect changes in a stimulus above that needed for saturation of receptors. We show that dose-to-duration signaling depends on Hog1 feedback, and that it allows Hog1 to encode both the switch and the rheostat. The Hog1 switch rapidly engages all cells in the adaptive process, but also allows individual cells to progress down a temporally graded adaptive program. Our findings reveal how a switch and rheostat can work simultaneously to ensure an appropriate response to an environmental stress.

Results

Hog1 is a switch-like timer that linearly transforms dose to duration

Our goal for this work was to identify the exact dose-to-duration relationship between input strength, Hog1 activity, and signaling output. We additionally endeavored to define the proteins and processes that encode this dose-to-duration profile. Hog1 is activated when the MAP2K Pbs2 phosphorylates the activation loop residues T174 and Y176[56]. Accordingly, activation of Hog1 has traditionally been measured using antibodies raised against the phosphorylated activation loop of a homologous MAPK, p38. Alternatively, activation of the

kinase has also been measured by tracking the translocation of a Hog1-GFP fusion into the nucleus. Neither method provides simultaneous measurement of the timing and amplitude of MAPK activation. The anti-phospho-p38 method does not provide the stoichiometry of activated and inactivated states and does not fully differentiate between the mono- and dually-phosphorylated forms of the kinase (**Figure 2.1**). Measurements of nuclear translocation suffer from similar shortcomings. For example, monophosphorylation is sufficient for nuclear translocation but not for full activation of the kinase[43,76]. Conversely, Hog1 promotes stress resistance and mitophagy under conditions that do not normally lead to nuclear translocation[77,78]. Thus it remains unclear the extent to which Hog1 phosphorylation and nuclear translocation are correlated. Given these limitations we sought an alternative method that accurately measures the dynamics and stoichiometry of Hog1 phosphorylation.

Phos-tag is a metal-coordinating small molecule with a high affinity for phosphorylated serine, threonine, and tyrosine[79]. Addition of Phos-tag to acrylamide gels slows the migration of polypeptides in proportion to the number of phosphorylations on the molecule. Accordingly, we analyzed whole cell lysates using our modified method for Phos-tag analysis. As compared to unstimulated cells, cells osmostressed with 550 mM KCl for five min exhibited slowed Hog1 migration (**Figure 2.2a**). Strains harboring integrated Hog1 mutations T174A or Y176F exhibited faster migration, in accordance with a reduced number of phosphorylations on the polypeptide. Deletion of the MAP2K Pbs2 resulted in migration of Hog1 identical to that observed in unstimulated cells. Interestingly, we never observed accumulation of mono-phosphorylated Hog1 in wildtype cells. Strains lacking each of the phosphatases known to act on Hog1 likewise produced only the dually phosphorylated species, suggesting redundant functions of the MAPK phosphatases. These results

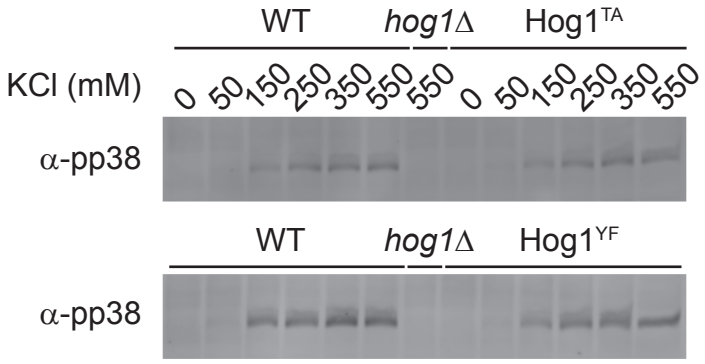

Figure 2.1. Phospho-p38 antibodies recognize monophosphorylated forms of Hog1.
The indicated strains were treated with KCl for 5 min and probed with phospho-p38 antibodies.

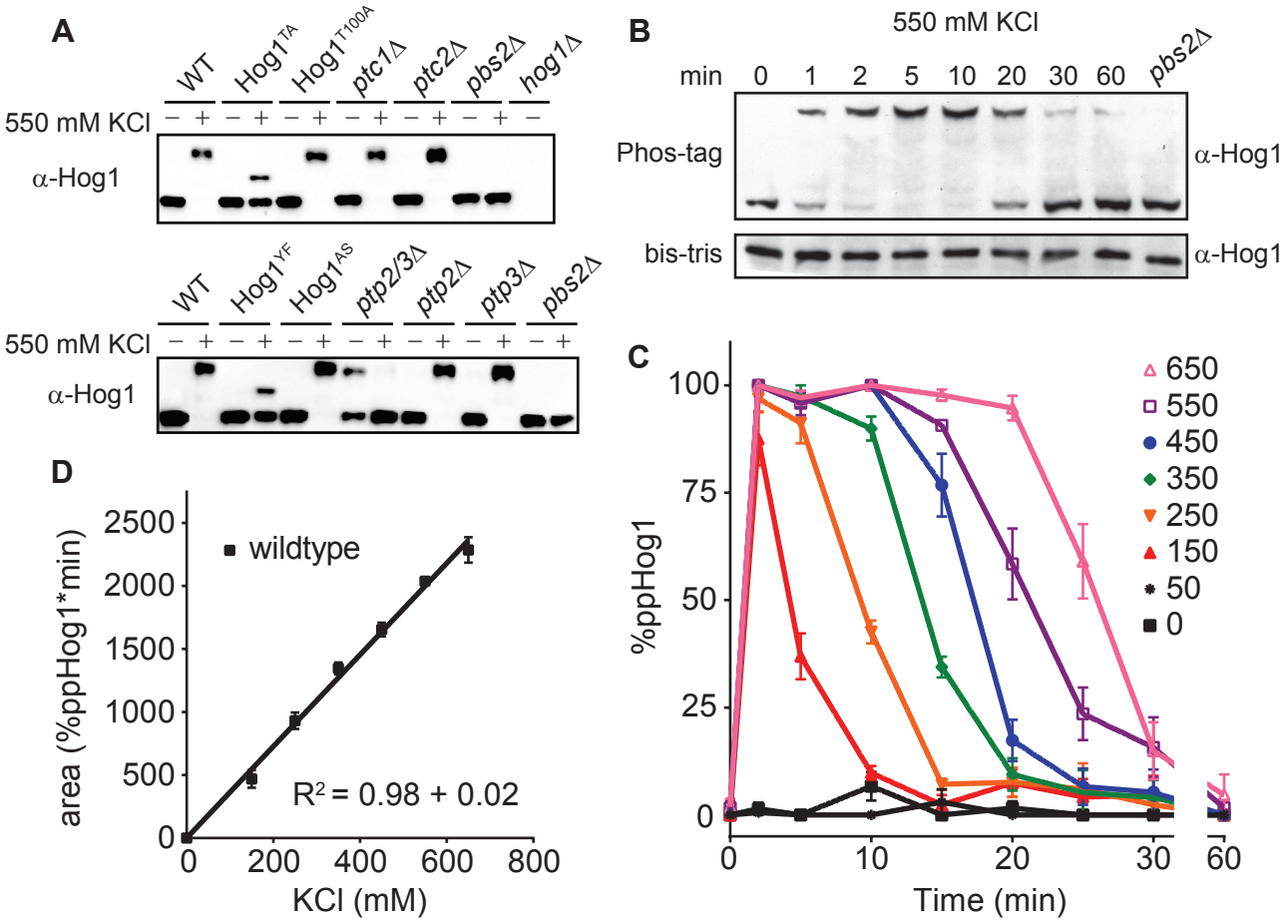

Figure 2.2. The Hog1 signaling profile is a linear function that converts dose-to-duration.

A. Validation of Phos-tag method for resolving dual-phosphorylated and activated (top band) or unactivated (bottom band) Hog1. Cells untreated (-) or treated for 5 min (+) with 550 mM KCl were lysed, resolved by Phos-tag SDS-PAGE, and immunoblotted with Hog1 antibodies. $Hog1^{TA}$ and $Hog1^{YF}$, mutants lacking one of two phosphorylation sites; $Hog1^{T100A}$, analogue sensitive mutant; ptc1Δ and ptc2Δ, serine/threonine phosphatase mutants. ptp2Δ and ptp3Δ, tyrosine phosphatase mutants; pbs2Δ and hog1Δ, MAP2K and MAPK mutants, respectively.

B. Hog1 activation over time. Wildtype cells were treated with 550 mM KCl, lysed and probed by immunoblotting with Hog1 antibodies. Top, Phos-tag Bis-Tris SDS PAGE. Bottom, identical samples in the absence of Phos-tag.

C. Hog1 signaling profile. Wildtype cells were treated with the indicated doses of KCl. Percentage of dually phosphorylated Hog1 was calculated by dividing intensity of the upper band by the total intensity of all Hog1 bands in each lane. Data are means +/- SEM (n > 3).

D. Integration of the Hog1 signaling profile. Data from C are presented as mean area under the curve +/- SEM.

demonstrate that the entire pool of cellular Hog1 is dually phosphorylated in response to osmotic stress.

Our next objective was to define the Hog1 signaling profile; that is, the amplitude and duration of Hog1 activation as a function of time and dose of stimulus. We therefore performed eight time course experiments (**Figure 2.2b-c**) using a range of salt concentrations up to 650 mM, a dose past which cellular compression begins to restrict molecular diffusion[80]. From these experiments it is evident that Hog1 is activated processively and phosphorylated maximally in response to low doses of osmostress. In particular, we observed full activation of Hog1 between 50 mM and 150 mM KCl, doses that we had previously regarded as non-activating. While activation of Hog1 occurred rapidly at all doses tested, the duration of Hog1 activity was graded, with increasing stimulus concentrations producing longer periods of maximum phosphorylation. Additionally, deactivation of Hog1 was significantly slower than its activation and was relatively dose independent, with 95%-98% of the kinase dephosphorylating in a 10 min window. Integrating the area under each time series of Hog1 activity revealed a linear relationship between the dose of osmostress and the duration of total Hog1 activity (**Figure 2.2d**). Thus the activation of Hog1 is switch like, while the duration and deactivation of Hog1 are graded. This signaling profile allows Hog1 to reliably convert input strength to Hog1 activity duration. As shown below, this relationship can be used to identify regulatory components and predict the behavior of Hog1 under various experimental conditions.

The Hog1 signaling profile is encoded by multiple upstream components

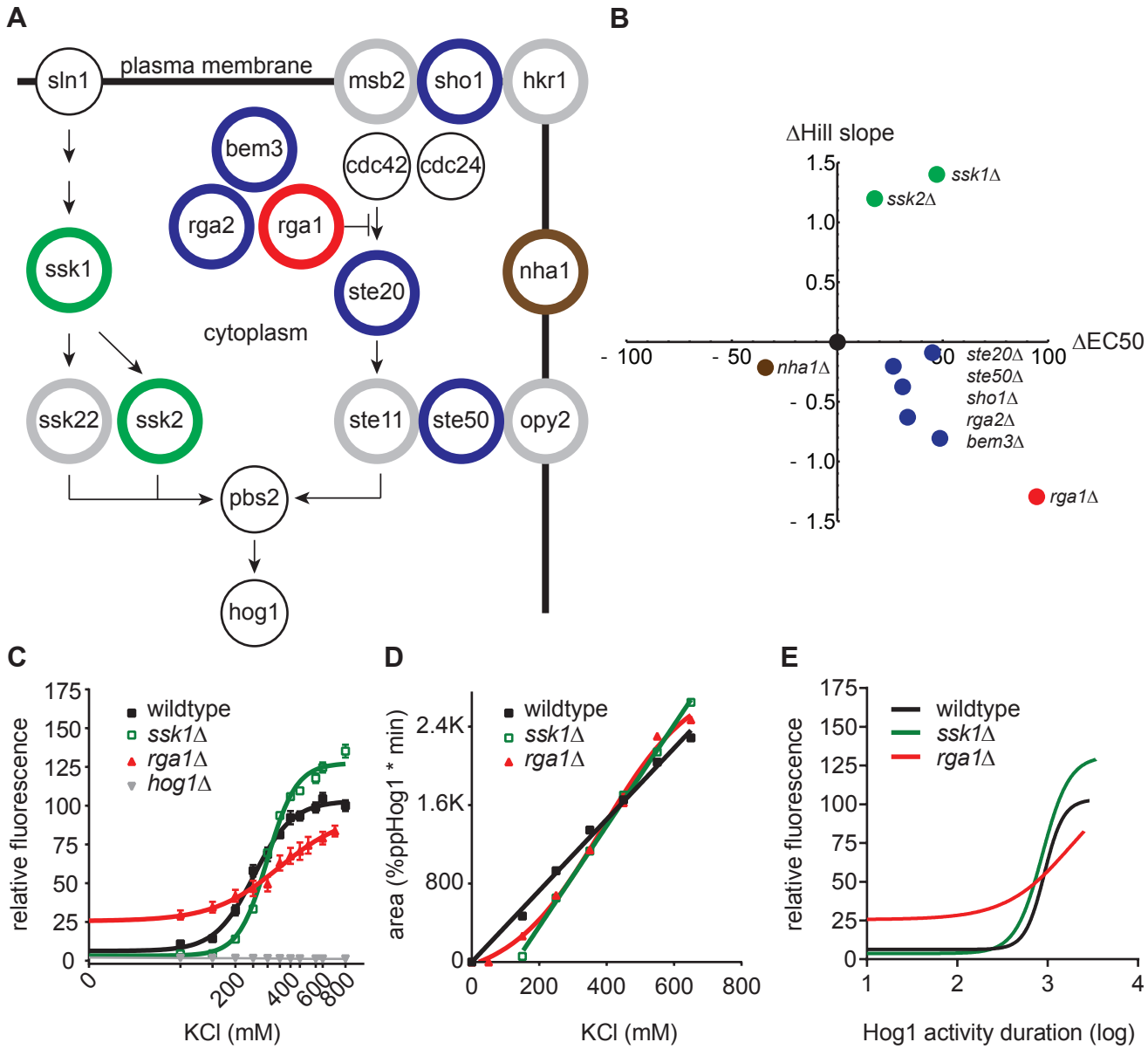

Figure 2.3. The Hog1 signaling profile can be re-engineered through component gene deletions.
A. Diagram of the Hog1 signaling pathway. Colored circles correspond to data points in B. Gray circles, pathway component deletions without effect. Black circles, essential pathway components that were not evaluated.
B. Summary of transcription reporter data. 8XCRE-LacZ Hill slope and EC50 for each mutant strain plotted relative to wildtype (black dot) and color coded as in A. Only significant ($p < 0.05$) changes are displayed. See Figure 2.3 for complete data set.
C. Transcription reporter data for wildtype, ssk1Δ, rga1Δ, and hog1Δ strains. Data are mean relative fluorescence +/- SEM ($n > 4$).
D. Integration of Hog1 signaling profiles for ssk1Δ and rga1Δ strains. Wildtype is shown for reference (see Figure 2.1). Data from Figure 2.3 are presented as mean area under the curve +/- SEM.
E. Comparison of transcriptional output to total Hog1 activity. Computational transformation of data in C, where X-axis values are replaced using Hog1 duration as determined in D for wildtype, ssk1Δ and rga1Δ.

Extensive effort has gone toward understanding how molecular signaling components encode, transmit, and decode information about environmental conditions[53–55,66,81]. One of the best known examples of an encoding component is the kinase scaffold Ste5, which is regulated via localization, feedback phosphorylation, and conformational changes that relate pheromone concentration to Fus3 MAPK activity[51,74,82,83]. Our studies of the Fus3 pathway were the first to suggest a dose-to-duration mechanism for MAPK signaling[75]. Above we demonstrate that Hog1 functions in a similar manner, converting input strength to total Hog1 activity duration. Below, we identify components of the Hog1 pathway responsible for this conversion, reengineer the pathway through deletion of these pathway components, and use those reengineered pathways to demonstrate how downstream output is determined by the duration of MAPK activation.

An input-output relationship has been established between Hog1 nuclear dwell time and transcriptional output[62]. We predicted that deletion of encoding components upstream of Hog1 would transform the functional dependence of Hog1 activity on salt concentration, leading to commensurate changes in downstream transcription. We therefore monitored pathway output using a Hog1-dependent promoter fused to the β-galactosidase gene (CRE-lacZ, CLZ). Using this reporter we conducted a screen wherein we individually deleted each of 15 non-essential upstream components of the Hog1 pathway and calculated dose-response curves for transcriptional output (**Figure 2.3a-b**). CRE-lacZ induction in wildtype cells requires a minimum of 200 mM KCl, and exhibits a Hill slope of approximately 3 (**Figure 2.3c**). As compared to wildtype, deletion of *SSK1*, *SSK2*, *SHO1, STE20,* or *STE50* increased the EC50 (**Figures 2.3b and 2.4a**). Deletion of *SSK1* or *SSK2* increased the Hill slope. These results reveal several components that act as potential encoders of Hog1 activity. In addition

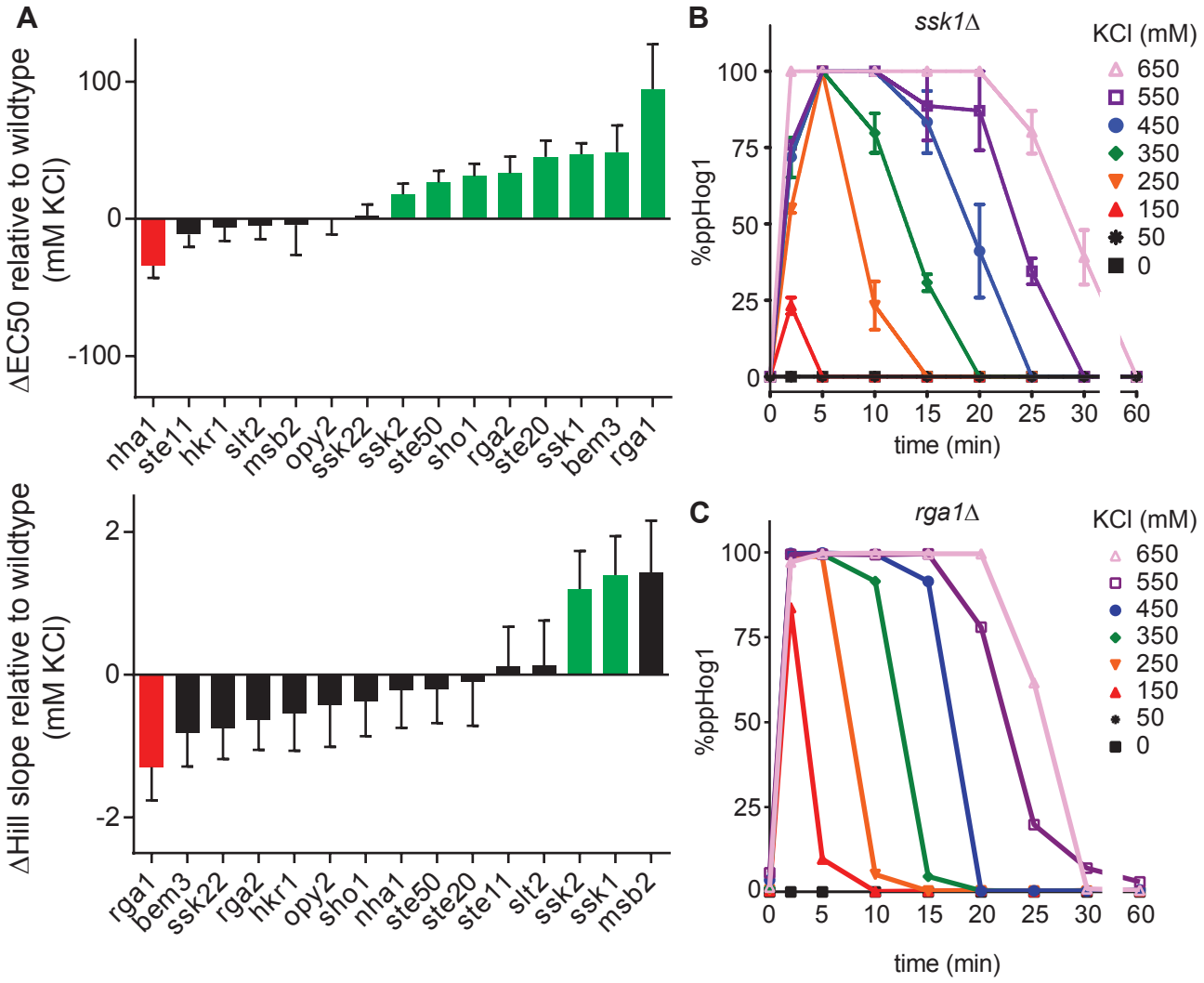

Figure 2.4. The complete transcription and Hog1 activity quantifications for Figure 2.3

A. Rank order of change in transcription reporter Hill slope and EC50 for each mutant strain, relative to wildtype. Significant ($p < 0.05$) increases or decreases are annotated by green or red shading, respectively. Data are mean relative fluorescence +/- SEM ($n > 4$).

B. Hog1 signaling profile in an ssk1Δ strain determined as described in Figure 2.2. Data are means +/- SEM ($n = 3$).

C. Hog1 signaling profile in an rga1Δ strain, determined as described in Figure 2.2 ($n = 1$).

to these known pathway components we also assessed the contribution of the GTPase activating proteins for Cdc42; *RGA1*, *RGA2* and *BEM3*[84,85]. Cdc42 is essential for Sho1 branch activity[86]. Of the Cdc42 regulators, deletion of Rga1 had by far the largest effect on transcription reporter activity, increasing the EC50 and decreasing the Hill slope substantially. These data reveal a unique and previously unrecognized role of Rga1 in the Hog1 signaling pathway.

Our next step was to determine the functional relationship between Hog1-mediated transcription and Hog1 activation. Having identified several candidate encoders of transcription, we selected Ssk1 and Rga1 for in-depth analysis of Hog1 function. Ssk1 is essential for the Sln1 branch of the HOG pathway. Rga1 represents a novel regulator of the Sho1 branch of the pathway. Deletion of these components had the most prominent effects on both the Hill slope and EC50 for our transcriptional reporter. As shown in **Figure 2.4b-c**, deletion of *SSK1* produced a delay in Hog1 activation. Deletion of *RGA1* shortened the duration of Hog1 activity at low doses and prolonged activity at high doses. Integration of these signaling profiles revealed that both deletions affect the relationship between dose and duration for Hog1 activity (**Figure 2.3d**). Deletion of *SSK1* preserved the linear relationship, but produced a steeper slope and x-intercept that was right-shifted as compared to wildtype. Deletion of *RGA1* produced a sigmoidal relationship, with less total Hog1 activity at low doses and greater Hog1 activity at high doses. Thus, the Sln1/Ssk1 branch increases the dynamic range of the pathway by allowing Hog1 to become activated at low doses and limits the duration of Hog1 activation at high doses. The Sho1 branch establishes the linearity of the input-output relationship for the Hog1 pathway.

Having determined the contributions of Ssk1 (Sln1 branch) and Rga1 (Sho1 branch) to Hog1-mediated transcription and Hog1 activation, we next sought to determine the functional relationship between transcriptional output and Hog1 activity. Accordingly, we plotted transcriptional output as a function of the duration of Hog1 activation, as measured by the area under the curve, for wildtype, *ssk1*Δ, and *rga1*Δ strains (**Figure 2.3f**). When plotted using this transformation we observed nearly identical induction and output EC50 values for the wildtype and *ssk1Δ* strains (**Figure 2.3f**). When plotted using this transformation we observed nearly identical induction and output EC50 values for the wildtype and *ssk1Δ* strains (**Figure 2.3f**). However, the behavior of these strains differed from that of the *rga1Δ* strain. Part of this difference may be due to pre-adaptation in the rga1D mutant, given that basal transcription is elevated in this strain and suppressed in the ssk1D mutant[87] (**Figure 2.3e**). Taken together, our results suggest that the Hog1 signaling profile is encoded differently by the two branches of the Hog1 pathway. Additionally, Hog1 activity duration is insufficient to predict transcriptional output under conditions where integrity of the Sho1 branch is perturbed.

Hog1 feedback phosphorylation encodes dose-to-duration signaling

In our previous modeling analysis we postulated that dose-to-duration signaling is mediated by a feedback mechanism[75]. Theoretically, the MAPK may be the origin of this feedback, conveying information via phosphorylation to tune upstream pathway output. Positive feedback drives switch-like behavior, while negative feedback tunes oscillators and rheostats[88]. The Hog1 profile has features of both a switch and rheostat. Therefore, feedback in this pathway may a combination of positive and negative feedback loops (**Figure 2.5a**).

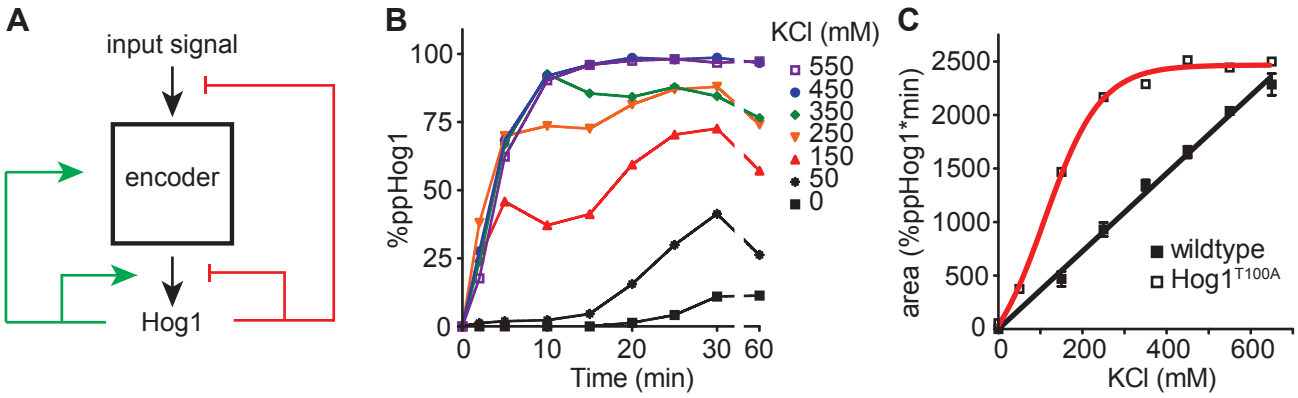

Figure 2.5. The Hog1 signaling profile is encoded through feedback phosphorylation.

A. Diagram of potential positive and negative feedback represented by green and red lines, respectively.

B. Hog1^{T100A} signaling profile in the presence of the kinase inhibitor 1-NA-PP1 (n = 1).

C. Integration of the Hog1T100A signaling profile. Wildtype signaling profile is shown for reference (see Figure 2.2).

Indeed, we previously identified two feedback targets of Hog1 in this pathway[49,50]. To assess the overall contribution of Hog1 feedback we set forth to directly block all Hog1 catalytic activity. In so doing we predicted that we would disrupt the dose-to-duration relationship between input strength and Hog1 activation. To test this prediction, we blocked Hog1 activity using a variant of the kinase ($Hog1^{T100A}$)[89] engineered to be sensitive to the ATP-analogue 1-NA-PP1[90]. This method of inhibition has several important advantages over mutations that permanently disrupt the catalytic activity of the kinase. In the absence of inhibitor the T100A mutation has no detectable effects on Hog1 activity. Conversely, the presence of the inhibitor has no effect on the wildtype kinase (**Figure 2.6**). Thus, cells bearing $Hog1^{T100A}$ will signal normally but are selectively inactivated within minutes of analogue addition. Such acute inhibition limits the opportunity for genetic adaptation or changes in basal activity of the pathway.

For our experiment, cells were pre-treated for two minutes with 1-NA-PP1, then exposed to a range of salt concentrations and harvested at different times. As shown in **Figure 2.5b**, acute inhibition of kinase activity significantly decreased the amplitude and increased the duration of Hog1 activation (dual phosphorylation). As expected for such a signaling profile, we calculated a non-linear relationship between salt concentration and area under the curve for Hog1 activation (**Figure 2.5c**). In particular, we observed a requirement of Hog1 catalytic activity for switch-like activation of the kinase, indicative of a Hog1-mediated positive feedback loop. We also observed a requirement of Hog1 catalytic activity for its own dephosphorylation, indicative of a Hog1-mediated negative feedback loop. Taken together, our results point to the existence of at least two feedback mechanisms: a positive feedback loop that ensures switch-like activation at all doses of stimulus and a negative

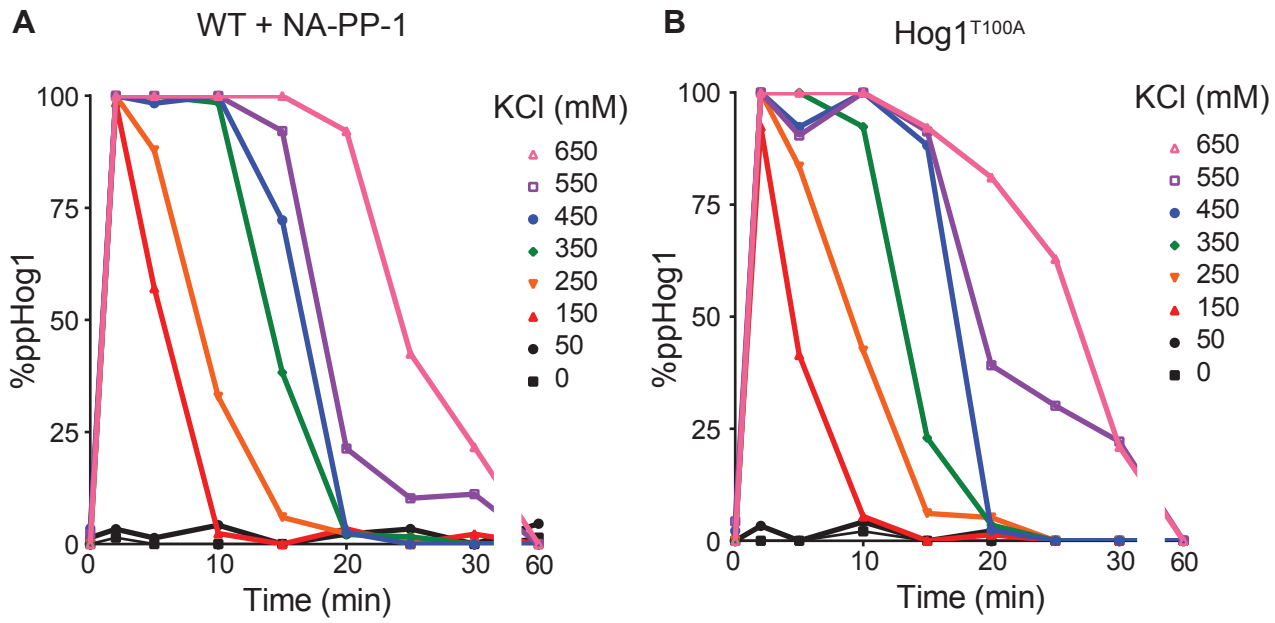

Figure 2.6. Only the combination of Hog1 inhibitor and mutant disrupt dose-to-duration.

A. Hog1 signaling profile with 1-NA-PP1 inhibitor (n=1).

B. Hog1^{T100A} signaling profile without inhibitor (n=1).

feedback loop that ensures graded inactivation over time. We conclude that Hog1 feedback encodes both a rapid switch and a tunable rheostat.

Hog1 feedback encodes dose as graded bits of patterned phosphorylation

For Hog1 to encode dose-to-duration, some target of Hog1 must be regulated in a graded manner. Phosphorylation is the currency of MAPK signaling, and many MAPK substrates are phosphorylated at multiple sites. Such multi-site phosphorylation can be compared to the binary bit language of computing[91]. By this analogy, a single protein phosphorylation event shifts the bit state of the substrate amino acid from 0 (unphosphorylated) to 1 (phosphorylated). The number of potential phosphorylation sites on a protein represents its bit length. For example, Hog1 can accept two phosphorylations and thus it has a bit length of 2, coding 2^2 or 4 bit states. However, we have demonstrated that Hog1 only persists in 2 of its 4 potential states, unphosphorylated or dually phosphorylated. Thus Hog1 functions as a binary switch with just two potential states, on or off. Additionally, we have shown that feedback regulation is a critical component of dose-to-duration, and that feedback phosphorylation converts the Hog1 switch into a tunable rheostat. Here we consider how this switch-to-rheostat conversion might be accomplished via bit state encoding on feedback substrates.

In our forward genetic screen we identified multiple components that affect Hog1 activity, all of which contain consensus sites for MAPK phosphorylation. Even in this limited analysis of 15 pathway components, we counted over 100 potential MAPK phosphorylation sites. Discerning the phosphorylation state of each feedback site, and its individual contribution to dose-to-duration signaling is impractical. Additionally, no single feedback

loop is likely to encode the entire complex topography of the Hog1 signaling profile. However, the relative contribution of a single loop can be investigated in isolation. We and others have previously demonstrated that Ste50 is a substrate of Hog1[49,66,92], and contains 5 documented sites for MAPK phosphorylation, amounting in 2^5 or 32 bit states. This rich diversity of Ste50 bit-states can be observed using Phos-tag, as demonstrated in **Figure 2.7a**. Upon treatment with a high dose of salt, Ste50 rapidly accumulates as a high-migrating species and then relaxes back to the original migration pattern over time. Since the phosphorylated species is absent in a *pbs2*Δ mutant, Ste50 feedback phosphorylation is dependent on Hog1 activity.

We then considered whether the phosphorylation of Ste50 is graded. To that end we measured the bit states occupied by Ste50 over a range of doses and times. These data were then internally normalized for intensity and aligned computationally (see methods) to generate an average bit state occupancy histogram for each condition. As shown in **Figure 2.7b**, Ste50 phosphorylation was indeed graded, occupying a smaller number of increasingly higher bit states as input strength increased. These phosphorylation events occurred rapidly, with obvious shifts after 2 min of stimulus addition. Peak Ste50 phosphorylation occurred by 15 min for all doses, and returned to baseline by 30 to 60 min. This trend is highlighted via plotting of the median migration distance of all Ste50 molecules (**Figure 2.8a**). Integrating each median curve demonstrates a linear relationship between input strength and the accumulation of phosphorylated Ste50 (**Figure 2.7c**). Thus, Hog1 encodes dose as a pattern of graded bit state phosphorylations on the Ste50 scaffold. While Hog1 is phosphorylated as a switch, Ste50 is phosphorylated as a rheostat.

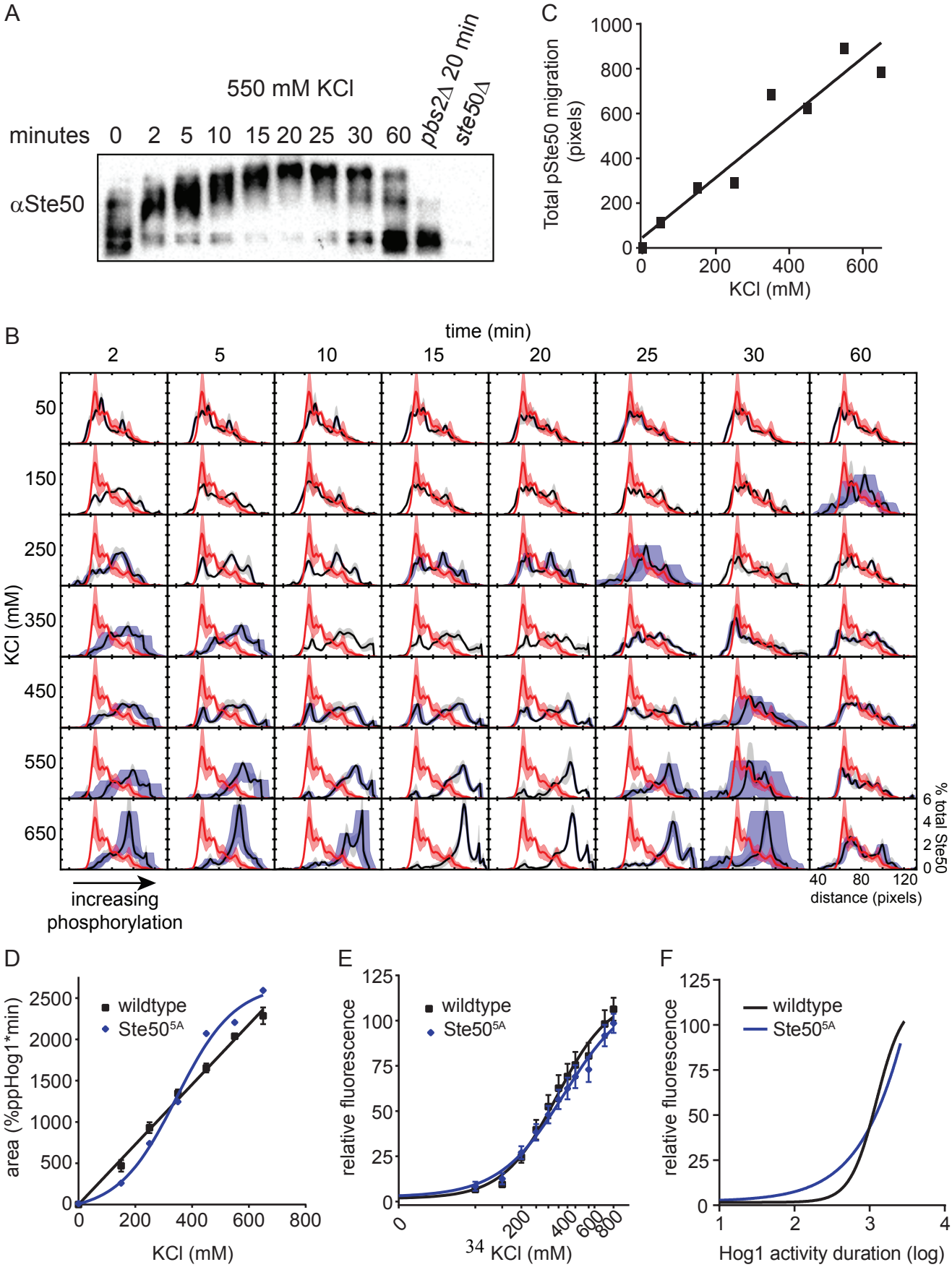
A
550 mM KCl
minutes 0 2 5 10 15 20 25 30 60
pbs2Δ 20 min
ste50Δ
αSte50
C
Total pSte50 migration (pixels)
KCl (mM)
B
time (min)
KCl (mM)
increasing phosphorylation
distance (pixels)
% total Ste50
D
wildtype
Ste50^5A
area (%ppHog1*min)
KCl (mM)
E
relative fluorescence
KCl (mM)
F
relative fluorescence
Hog1 activity duration (log)

Figure 2.7. Hog1 encodes dose-to-duration signaling through graded phosphorylation

A. Ste50 phosphorylation over time. Wildtype and the indicated mutant strains were treated with KCl, processed via Phos-tag immunoblotting, and probed with Ste50 antibodies.

B. Ste50 phosphorylation profile. Wildtype cells were treated as in A with the indicated concentrations of KCl. Each histogram represents > 2 biological replicates. Red, mean Ste50 distribution measured from unstimulated cells; black, mean Ste50 distribution measured for each dose-time in the variable matrix. Shading, +/- SEM (red and gray) or the positional confidence of our computational alignment for the data (blue).

C. Integration of the Ste50 phosphorylation profile (see Figure 2.8a). Data are mean area under the curve +/- SEM.

D. Integration of the Hog1 signaling profile for the $Ste50^{5A}$ strain. Wildtype is shown for reference (see Figure 2.2). Data from Figure 2.8b are presented as mean area under the curve +/- SEM.

E. Transcription reporter data for wildtype (black) and $Ste50^{5A}$ (blue). Data are mean relative fluorescence +/- SEM ($n > 4$).

F. Comparison of transcriptional output to total Hog1 activity. Computational transformation of data in E, where X-axis values are replaced using Hog1 duration as determined in D for wildtype (black), and $Ste50^{5A}$ (blue).

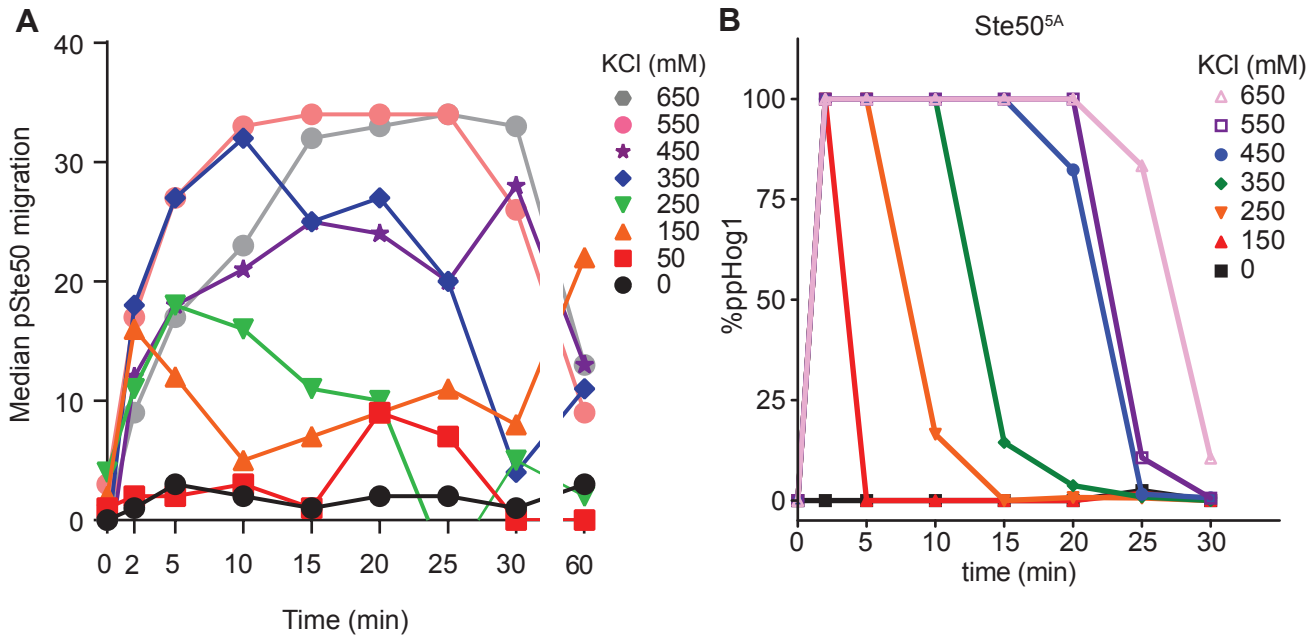

Figure 2.8.

A. Average Ste50 migration. Data are means derived from the alignments in Figure 2.7c +/- SEM (n > 2).

B. Hog1 signaling profile in the Ste505A strain (n = 1).

Our next goal was to determine if graded feedback to Ste50 contributes to establishing the Hog1 dose-to-duration signal. To that end we replaced all documented Hog1 feedback sites on Ste50 and determined the Hog1 signaling profile for this mutant. Ablation of Ste50 feedback phosphorylation modulated Hog1 activity duration, rather than signaling amplitude, and disrupted the linearity of the Hog1 dose-to-duration response (**Figures 2.7d and 2.8b**). In contrast, the CRE-lacZ profile for the $Ste50^{5A}$ mutant was identical to wildtype (**Figure 2.7e**). This seemingly incongruous behavior appears to be a consequence of a reduced gene induction threshold in this mutant. This reduction can be highlighted using the dose to duration conversion method outlined in Figure 2.3 (**Figure 2.7f**). Again, we discover that perturbation of components in the Sho1 branch results in a failure of Hog1 duration to predict gene induction. Thus the effects of the $Ste50^{5A}$ mutant are largely masked in the reporter assay, but revealed through direct observation of Hog1 activity over time.

Taken together, these data reveal a time- and dose-dependent increase in Ste50 phosphorylation. As with activation of Hog1, the increase in phosphorylation is rapid and transient. In contrast to Hog1, the increase in phosphorylation occurs with a dose-dependent profile that is clearly graded. Thus the switch-to-rheostat conversion occurs at the level of Hog1-mediated phosphorylation.

Hog1 activity duration coordinates a tiered adaptive program

Switch-like signals usually underlie commitment to a binary developmental or adaptive output such as cell division[93], neuronal potentiation and backfiring[94,95], or cell differentiation[96,97]. These processes have high energy costs, are often irreversible, and produce a consistent set of outputs. Therefore, most switches are carefully regulated by

graded inputs that either (i) overcome dose thresholds to filter environmental noise or (ii) traverse a buffered signaling cascade before initiating the switch. In contrast, Hog1 employs an inverse switching regime, referred to here as a tunable bifurcated response, wherein commitment to adaptation is switch-like and the resolution of this commitment is graded. This hypothesis is supported by multiple observations. First, Hog1 is activated in a switch-like manner, while substrate phosphorylation is graded. Second, the time that Hog1 spends in the nucleus dictates the sequential production of Hog1-regulated genes[62]. Third, the occupancy of Hog1-regulated transcription factors to their gene promoters is time dependent[98]. Paradoxically, Hog1 activation does not correlate precisely with CRE-lacZ induction when the Sho1 pathway is perturbed. Here we build on this observation to determine if Hog1 activity duration encodes an alternative, graded adaptation program.

We began by analyzing an existing microarray data set[60] where cells were treated with a high dose of salt and monitored for gene expression under continuous stimulation. In this analysis we identified 4 gene clusters, each with distinct time-dependent activation thresholds (**Figure 2.9a**). All four clusters are highly enriched for genes regulated by Hog1 and its canonical transcription factors Msn2, Msn4, Sko1, and Hot1 (**Table 2.1**). However, each cluster dictates progressively higher levels of energy commitment, as determined via gene ontology (GO) analysis (**Figure 2.9b**). Each cluster encodes its own progressive and unique set of general stress response elements, such as heat shock proteins, chaperones, and cytotoxic response elements. Cluster 1 encodes for catabolism of proteins and carbohydrates while driving strong induction of genes for osmolyte synthesis and energy storage. Cluster 1 operates in isolation for the first 15 minutes of the stress response. Between 15 and 30 minutes cluster 2 is engaged, demarcating a pronounced change in the cellular energy

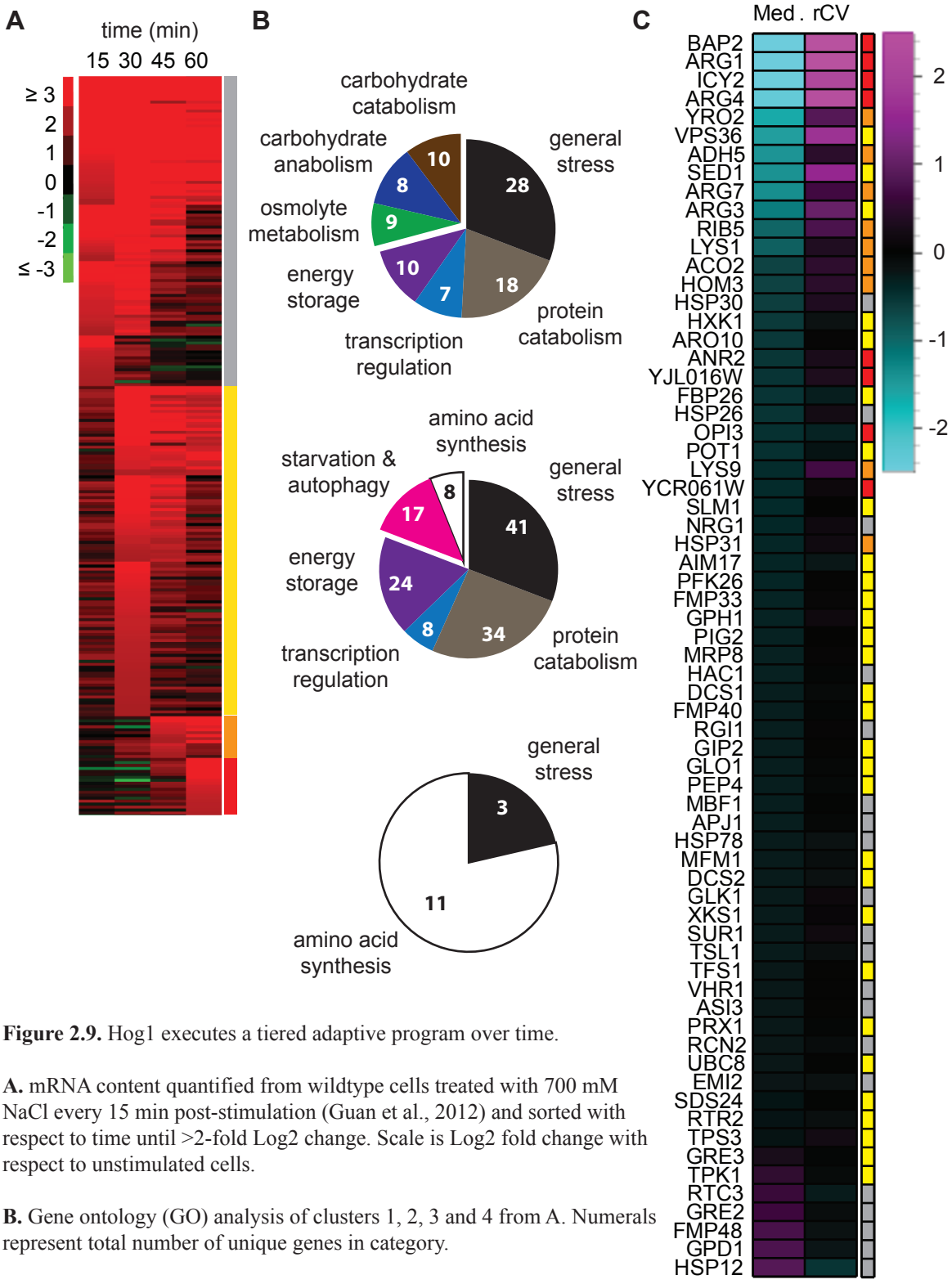

Figure 2.9. Hog1 executes a tiered adaptive program over time.

A. mRNA content quantified from wildtype cells treated with 700 mM NaCl every 15 min post-stimulation (Guan et al., 2012) and sorted with respect to time until >2-fold Log2 change. Scale is Log2 fold change with respect to unstimulated cells.

B. Gene ontology (GO) analysis of clusters 1, 2, 3 and 4 from A. Numerals represent total number of unique genes in category.

C. GFP-tagged protein abundance measured via flow cytometry. Candidate genes were selected at random from those listed in A and treated with 0, 350, or 650 mM KCl for 30 min. Displayed are 67 GFP fusion for which expression increased following stimulation. Change in median intensity and robust CV are reported as Log2 fold-change of 350 mM over 650 mM. The parent cluster for each protein is represented by the color key (right) in gray (cluster 1), yellow (cluster 2), orange (cluster 3), and red (cluster 4).

landscape. Cluster 2 greatly increases synthesis of genes driving protein catabolism and energy storage while generating starvation mediators and components necessary for autophagy. This starvation and survival profile is likely a consequence of the rapid conversion of freely available carbohydrates such as glucose and fructose to osmolytes such as trehalose and glycerol. Lastly clusters 3 and 4 ramp up amino acid synthesis, potentially to compensate for the pronounced protein catabolism and autophagy driven by clusters 1 and 2. We presume that sequential induction of these clusters would serve to tune the adaptive response by facilitating sufficient catabolism and stress mediation while optimizing for fitness after recovery. We propose that this step-wise pattern of gene induction is facilitated through dose-to-duration signaling.

To directly assess the consequences of dose-to-duration signaling we next measured changes in the abundance of the proteins encoded by each of the gene clusters. Accordingly, we measured induction of an unbiased subset of 95 proteins from clusters 1-4. Each protein was expressed from the native gene locus as a GFP fusion and measured by fluorescence cytometry (**Figure 2.9c**). Cells were treated with 350 mM or 650 mM KCl, doses sufficient to activate Hog1 for 20 or 30 min, respectively. As predicted, the median production of proteins from cluster 1 was nearly identical following treatment with 350 or 650 mM KCl, while production of proteins from clusters 2, 3 and 4 were higher following treatment with 650 mM as compared to 350 mM KCl. Collectively, these results indicate that translational output is graded even as Hog1 activation is switch-like.

While the order of protein synthesis was graded, it was not uniform in all cells. For example, the 650 mM treatment group maintained tight population distributions for all proteins, while cells treated with 350 mM KCl exhibited an increasing coefficient of

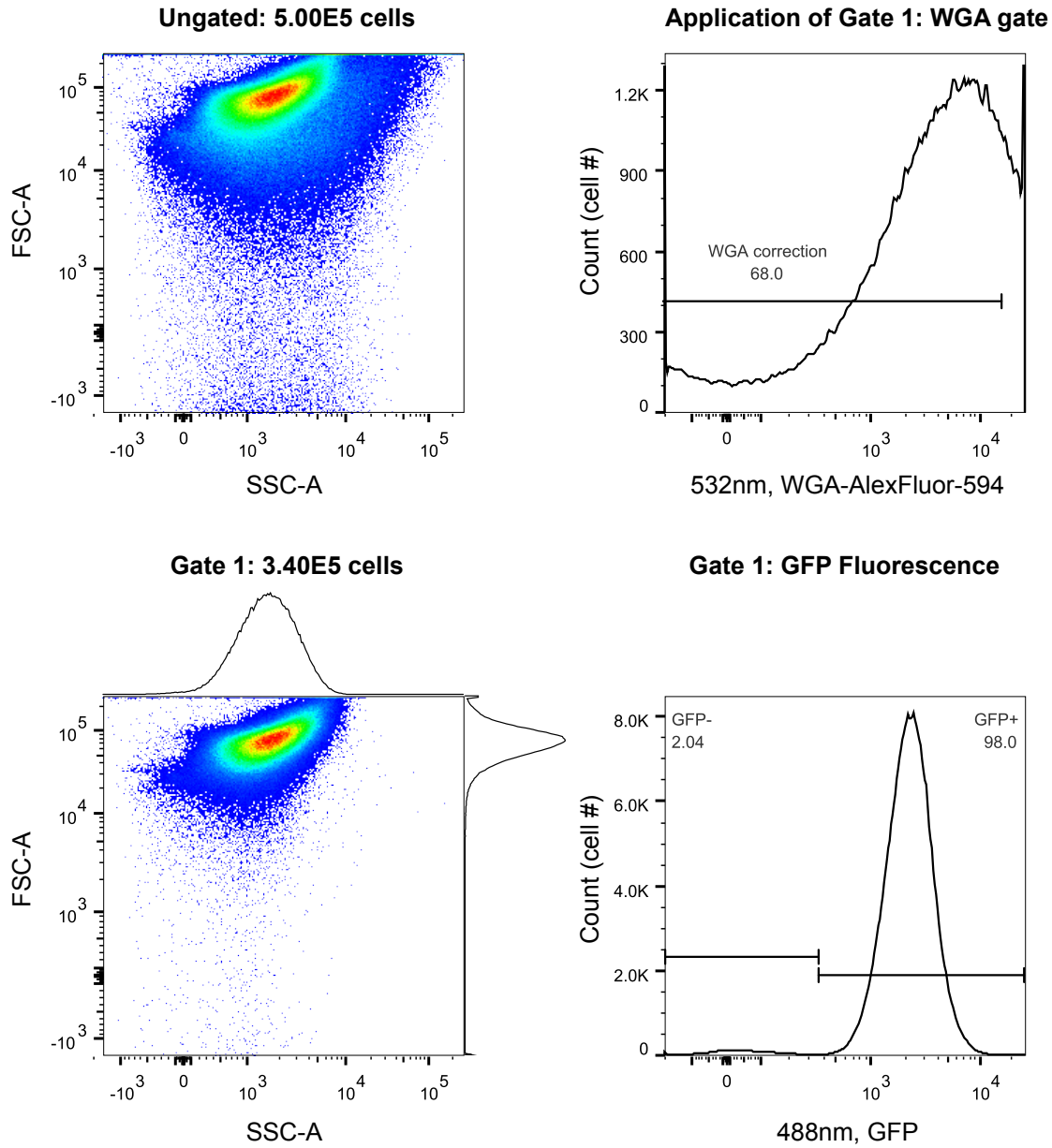

Figure 2.10
Gating parameters for flow cytometry data. Gate 1 establishes a cut-off for auto-fluorescent debris and dead cells determined by staining with wheat germ-agglutinin (WGA) conjugated to AlexFluor-594. Fluorescence minus one (FMO) experiments were performed to compensate for bleed-through on line. Data is compensated fluorescence values. FSC-A, forward scatter area; SSC-A, side scatter area.

variation (CV) for weakly induced proteins. Thus there is an apparent cell-to-cell variability in this system occurring at the level of signaling deactivation. In this context it is worth noting that Hog1 is fully activated, indicating that all cells respond maximally to osmotic stress. This is in striking contrast to the pattern of ERK activation and mitosis in *Xenopus* eggs[72] where switch-like MAPK signaling was first characterized. In those experiments, measurements of whole cell populations indicated a graded response, while measurements of individual eggs uncovered a mix of unresponsive and fully responsive (switch-like) behaviors. Thus, in keeping with our proposal that Hog1 represents an inversion of the standard switch-like model, variability of this system appears to occur at the back-end of signal resolution, rather than at the outset of signal initiation.

Collectively these results indicate that adaptive output is ordered, but not uniform in all cells. Rather, each cell progresses down a graded adaptation program encoded by Hog1 duration, before deactivating stochastically. This stochastic deactivation introduces a noisy adaptive output at the level of individual cells that can be attributed to variable Hog1 deactivation. Thus, Hog1 appears to encode two rheostats, one at the level of MAPK duration and another at the level of MAPK deactivation. The first dictates induction of the cells adaptive program, while the second accommodates variable persistence of this program in individual cells.

Discussion

Hog1 has long served as a prototype for cellular stress adaptation systems. Here we elucidate the mechanism by which switch-like activation of Hog1 converts a linear input of osmotic stress stimulus to a graded adaptive response. We make three observations that

account for these seemingly incongruous behaviors, and reveal how they act to coordinate the stress response program.

First, using a new method to quantify protein phosphorylation, we define the Hog1 signaling profile and use these data to calculate a linear function for Hog1 activity, demonstrating that this pathway encodes a perfect dose-to-duration signal. We then identify encoder components of this function and use them to establish the relationship between Hog1 activity duration and downstream gene induction.

Second, we demonstrate that the relationship between Hog1 activity and transcription extends to induction of the cellular adaptive machinery. In particular, Hog1 exhibits a tunable bifurcated response, having features of both a switch and a rheostat. As a switch Hog1 commits the cell to adaptation, regardless of input strength, ensuring the fastest possible response to stress. As a rheostat, Hog1 tunes recovery through sequential and variable production of proteins needed for adaptation. Two distinct rheostats facilitate this adaptation response. The first is a dose-to-duration rheostat encoding the persistence of maximum Hog1 activity and a sequential gene induction program. The second is a stochastic rheostat encoding cell-to-cell variability in induced protein expression.

Third, we demonstrate that Hog1 feedback is essential to the tunable bifurcated response. Without feedback neither the activation switch nor the graded adaptation response can be established. Ste50 is a major target of Hog1 feedback, a relationship we demonstrate here to be necessary to properly tune Hog1 activity. Further, we show that the total accumulation of phosphorylation on all Ste50 proteins is graded with respect to input strength. Thus, while Hog1 is phosphorylated as a switch Ste50 is phosphorylated as a rheostat.

MAPK signaling pathways are often characterized as being inherently switch-like [74,99]. This conclusion is derived from a viewpoint that MAPK signaling cascades function as ultrasensitive biochemical reactions with zero-order kinetics, a term that differentiates these reactions from more graded first-order Michaelis-Menten systems[29,30]. In contrast, we demonstrate that switch-like activation of Hog1 is largely dependent on feedback. When feedback is abrogated, Hog1 activation is graded. In this way, the Hog1 switch resembles other regulated switch-like systems, such as the Cdk1/Cdc25C positive feedback loop regulating mitosis commitment in *Xenopus* eggs[100].

Many investigators have commented on the relative merits of MAPK pathways operating as either switches or rheostats[47,99,101,102]. Whereas switches encode deterministic action, rheostats can scale their responses to input strength. When a rheostat begets a switch, the system is designed to integrate information to engage a decision making process. We propose that the Hog1 system functions in the inverse, utilizing a switch initiate adaptation before integrating information and tuning the response over time. Moreover, we demonstrate that Hog1 confers graded feedback regulation, through bit state encoding of Ste50 phosphorylation. While phosphorylation has been highlighted in this study, other modifications can regulate protein activity[103]. For MAPK pathways such modifications include ubiquitination[104,105], acetylation[106,107], methylation[108], sumoylation[109,110], and others. Thus, while the currency of MAPK modules remains phosphorylation, this modification is likely to be a precursor to other modifications that serve to further expand the bit lengths of substrate proteins. In fact, phosphorylation has been identified as a requirement for certain ubiquitination reactions[111]. And in at least one case, ubiquitination of a MAPK pathway component has been shown to dictate MAPK signaling specificity[105]. Just as protein

induction occurs in a graded and sequential manner (Figure 2.9), different post-translational modifications may occur sequentially and thereby contribute to the graded output.

Finally, Hog1 activity duration encodes a temporally graded protein induction program. The protein content of each step suggests that the cell is steadily progressing in its energy commitment to the stress adaptation process. Some cells progress further than others in this process, indicating differing needs of individuals in the population. We observed that perturbation of Sho1 branch components alters the relationship of Hog1 duration to gene induction. This observation may underlie reprogramming of the adaptive needs for those mutants. Indeed, deletion of RGA1 results in significant basal output of the reporter. This pre-adaptation may adjust the relationship between Hog1 activity duration and transcriptional output. Additionally, $Ste50^{5A}$ is known to generate cross-talk between the Hog1 stress adaptation and Kss1 nutrient deprivation pathways [49,92]. This crosstalk may introduce signaling interference in the MAPK transcriptional circuit.

The results of our cytometry analysis indicate that each induced gene, or perhaps cluster of genes, exhibits a tiered (graded) relationship to Hog1 activity duration. Elucidation of these relationships would allow for a more complete predictive model of total system output. Comprehensive identification of Hog1 substrates, and establishing the consequences of those phosphorylation events, could eventually produce a complete predictive model of the pathway. Further, multiple MAPK signals are likely to regulate many of these same genes. Identification of all functions for all kinase signals, over a time-dose matrix, will be necessary to complete a deterministic model for a given cell stimulus.

An ideal stress response system is one that responds immediately, in a strictly dose-dependent manner, and in a manner that protects the population. We propose that Hog1

meets this ideal. We have shown that Hog1 is activated rapidly and in a dose-to-duration manner, but with sufficient variability to accommodate a rapidly changing environment. Ultimately, our goal is to generate a universal function for this MAPK transduction pathway – wherein the encoding components for any input at any dose are known. This will require development of new analysis techniques capable of quantifying the sum of modifications on signaling proteins. We expect that such efforts will eventually reveal new avenues for therapeutic intervention and control of disease networks.

Experimental Procedures

Strains

All yeast strains in this study were derived from BY4741 (**Table 2.2**). Deletion of open reading frames was performed using standard methods, either with antibiotic or auxotrophic markers. PCR was used to validate all deletions. Strains used for flow cytometry were taken directly from the green fluorescent protein (GFP)-tagged library (Life Technologies)

Cell Culture

Cells were cultured using standard methods with minor modifications. Yeast were grown on yeast-peptone-dextrose (YPD) agar medium at 30^{o}C for 3 days. Fresh, single colonies were isolated and grown overnight in synthetic complete + dextrose (SCD) liquid medium, diluted 1:500, grown for 6 hr, and diluted again to OD_{600nm} = 0.001. Experiments were performed the following day when the culture reached OD_{600nm} = 1.

Stress Treatment and Cell Lysis for Immunoblotting

Cells were stressed and lysed as described previously[50]. Notable exceptions, dosage, and considerations for Phos-tag sample preparation follow. Cell cultures were split into 8 x 75 ml volumes and 25 ml of SCD+KCl medium was added to a final concentration of 0, 50, 150, 250, 350, 450, 550, or 650 mM KCl. Where noted 1-NA-PP1 ATP-analogue (Cayman Chemical, 10954) was applied to cells at 12 uM final concentration as described previously[89]. Time-points from each flask were taken as 10 ml samples, quenched in 5% (% w/v throughout) trichloroacetic acid (TCA), and held on ice until the end of the time course. Samples were then centrifuged at 3000 *x g* for 3 min, aspirated, washed in 1 ml 5% sodium azide, and frozen at -80^{o}C.

Cell pellets were thawed on ice, resuspended in 200 ul TCA lysis buffer (10 mM Tris-HCl pH 8.0, 10% TCA, 25 mM NH_4OAc), and lysed by vortexing at 4^{o}C for 10 min. Lysate was centrifuged at 13000 *x g* at 4^{o}C for 10 min, aspirated, and mixed with 100 ul resuspension buffer (0.1 M Tris-HCl, pH 8.5, 3% SDS). Each sample was then heated to 90^{o}C for 10 min, cooled at room temperature for 10 min, and centrifuged at 13000 *x g* for 1 min. 60 ul supernatant was isolated and protein concentration was determined using the BioRad DC Protein Assay (500-0112) with detergent-compatible reagent. Each sample was diluted to a final concentration of 2 ug/ul in resuspension buffer and mixed 1:1 with 2x sample buffer (0.1% bromophenol blue, 2% SDS, 20% glycerol, 500 mM Tris-HCl pH 8.5, and 200 mM dithiothreitol). Samples were run immediately or stored for use in 1-2 days at -80^{o}C.

Bis-Tris Acrylamide Gels, Phos-Tag, and Gel Transfer for Immunoblotting

Phos-Tag conjugated to acrylamide has been previously reported to function best in neutral pH conditions such as those found in Bis-Tris SDS-PAGE gels[79,112]. We optimized the Bis-Tris gel formulation to properly resolve a wide range of protein sizes and phosphorylations from yeast whole-cell lysates. Reagents for each gel layer were added in the order listed and, importantly, were vigorously vortexed in a 14 ml screw-cap conical bottom tube for 5 sec where indicated. Resolving layer; 8% 29:1 acrylamide/bis-acrylamide (BioRad, #161-0156), 350 mM Bis-Tris pH 6.8 (Fisher Scientific, #BP301100), 20 uM Phos-Tag (Wako Chemical Industries, #304-93521), 40 uM $Zn(NO_3)_2$, vortex, 0.05% ammonium persulfate (APS), vortex, 0.1% tetramethylethylenediamine (TEMED), vortex, pour immediately and very gently layer with isopropanol and polymerize for a maximum of 1 hr. Rinse resolving layer 5 times with deionized water and add stacking layer; 4% 29:1 acrylamide/bis acrylamide, 350 mM Bis-Tris pH 6.8, vortex, 0.05% APS, vortex, 0.1% TEMED), vortex. Gels were cast, run, and transferred using the 1.5 mm BioRad Mini-PROTEAN gel system (165-8006). Gels were used immediately or stored at 4^{o}C in 350 mM Bis-Tris pH 6.8 buffer for up to 4 weeks.

Prior to running, protein samples were heated at 70^{o}C for 10 min, allowed to cool, and loaded to 15 ug of protein lysate per lane. Running buffer [50 mM Tris-HCl, 50 mM 3-(4-Morpholino)propane sulfonic acid (MOPs), 0.1% SDS, 5 mM sodium bisulfite, pH 7.2] was added and each gel was run at a constant 150V for 1.5 hr. Upon completion the resolving layer was removed and equilibrated in transfer buffer [1x NuPage transfer buffer (Life Technologies, NP0006-1) supplemented with 20% methanol, 2.5 mM sodium pyrophosphate, and 5 mM sodium bisulfite] shaking at room temperature for 20 min to release

phosphopeptides from Phos-Tag. Wet transfer to an Immobilon-P PVDF membrane (Millipore) was then performed at 4^{o}C for 20 hr at 20V.

Immunodetection and Quantification

All blots were incubated in blocking buffer (TBS-T; Tris buffered saline, 50 mM Tris, 150mM NaCl plus 0.05% Tween 20 with 5% non-fat dry milk) for 1 hr at room temperature. Membranes were then transferred to heat-sealable pouches, filled with 3 ml primary antibody solution (blocking buffer + primary antibody), sealed, and rocked gently for 14 hr at 4^{o}C. The primary antibodies were directed against Hog1 (Santa Cruz sc-6815, 1:500), phospho-p38 (Cell Signaling 9216, 1:500), Ste50 (gift of Roger Brent, 1:500) and Protein-A (Sigma-Aldrich P2921 1:50,000). Blots were washed 4 x 15 min with TBS-T and probed with 5 ml goat anti-rabbit (Santa Cruz sc-2030, 1:50,000) or rabbit anti-goat (Santa Cruz sc-2922, 1:50,000) secondary antibody solution (blocking buffer + secondary antibody) for 1 hr with rocking at room temperature. Blots were again washed 4 x 15 min with TBS-T before incubating with 5 ml Clarity Western ECL Substrate (BioRad 170-5060) for 5 min in the dark. Blots were then developed on radiography film for qualitative images or using the BioRad ChemiDoc MP System (170-8280) for quantification of proteins. Briefly, ECL images were captured over time and sequentially integrated using a CCD camera. Images were acquired until all blot lanes contained saturated pixel intensities, and then hand selected exposure times occurring just prior to pixel saturation to maximize the dynamic range of each band for quantification.

Immunoblot image quantification was performed using Fiji[113]. Protein quantitation data are presented as a percentage determined by dividing the intensity value for the band identified as dually phosphorylated protein by the intensity value of all protein bands.

Microarray Data Analysis, Transcription Factor Association, and Gene Ontogeny Analysis

All microarray data were downloaded from the National Institutes of Health Gene Expression Omnibus database, accession number GSE32196. Data were clustered based on time to > $Log_2$2-fold change in mRNA expression relative to unstimulated cells. Determination of transcription factor association was performed using the "Rank by TF" algorithm from YEASTRACT[114] scanning for binding plus expression evidence with standard statistical cut-offs calculated from whole genome background values. These genes were further clustered by their gene ontology classification using the "Functional Annotation Clustering" algorithm from DAVID[115,116] and then grouped by hand into broad, distinguishable classes.

Fluorescence-based Flow Cytometry and Data Analysis

Cell culture and stress treatment were performed as above, but in 96-well plate format. Cells were treated with 0, 350, or 650 mM KCl final concentration and incubated at 30^{o}C for 30 min. After stress treatment cycloheximide was added to 10 ug/ml final concentration to halt protein translation. Cells were immediately centrifuged at 3000 x g for 2 min. Cell pellets were resuspended and fixed with 2% paraformaldehyde, 1 M phosphate buffer (PB, 5:1 ratio of K_2HPO and KH_2PO_4, pH 7.5), and 10 ug/ml cycloheximide. Fixation was carried out at room temperature for 15 min. Plates were then recentrifuged as before and

washed at room temperature 2 times in 150 ul PB + 75 mM lysine HCl to quench fixative. The cell pellets were then resuspended in 100 ul PB + 100 U benzonase (Sigma-Aldrich) and incubated at 37^{o}C for 15 min to cleave free nucleotides. Pellets were again washed in 150 ul PB and then incubated with 0.5mg/ml wheat germ-agglutinin, a yeast bud scar stain[117] conjugated to Alex Fluor 594 (Invitrogen, W11262) for 15 min and rinsed 3 times in 150 ul PB. The fixed and stained cells were stored in the dark at 4^{o}C. Prior to cytometry cells were sonicated in a 96-well plate sonicator ('SonicMan' Brooks Life Science Systems) at power 30 for 15 sec at 4^{o}C using a SL0096-P21-SS sonication head.

Fixed cells were run on an LSRII flow cytometer (BD Biosciences) modified with a 96-well plate HTS system (BD Biosciences). A maximum of 500,000 counts were processed per run. Data were gated and analyzed using FlowJo v.10 analytic software (**Figure 2.10**) and a custom statistical analysis for defining a unique α cut-off value for each protein analyzed. For this statistical analysis test populations for each cytometry data set were generated using random sampling with replacement up to the n of the data set. These test populations were paired and the student t-test was performed on each pair. This process was iterated 100 times, generating p-values for each pairing. These p-values were rank ordered and the 5th was taken as a cut off distinguishing the α value. This α value represents the p-value threshold for a 5% false-positive assumption. The α value determination was repeated 5 times, ranked, and the median of those values taken as the true α value for the data set. This was repeated for all cytometry samples. These α values were then used to set the unique p-value thresholds for t-tests between each treatment type. The t-tests were performed in both directions. A significant difference between cytometric data sets was assumed to exist only if the p-value threshold was met for both analysis directions.

Transcription Reporter Assay

The pRS416-8XCRE-LacZ plasmid was used in these studies, as described previously[118]. Cells were transformed with the reporter plasmid using standard methods and evaluated as previously[119], with several notable exceptions. Single colonies were isolated and cultured as noted above, except using SCD lacking uracil to maintain selection for the reporter plasmid. 96-well plates were preloaded with 40 ul SCD+KCl to achieve final experimental concentrations between 0 and 800 mM KCl. Each plate was loaded with 60 ul cell culture per well and incubated at 30^{o}C for 90 min. Two technical replicates for four biological replicates were conducted per plate. The assay was stopped by addition of 20 ul development solution [135 mM piperazine-N,N'-bis(2-ethanesulfonic acid) sodium salt (PIPES), 0.25% Triton-X100, 0.5 mM fluorescein di-β-D-galactopyranoside (FDG, Marker Gene Technologies, 17817-20-8)] and incubated at 37^{o}C for 6 hr. The OD_{600nm} and 485nm/580nm fluorescence ratio was measured for each plate using a Molecular Devices SpectraMax M5.

Fluorescence values were normalized using OD_{600nm} reads from unstimulated wells. Technical replicates were averaged and a minimum of four biological replicates were plotted in Prism 6 (GraphPad Software) and fit using a log(agonist) vs. response variable slope equation. Change in EC50 and Hill slope were assessed via two-tailed t-test with a $p < 0.05$ cut off.

Ste50 Quantification, Data Alignment, and Statistical Comparison

Ste50 was quantified as pixel intensity with respect to distance from an anchor point, a consistent non-specific band on the immunoblot. Experimental replicates ($\geq$2) were then paired and aligned in Python using a custom analytical program. Briefly, data set 2 was scanned past data set 1 pixel by pixel and 2 was subtracted from 1 for each alignment. The root mean-squared (RMS) sum of their intensities at each scanned position was then tallied. The positional alignment scoring the lowest RMS value was then chosen as the best-fit alignment. Data set 3 was then scanned against the first two and fit similarly. All potential data-set alignment orders were tested for all data sets and each produced identical alignments, this was done to ensure no alignment bias was injected due to operational ordering. The alignments were then averaged and a standard error (SE) was generated and displayed as black shading. For each alignment the anchor value was omitted to ensure only real data influenced the alignment. The anchor was then reinserted for each aligned dataset and the mean distance between anchors was computed. This mean was set at X=0 for each graph and the anchor SE was displayed with blue shading. The median of each alignment was then computed and used to generate the plots in Figures 2.7 and 2.8.

Dose-to-Duration Conversion Calculations

Transcriptional reporter curve fits were converted from dose to Hog1 duration using functions fit to the Hog1 area plots. These functions were generated using the analytical software Eureqa (Nutonian) by randomly sampling basic and exponential mathematical functions. Approximately 1e11 formulations were evaluated and the function with the highest score (size vs. R^2) was selected for each strain.

Plasmid Synthesis and Mutagenesis

Pbs26A construct was purchased through nucleotide synthesis by GenScript.

Table 2.1

Transcription factor (TF) binding and interaction analysis. Percent value represents number of query set gene promoters associated with TF. p-value calculations and cut-offs determined as outlined on YEASTRACT. Significance of gene set (left) to transcription factor (top) association indicated as highly significant (**, $p < 1E^{-5}$), significant (*, $p < 1E^{-5}$), or non-significant ($p > 0.01$). 67 random genes were selected from the yeast genome as a negative control.

	Msn2	**Msn4**	**Sko1**	**Hot1**	**Hog1**
random (67)	51.56% (0.245)	37.50% (0.346)	21.88% (0.016)	1.56% (0.152)	9.38% (0.003)
All microarray (252)	95.63% (0**)	87.30% (0**)	46.83% (0**)	17.86% (0**)	10.71% (1.2E-09**)
C1 (107)	98.10% (0**)	94.39% (0**)	57.94% (0**)	28.97% (0**)	13.08% (5.4E-07**)
C2	96.40% (0**)	87.39% (0**)	37.84% (6.3E-12**)	11.71% (8.3E-12)**	10.81% (2.4E-05**)
C3&4	85.29% (1E-06**)	64.71% (1.8E-4*)	41.18% (8.0E-08**)	2.94% (0.052)	2.94% (0.27)
flow cytometry (67)	94.03 (0**)	82.09% (1E-15**)	49.25% (9.3E-14**)	14.93% (9.24E-11**)	13.43 (2.55E-05**)

Table 2.2

Strains used in this study.

Strain	Genotype	Background	Reference
BY4741	*MATa, his3Δ1, leu2Δ, met15Δ, ura3Δ*	BY4743	Brachmann et al., 1998
JGE001	$Hog1^{T100A}$	BY4741	This study
JGE002	*ssk1Δ::KanMX4*	BY4741	This study
JGE003	*ssk2Δ::KanMX4*	BY4741	This study
JGE004	*ssk22Δ::KanMX4*	BY4741	This study
JGE005	*pbs2Δ::KanMX4*	BY4741	This study
JGE006	*msb2Δ::KanMX4*	BY4741	This study
JGE007	*hkr1Δ::KanMX4*	BY4741	This study
JGE008	*rga1Δ::KanMX4*	BY4741	This study
JGE009	*rga2Δ::KanMX4*	BY4741	This study
JGE010	*bem3Δ::KanMX4*	BY4741	This study
JGE011	*ste20Δ::KanMX4*	BY4741	This study
JGE012	*ste11Δ::KanMX4*	BY4741	This study
JGE013	*opy2Δ::KanMX4*	BY4741	This study
JGE014	*ste50Δ::KanMX4*	BY4741	This study
JGE015	*hog1Δ::KanMX4*	BY4741	This study
JGE016	*ptc1Δ::KanMX4*	BY4741	This study
JGE017	*ptc2Δ::KanMX4*	BY4741	This study
JGE018	*ptp2Δ::KanMX4 ptp3□::LEU2*	BY4741	This study
JGE019	*ptp2Δ::KanMX4*	BY4741	This study
JGE020	*ptp3Δ::LEU2*	BY4741	This study
JGE021	$Hog1^{T174A}$	BY4741	This study
JGE022	$Hog1^{Y176F}$	BY4741	This study
JGE023	Ste505A; S155A, S196A, S202A, S248A, Thr341A	BY4741	Nageic et al., 2012

CHAPTER III

SPECTATING THE SYMPHONY OF YEAST STRESS ADAPTATION THROUGH BIOINFORMATICS[1, 2]

For cell adaptation, as for a symphony, harmony is essential. Maintaining harmony in these complex systems requires a conductor. The conductor does not play. Instead, the conductor establishes a tempo upon which harmonious actions are linked. In the same fashion, the work of the previous chapter establishes Hog1 as a conductor of yeast osmoadaptation. This observation then begs the question, what is the opus that Hog1 conducts?

Soon after the discovery of Hog1 it was assumed that its sole purpose was to coordinate glycerol production[120], thereby reestablishing osmotic balance. Since that time, microarray analyses have demonstrated that Hog1 engages a dynamic gene regulatory network[60,121]. By setting this gene induction symphony to the timing of the conductor, as was done in Figure 2.9, a compelling motive for the actions of the cell were uncovered. As Hog1 signaling duration increases the cell engages an increasing number of stress adaptation and survival genes. In this way Hog1 generates sufficient adaptive output for the needs of the cell without engaging unnecessary systems. However, this conclusion is likely imperfect and our understanding of this complex system is narrow. Microarray is a woefully ineffective interpreter of cellular action, much like listening to music through a very thick wall. For

[1] All figures contributed by Justin G. English

[2] Metabolomics data collection performed with James P. Shellhammer

example, through fluorescent cytometry analysis we determined that only 60% of the largest mRNA induction events after osmostress result in increased protein abundance. This is not a rare occurrence, in fact it falls in line with numerous similar reports[122–125]. Thus, mRNA production does not necessitate an increase in protein abundance. The possible reasons for this are myriad but the conclusion remains the same; if we wish to understand how the cell reprograms its adaptive machinery then it is to that machinery we must focus our attention.

Hog1 modifies the production priorities of the cell during osmoadaptation. While the mechanics underlying changes in production are complex, the results are quite simple; the cell generates what it needs to respond and survive. To understand this process we must observe it. Thus, in the first section of this chapter we combine proteomic and metabolomic data sets to determine how Hog1 sets the cells adaptive priorities. In light of this question, we also sought to understand how the needs of individual cells may differ within the population. To this end we repeated our analysis of the flow cytometry data in Chapter II using a cell age discriminator. This experiment demonstrates that cell age directly alters both the basal and stress induced protein landscape in yeast. Through these analyses a small window, a single note, in the complex actions of the cell population are uncovered. While incomplete, these approaches hold promise for unlocking the cells stress-adaptive symphony.

Stress Induced Metabolic Restructuring in Yeast

If phosphorylation is the information currency of the cell then metabolites are its energy currency. Metabolites are chemicals that have been ingested or synthesized by the cell for the purposes of energy storage or expenditure. ATP is a canonical example. There are numerous chemical synthetic routes for synthesizing ATP. The most common in humans is

via cellular respiration. In this process oxygen, adenosine diphosphate (ADP), and sugar molecules are processed within the mitochondria to create ATP and carbon dioxide. This conversion stores the energy locked within sugar on to a cellular metabolite useable by numerous enzymes, such as kinases[126]. The synthesis of metabolites is a rapid and constant process; a balancing act guiding the survival of every organism. In fact, a human being turns over their body weight equivalent in ATP every single day[127]. Though of course, the mass is not lost, instead a small amount of energy is consumed to convert the ATP to adenosine diphosphate (ADP) and back to ATP. An iterative recycling of energy storage substrates.

ATP is but one example of thousands of cellular metabolites continually synthesized and consumed by the cell. Many of these are intermediary chemical substrates, the building materials fed in to complex enzymatic cascades, which lead to terminal metabolic products. By measuring how stress alters the abundance of terminal metabolites and their enzymatic processors we can begin to visualize the biological needs of a cell under distress. To this end, we conducted a metabolomic analysis of yeast via mass spectrometry before and after stress induction. Untreated cell cultures and cultures treated with 500 mM KCl for 15 minutes were snap frozen, lysed, and analyzed by mass spectrometry. The resulting output was then matched and quantified against a simultaneously processed panel of 297 terminal metabolites. Through this analysis we identified an astounding 181 (60%) terminal metabolites that undergo significant changes in abundance after only 15 minutes of osmostress. We then compared this metabolomics study to a similar proteomic experiment wherein the changing abundance of 296 proteins was quantified[128]. Comparison of these two datasets provides insight on how Hog1 signaling can reprogram the cells enzymatic framework. Here we will focus on three major themes of this analysis; production of

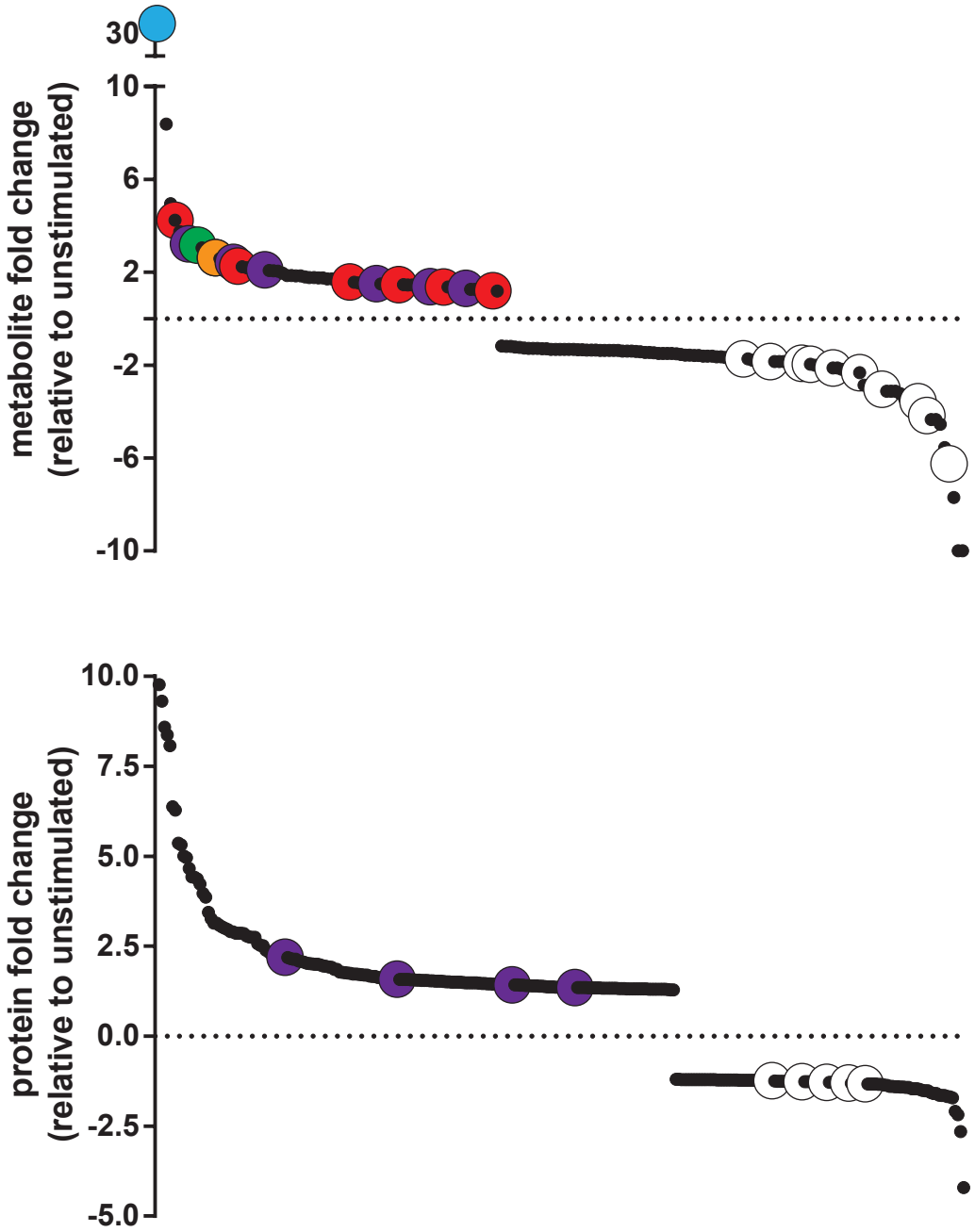

Figure 3.1. Rank order analysis of change in metabolite (top) and protein (bottom) concentrations after osmostress. Only statistically significant hits from each screen are displayed. Data is fold-change relative to measurements from unstimulated cells. Purple; products and enzymes of lipid catabolism. White, mature lipids and lipid synthesis enzymes. Red, polyamines. Green, glycerol. Orange, acetyl-CoA. Blue, trehalose.

osmolytes, conversion of lipids to energy, and the synthesis of a unique family of amino acid derivatives known as polyamines.

Yeast osmoadaptation requires the synthesis of osmolytes to restore turgor[63]. Metabolic research of the Hog1 pathway has focused primarily on glycerol production[63,129–131]; indeed the pathways namesake, HOG, stands for “high osmolarity glycerol”. Glycerol is presumed to function as the primary osmolyte for restoring cell turgor. Our metabolomic screen, coupled with bioinformatic analysis, corroborates that glycerol production increases after osmostress (**Figure 3.1**). Relative to unstimulated cells glycerol increases by 2.5 fold. It has been proposed that Hog1 directly increases the activity of enzymes that accelerate the conversion of respiration (glycolysis) by-products in to glycerol. Curiously, the branches of glycolysis necessary to generate these by-products appear inactive (**Figure 3.2**). Indeed, the end product of glycolysis, pyruvate, is reduced in osmostressed cells, as are many of the enzymes necessary to generate and process pyruvate. If glycerol is not being produced through glycolysis by-products, where is it originating?

The Krebs cycle is substantially activated after osmostress (**Figure 3.3**). Acetyl-CoA is necessary to fuel energy production through the Krebs cycle[132]. In our analysis we noted a considerable increase in Acetyl-CoA (2.4 fold) (**Figure 3.1**). Acetyl-CoA is generated through sugar or lipid catabolism. To produce acetyl-CoA from sugar glycolysis must synthesize pyruvate, which is then processed in to acetyl-CoA. As noted above, glycolytic activity is down in cells following osmostress. However, we noted that lipid catabolism, lipolysis, is significantly increased. The concentration of complex, intact triglycerides and lipids decrease after osmostress; while degraded lipid sub-species and the enzymes involved in lipid catabolism rise after osmostress (**Figure 3.1**). The process of lipolysis liberates

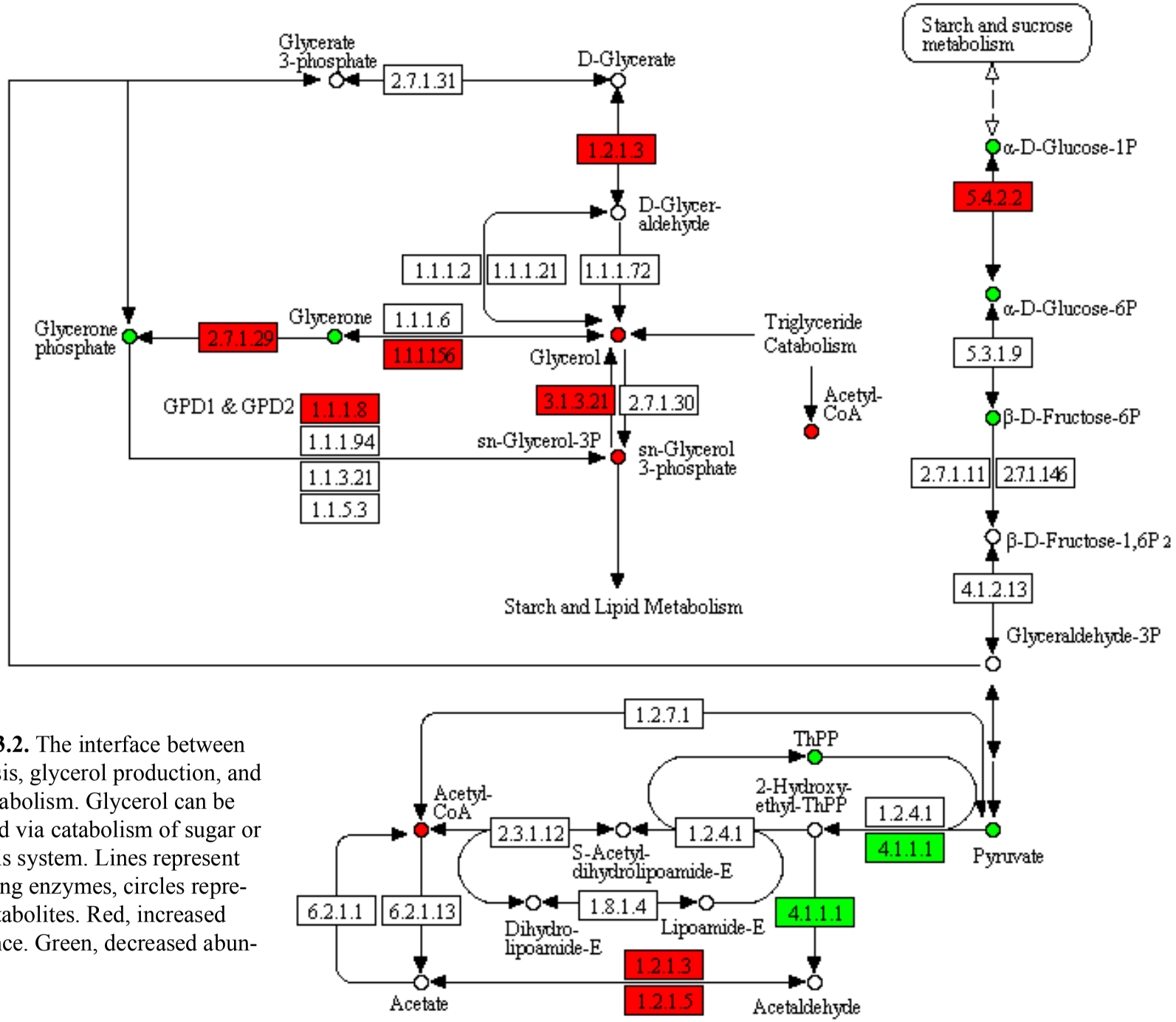

Figure 3.2. The interface between glycolysis, glycerol production, and lipid catabolism. Glycerol can be produced via catabolism of sugar or fat in this system. Lines represent processing enzymes, circles represent metabolites. Red, increased abundance. Green, decreased abundance.

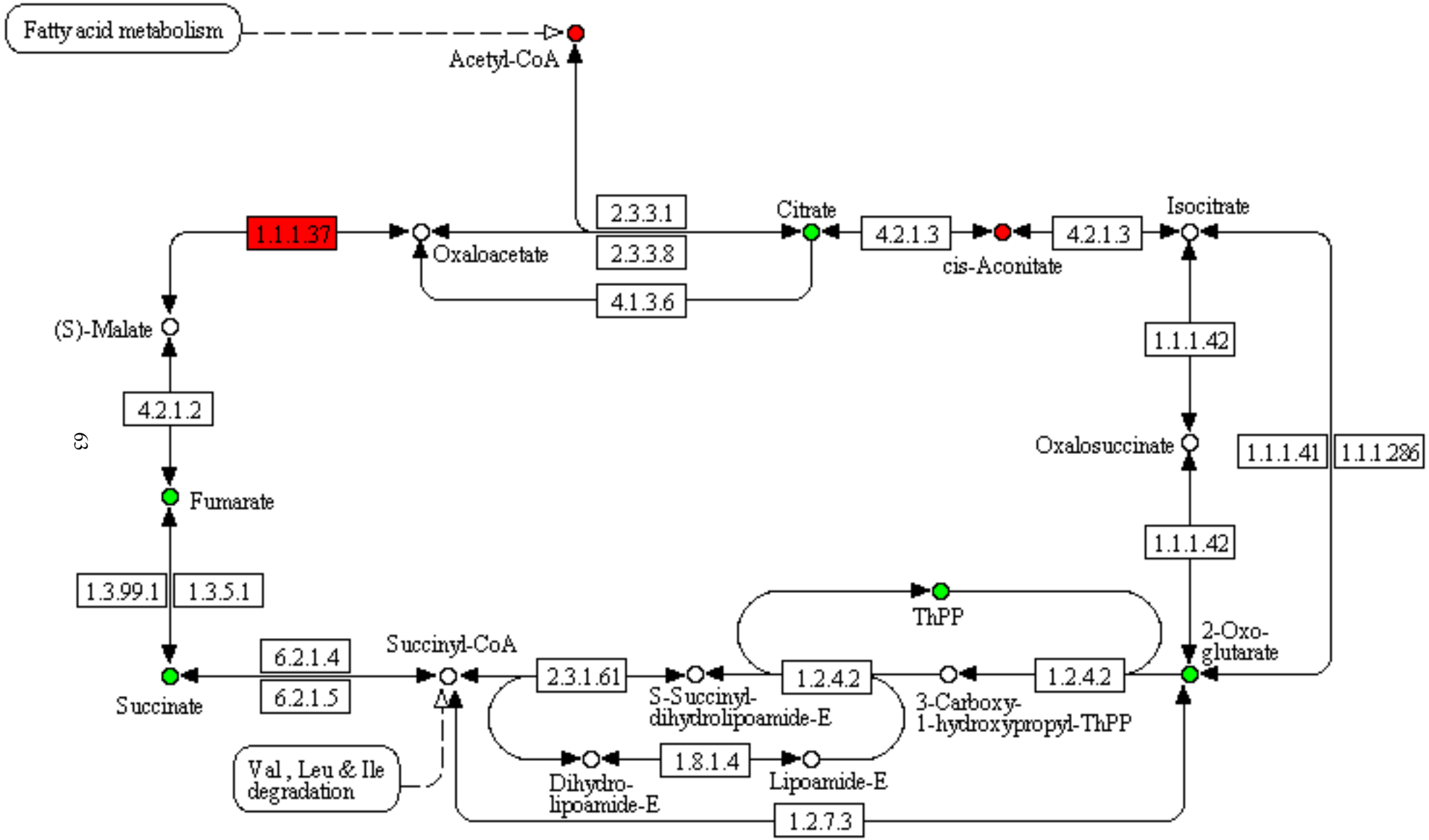

Figure 3.3. The Krebs (TCA) cycle. Acetyl-CoA derived from sugar or fat catabolism is processed to produce ATP. Lines represent processing enzymes, circles represent metabolites. Red, increased abundance. Green, decreased abundance.

glycerol from glycerolipids before processing fatty acids to produce Acetyl-CoA and hydrocarbons[133]. The observation that lipolysis, and not glycolysis, is increased during osmostress suggests that Hog1-mediated glycerol production may in fact be a result of lipolysis.

The yeast genes GPD1 and GPD2, both glycerol-3-phosphate dehydrogenases indicated on **Figure 3.2**, have been described as osmostress mediators[120,134]. Both are required for quick recovery from osmotic stress. The rationale for involvement of GPD1 and GPD2 has been through their role converting glycolysis by-products in to glycerol. We propose here that this conclusion is false. We observe that numerous glycerol containing molecules and processing enzymes increase following osmostress (**Figure 3.2**). GPD1 and GPD2 are among these, and are important not only for the synthesis of glycerol precursors, but for converting glycerol derivatives in to other metabolites. Without GPD1, GPD2, and other glycerol processing enzymes identified in our analysis glycerol would accumulate. A stockpile of glycerol would slow the overall rate of lipolysis. This would then decrease production of acetyl-CoA, a metabolite essential for energy production via the Krebs cycle.

From a biochemical standpoint glycerol production via lipolysis is a more logical conclusion than synthesis of glycerol as an osmolyte. The resting concentration of glycerol in cells is 21 mM[134]. The 2.5 fold increase observed in our study would amount to 52.5 mM of glycerol. The osmolality (osM) of a non-ionic compound is equivalent to its concentration, so the observed production of glycerol would increase intracellular osmopressure by 0.032 osM. However, we applied 500mM KCl, constituting an approximate 1 osM increase in extracellular osmopressure. It is therefore unlikely that glycerol production is serving as a potent osmolyte in this scenario. Glycerol is instead the by-product of lipolysis for the

purposes of energy. This analysis, while rational, brings up several questions. Why is the cell catabolizing lipids and processing acetyl-CoA for energy? The Krebs cycle is strongly activated in our system, but it is largely inferior for energy production when compared to glycolysis. The cells are floating in media containing approximately 2% glucose and ample oxygen. Why is glycolysis not operating to provide the cell with its energy needs? The answer appears to be that the cell is prioritizing use of its carbohydrates for synthesis of two actual osmolytes, trehalose and glycogen.

Trehalose is an absolutely fascinating molecule[135–139]. Trehalose is a critical dehydration stabilizer in all living organisms. It has been proposed to compensate for water loss due to its unique volume and hydrogen bond capacities. Trehalose is simply two alpha-linked glucose molecules. However, in this conformation trehalose fills a volume 2.5 times greater than all other sugars, by weight. Trehalose protects organelle integrity under osmostress conditions. This is achieved by replacing the lost water molecules necessary for maintaining protein folds and lipid layer organizations with trehalose-mediated hydrogen bonds. Through this trehalose-mediated mechanism several organisms, including *Tardigrades* and *Selaginella* can survive complete dehydration and “come back to life” upon application of water. Trehalose has also been identified as a significant survival component of wild mushrooms and other fungi.

In our analysis trehalose synthesis is the strongest metabolic hit of all metabolites in the cell (**Figure 3.1**). Trehalose increases by 32 fold relative to unstimulated cells in 15 minutes. The scope and scale of enzymatic reprogramming for production of trehalose has not been previously appreciated. As predicted in our GO analysis from **Figure 2.9**, our metabolomics analysis uncovered a frenzy of biomass catabolism. Glucose, fructose, and

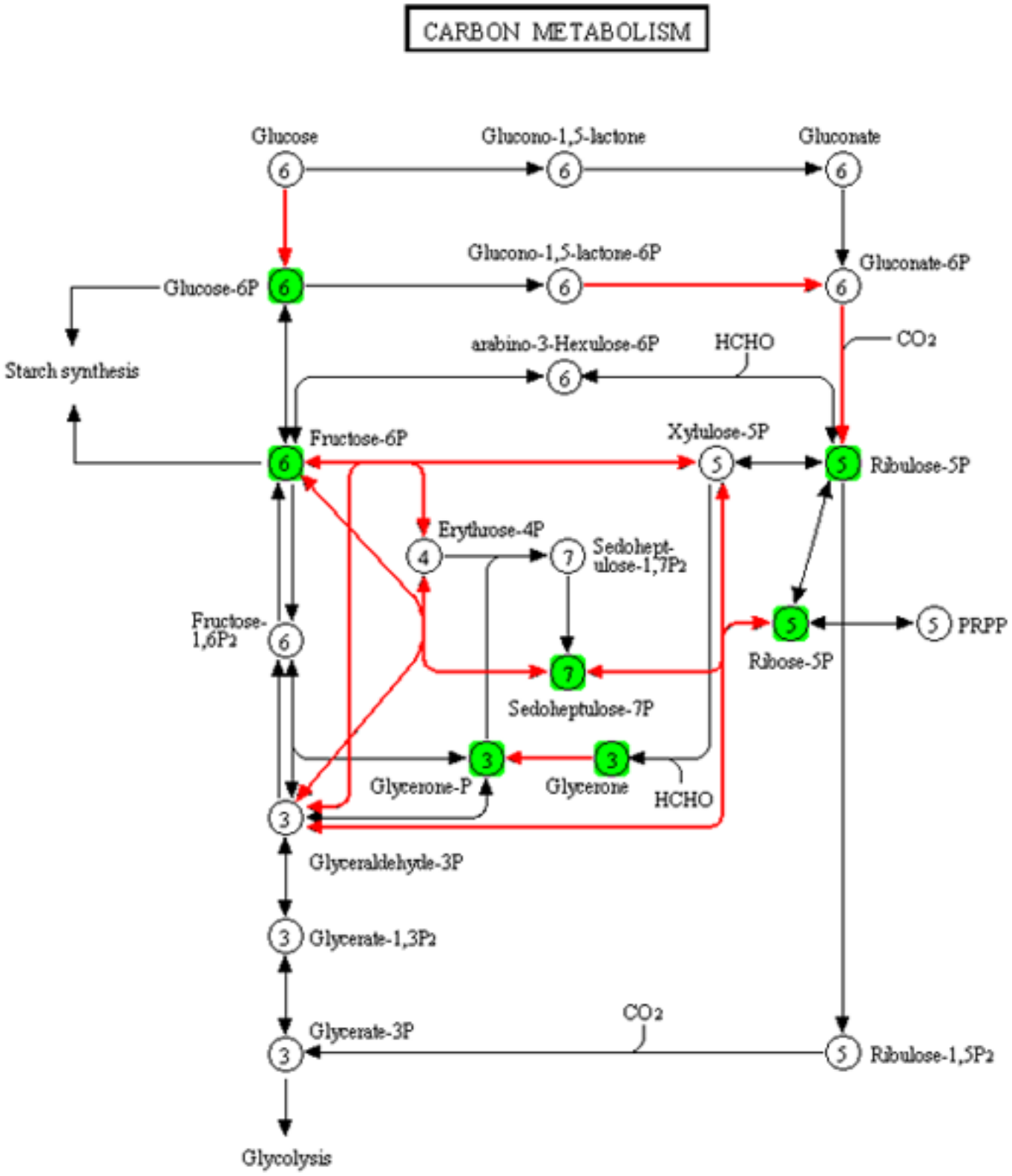

Figure 3.4. Carbon metabolism process of the cell. Sugar is processed for glycolysis or starch synthesis. Lines represent processing enzymes, circles represent metabolites. Red, increased abundance. Green, decreased abundance.

sucrose fall in abundance while the catabolic enzymes necessary for processing these nutrients in to complex starches, and ultimately trehalose, enrich (**Figure 3.4-3.5**). Alongside trehalose synthases a number glycogen-synthase enzymes are upregulated. Glycogen is an enormous starch-like energy storage molecule comprised exclusively of hundreds of linked glucose molecules (**Figure 3.6**)[140]. Hydration of glycogen can immediately release free glucose for use. Unfortunately, our metabolomics screen was unable to detect the glycogen, and thus we fail to determine if its abundance also increases alongside trehalose. However, the proteomic profile suggests this likely. Glycogen is normally synthesized as a carbon reservation mechanism during times of carbohydrate starvation. In this context, the cell may believe it is starving due to the rampant conversion of glucose to trehalose. However, glycogen may also serve as an additional osmolyte. Regrettably an alternate analysis will be necessary to assess this possibility.

Through our combined metabolomics and proteomic analysis we have determined that the cell is engaged in wholesale aggregation of energy molecules in to starchy osmolytes. This behavior underlies the immediate need of the cell to re-establish homeostasis. It therefore appears that the cell forgoes efficient energy metabolism via glycolysis, and suffices on the ATP produced through lipid energy sources. This observation coincides with the extreme drop in ATP levels in our analysis, to a level undetectable.

The majority of metabolic restructuring events after osmostress appear to be those related to nutrient catabolism, energy prioritization, and osmotic balance. However, we also noted a distinct enrichment of a unique class of molecules known as polyamines (**Figure 3.7**). These molecules include putrescine, cadaverine, spermidine, and spermine[141]. Grotesque as these may sound, they serve critically important but poorly understood roles in

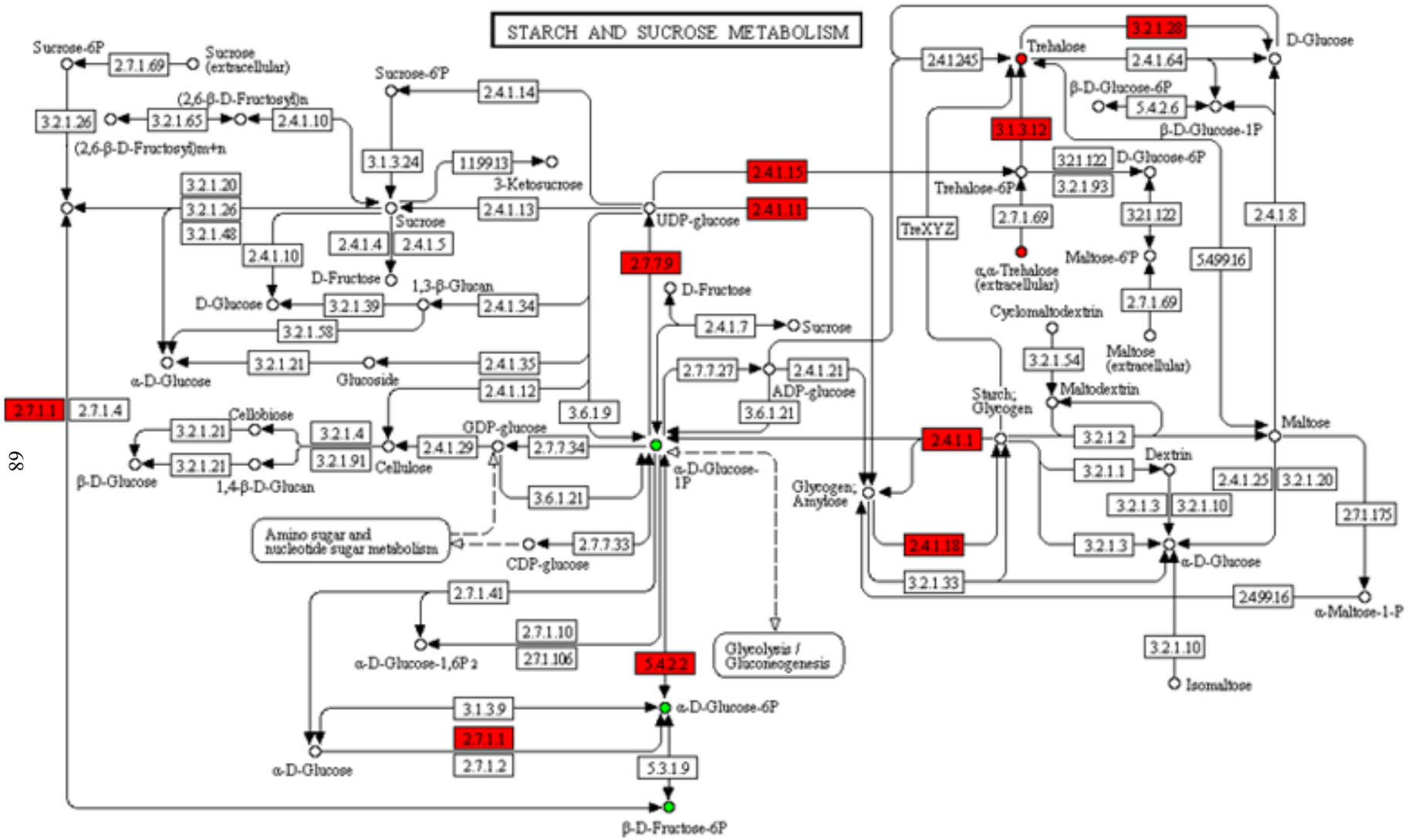

Figure 3.5. Starch metabolism process of the cell. Glucose-6P and Fructose-6P are processed in to glycogen or trehalose. Lines represent processing enzymes, circles represent metabolites. Red, increased abundance. Green, decreased abundance.

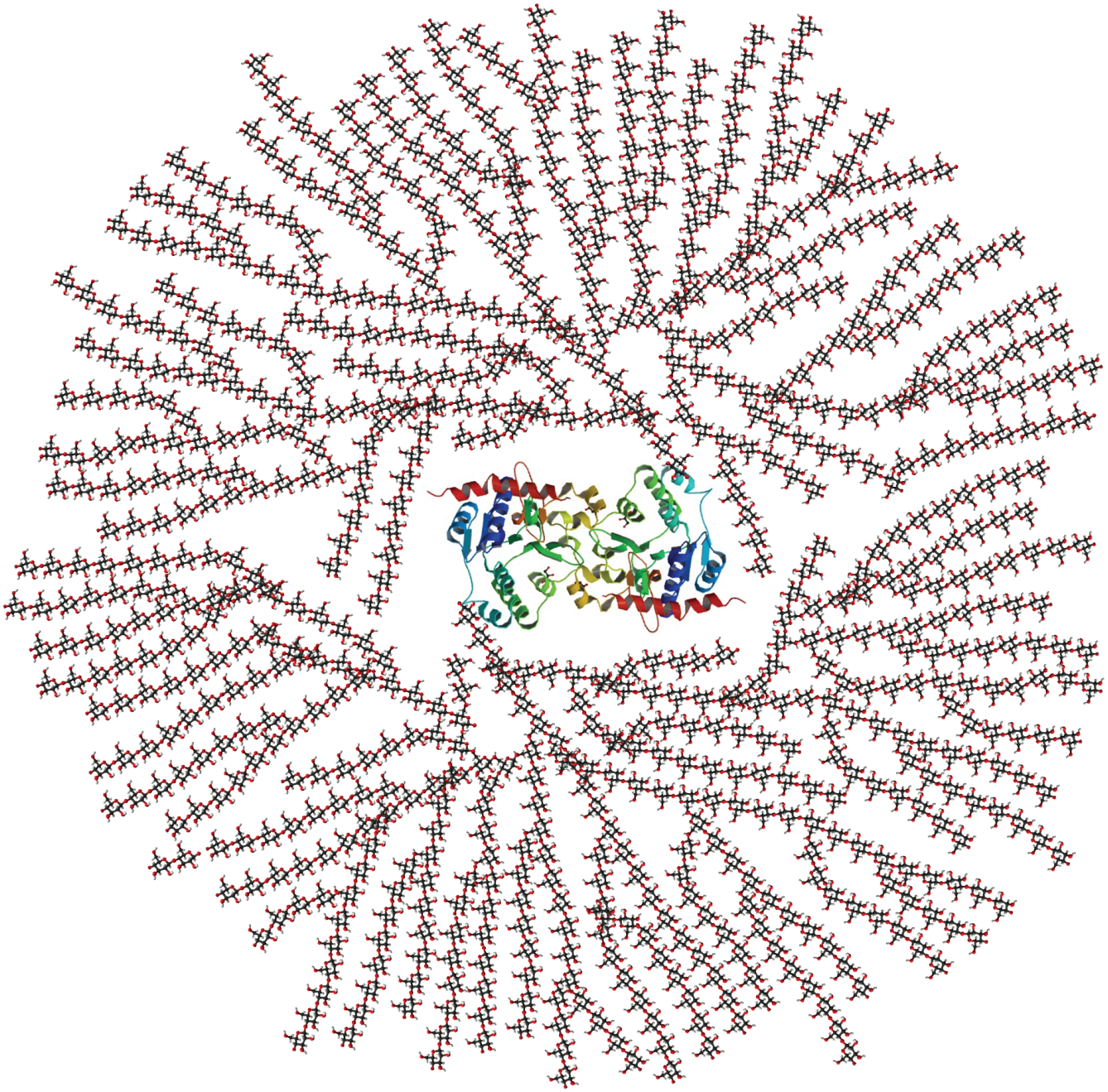

Figure 3.6. 2D Cross-sectional view of the metabolic molecule glycogen. Each unit on each chain is a molecule of glucose. Protein at center is glycogenin, the enzyme involved in linking glucose to form glycogen.

the process of cell stress adaptation, growth, and survival[142–144]. Their synthesis and production mechanisms are conserved among all eukaryotes; including plants, yeasts, and humans. Wildly enough, a study of salmon has found direct links between polyamine turnover and p38 signaling, the homolog of Hog1 in higher order animals[145]. Similar studies in human systems have since been conducted using polyamine precursors[146].

Notably, osmostress causes depletion of Spe1 (**Figure 3.7**), the synthase responsible for converting ornithine to putrescence. One would assume, then, that polyamine concentrations should decrease rather than increase during osmostress. However, the accumulation of polyamines induces translation of a Spe1-specific ubiquitin ligase[147]. Through this degradation mechanism polyamines self-regulate their own abundance. What role then are these carefully regulated molecules playing in the osmoadaptive process? This question remains to be answered, however hints from the literature suggest several possible mechanisms. The addition of polyamines to yeast, flies, worms, and mice induces autophagy and extends the lifespan of each organism[148,149]. Inversely, the abundance of polyamines in all organisms decreases with respect to that organism's age[150]. As osmostress induces polyamine production in yeast three questions surface. Does osmostress affect autophagy, cell aging, or both?

Certain forms of autophagy in yeast have been attributed to Hog1 activity. However, autophagy has been observed under non-osmostressed conditions[77]. These observations suggest Hog1 may play alternative roles in regulating nutrient availability and starvation responses. Indeed, the breadth of control that Hog1 exercises over the cells energy stores during osmostress indicates a potentially potent interplay between these two pathways. As glucose and other sugars are the principal foods of yeast, this would make logical sense. It

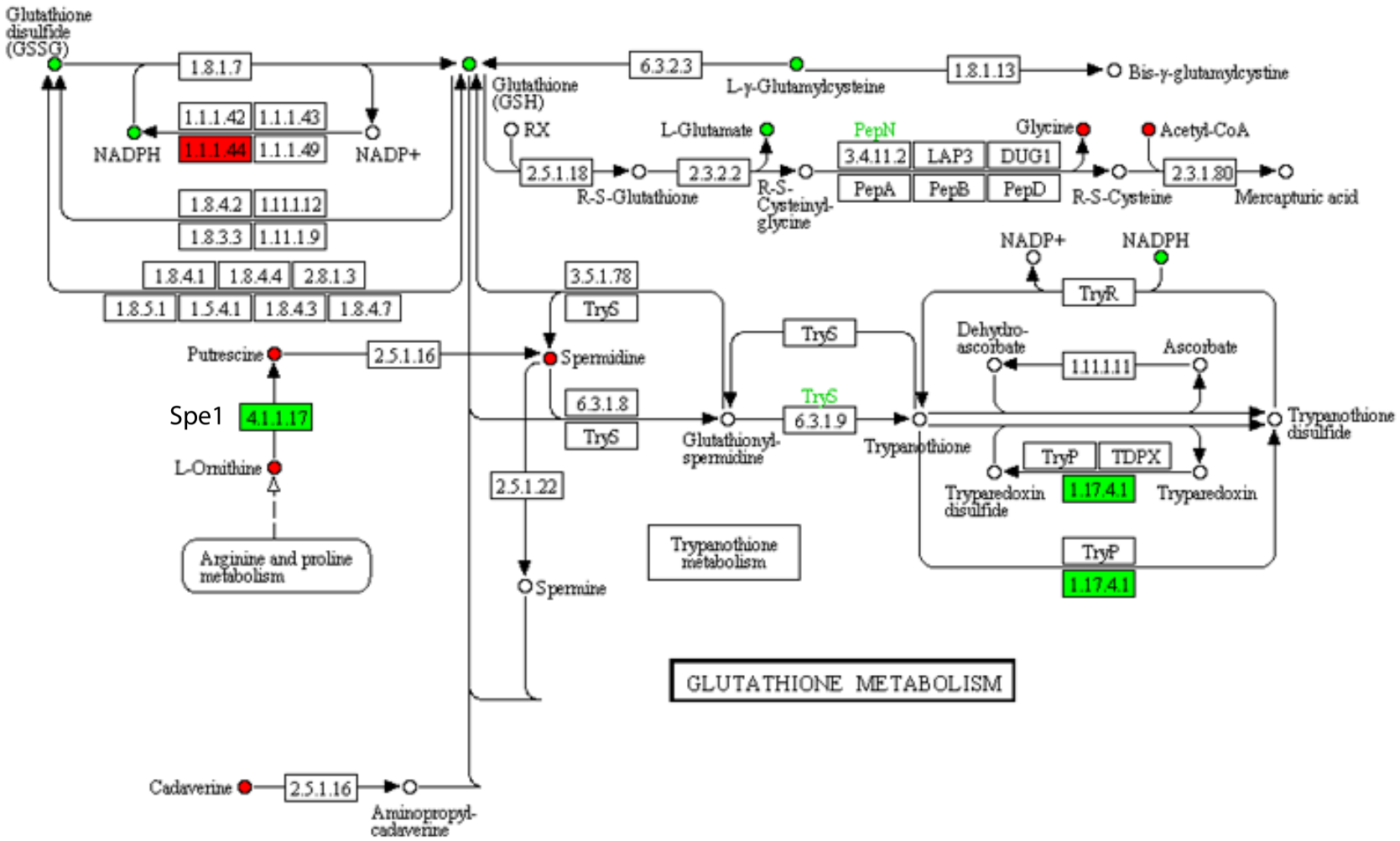

Figure 3.7. Polyamine metabolism in the cell. Ornithine and other amines are processed in to putrescine, spermidine spermine, and cadaverine. Lines represent processing enzymes, circles represent metabolites. Red, increased abundance. Green, decreased abundance.

would be important for individual cells invading a piece of fruit, for example, to rapidly determine whether the rush of osmotic pressure in their extracellular space was a cytotoxin or a life giving nutrient. Perhaps, however, a distinction is unimportant. The only role of Hog1 may be to coordinate re-establishment of cellular turgor. To accomplish this goal Hog1 induces production of the trehalose synthase enzyme network, converting sugar to osmolyte. Perhaps polyamine synthesis, and subsequently autophagy, occurs when free sugar or energy from lipolysis is no longer available to meet the cells stress response needs. If the cell runs out of raw material, polyamine synthesis and autophagy could provide a relatively simple biomass generating solution. It remains to be determined whether osmostress induces autophagy by way of Hog1 and polyamines, however we propose that it may very well do just that.

Polyamine concentrations are closely related cell age[143,150,151]. As mentioned above, older cells contain a lower abundance of polyamines compared to their younger counterparts. As with all biological systems, some balance of states and costs must be associated with this correlative decline. Indeed, the capacity of polyamines to extend cell life suggests that it would be disadvantageous to deplete them, unless depletion carried with it significant advantages for that cell. Perhaps maintaining high levels of polyamines requires a large investment of nutrients or energy. Additionally, polyamines are cations that bind directly to DNA. Perhaps young cells are more capable of mitigating damage or defects caused by these interactions than older cells. Lastly, perhaps older cells lose polyamine concentrations with age only if they exist in a low stress environment – weighing the benefit of maintaining an adaptive safety net against the detrimental costs of high polyamine synthesis. Direct experiments to answer these questions remain to be completed, however data are available

from our studies to address how old and young cells may differ in their capacities to mount a stress adaptive response. Through analyzing these data we may gain a better understanding of how age, metabolism, and polyamines are linked.

Weak or Wise?: the Alternative Stress Adaptive Network of Aged Yeast

Age can be an organism's weakness and its strength. As we age we accumulate damage, disease, and disabilities; both within our bodies and cells. However, we also accumulate experience, expertise, and endurance to see us through future challenges. There are numerous methods for approximating the relative age of an organism. However, doing so for an intact, individual cell has proven to be far more difficult. This challenge has been overcome for the observation of individual yeast cells. As yeast divide, roughly once every two hours, they produce a chitinous scar on their cell wall. The sugar composition of this scar is unique with respect to the rest of the extracellular surface[152,153]. Wheat germ agglutinin (WGA) is a lectin synthesized by *T. vulgaris* for protection of the plants offspring from, among other parasites, yeast. Fortuitously, or perhaps ingeniously, WGA binds to high-abundance sugars of the yeast bud scar. Conjugates of WGA to fluorescent dyes have recently become commercially available, making it possible to rapidly quantify the number of bud scars on a yeasts surface[117]. This measurement can be used to correlatively determine the age of individual cells in a population. By applying fluorescently conjugated WGA to cells prior to our flow cytometric analyses, as outlined in the previous chapter, we were able to determine both the age and abundance of stress adaptive protein accumulation in

individual cells. Analysis of this data sheds light on the question of whether old cells may be weak or wise to environmental stressors.

As in Chapter II, we measured induction of an unbiased subset of 95 proteins from the microarray clusters 1-4 in **Figure 2.9**. Each protein was expressed from the native gene locus as a GFP fusion and measured by fluorescence cytometry. Cells were treated with 350 mM or 650 mM KCl, fixed, and stained with fluorescent WGA. As a control yeast stained with WGA, but lacking GFP, were observed first. These cells produced similar fluorescent intensity and population distribution profiles (**Figure 3.8)**. Roughly 60% of our screened stress proteins demonstrated age-dependent expression patterns (for contrast, see **Figure 3.9**, a homogenously expressed protein). In the following we group these expression patterns in to classes and present representative cytometry examples for each.

Many stress proteins exhibit higher basal expression in older cells (**Figure 3.10 – 3.13)**. In these four examples the proteins in question are Glk1, Gsy1, Gph1, and Dcs1. Glk1 is a glucokinase responsible for the first step in the irreversible maturation of glucose-6-phosphate, the substrate of trehalose and glycogen synthesis[154]. Gsy1 and Gph1 both mature glycogen[155,156]. Dcs1 inhibits the enzymes that degrade trehalose[157]. Presumably, the increased basal expression of these proteins in older cells may underlie a higher capacity for mediating stress.

Multiple instances were observed where the expression level of the young cell rose to meet that of the older cell after osmostress – with higher osmostress bringing more of the young cells in to line with that of the old (**Figure 3.14 – 3.17**). In these 4 examples the proteins in question are Hsp26, Tsl1, Hsp30, and Mbf1. Hsp26 chaperones unfolded proteins[158]. Hsp30 down-regulates Pma1, an essential proton pump with significant effects on

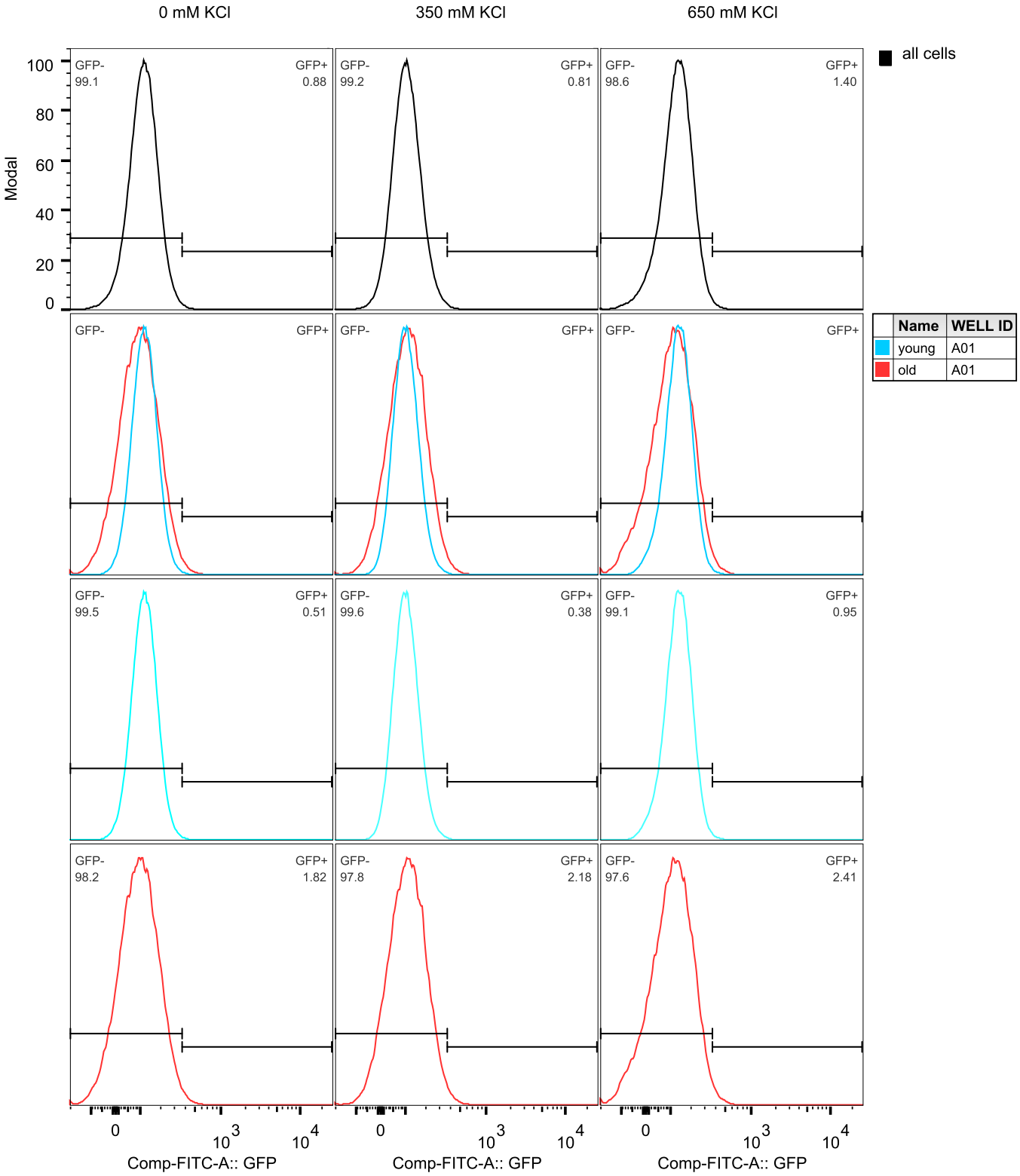

Figure 3.8. Age distribution analysis of yeast population. Y axis is a linear modal normalization of data. X axis is a biexponential scale of GFP fluorescence. Black, all cells. Cyan, young cells (low WGA signal). Red, old cells (high WGA signal). There is no GFP-tagged protein in this analysis.

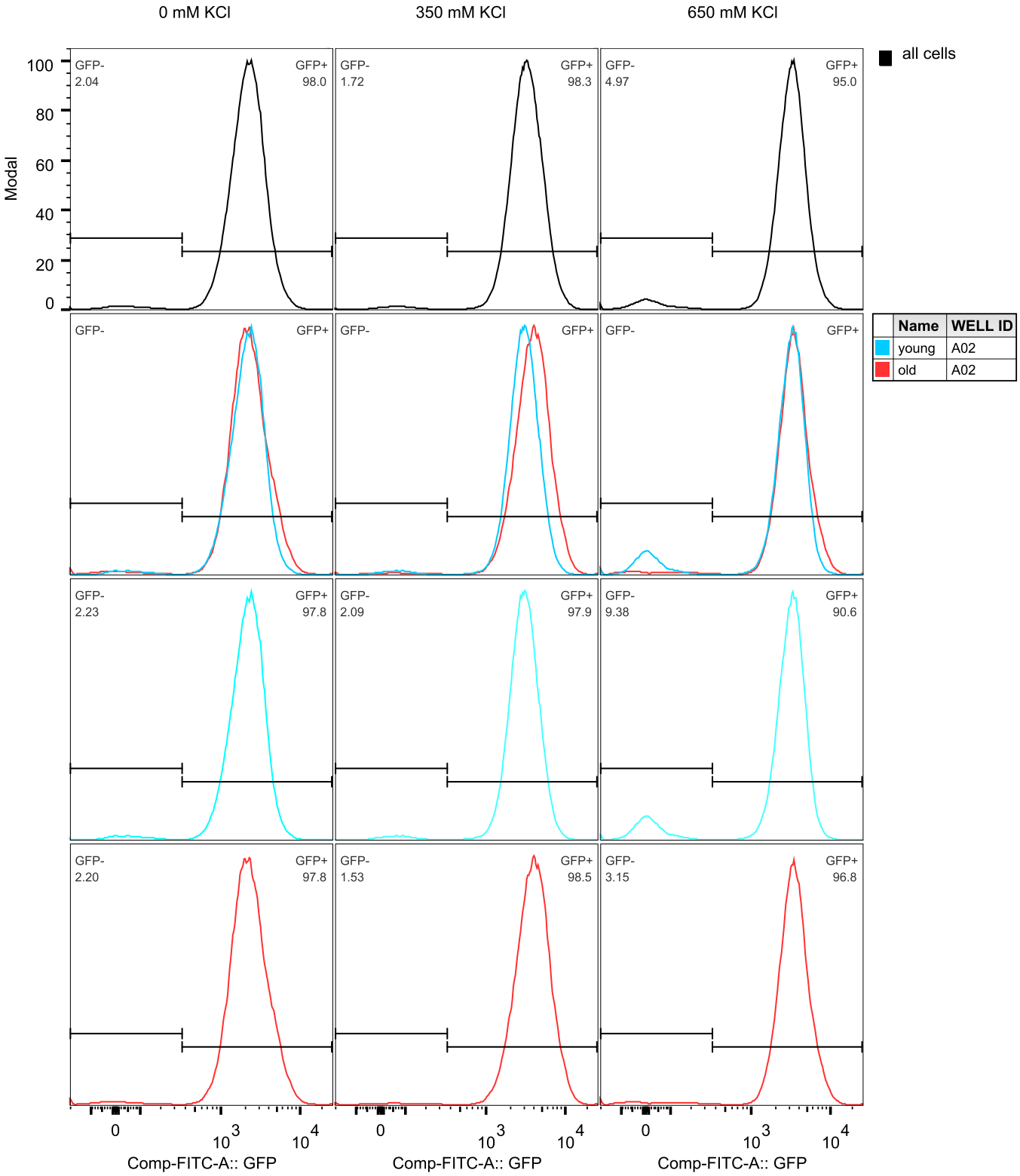

Figure 3.9. Age distribution analysis of yeast cell population. Y axis is a linear modal normalization of data. X axis is a biexponential scale of GFP fluorescence. Black, all cells. Cyan, young cells (low WGA signal). Red, old cells (high WGA signal). The GFP-tagged protein in this analysis is Hor7.

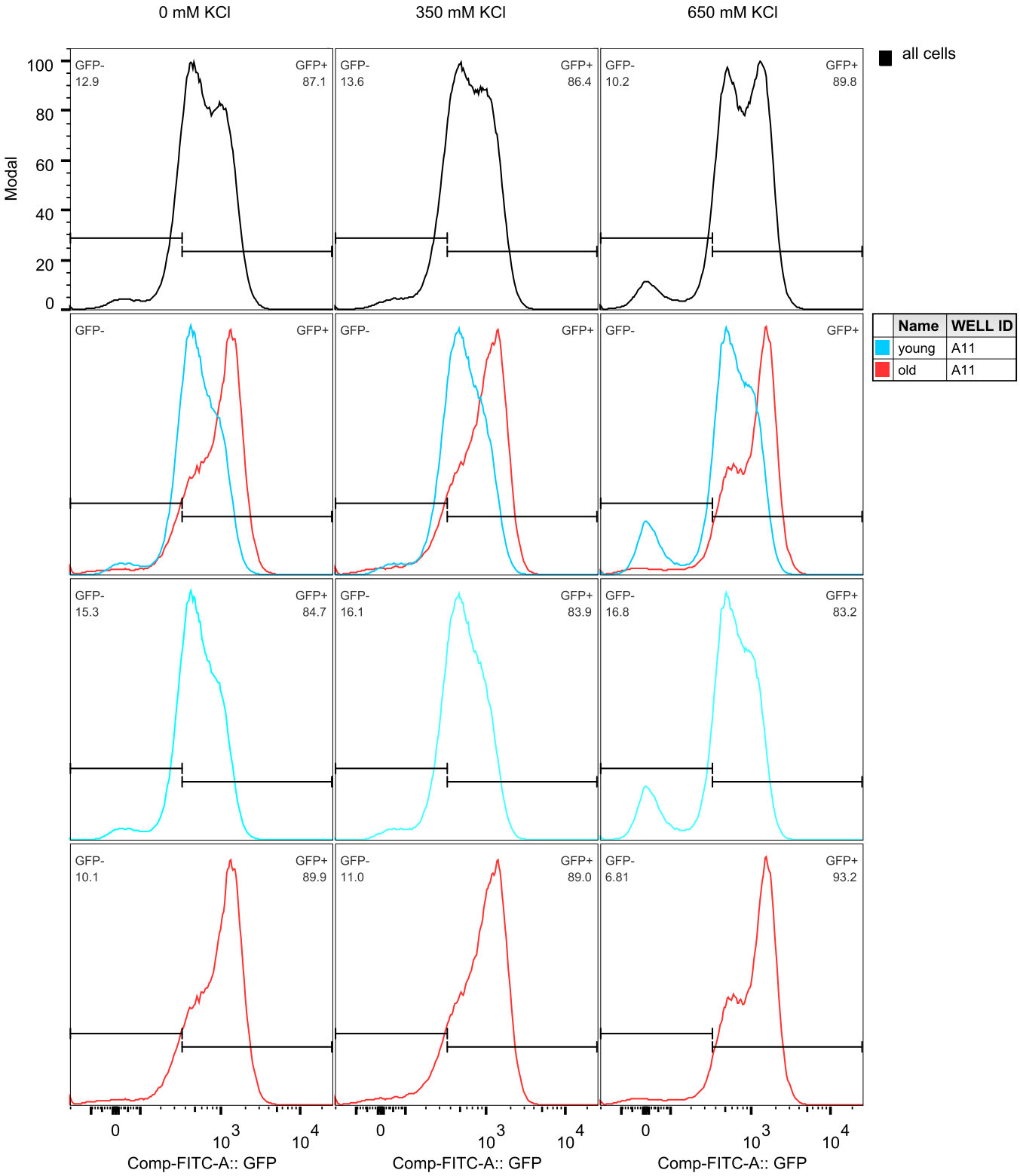

Figure 3.10. Age distribution analysis of yeast cell population. Y axis is a linear modal normalization of data. X axis is a biexponential scale of GFP fluorescence. Black, all cells. Cyan, young cells (low WGA signal). Red, old cells (high WGA signal). The GFP-tagged protein in this analysis is Glk1.

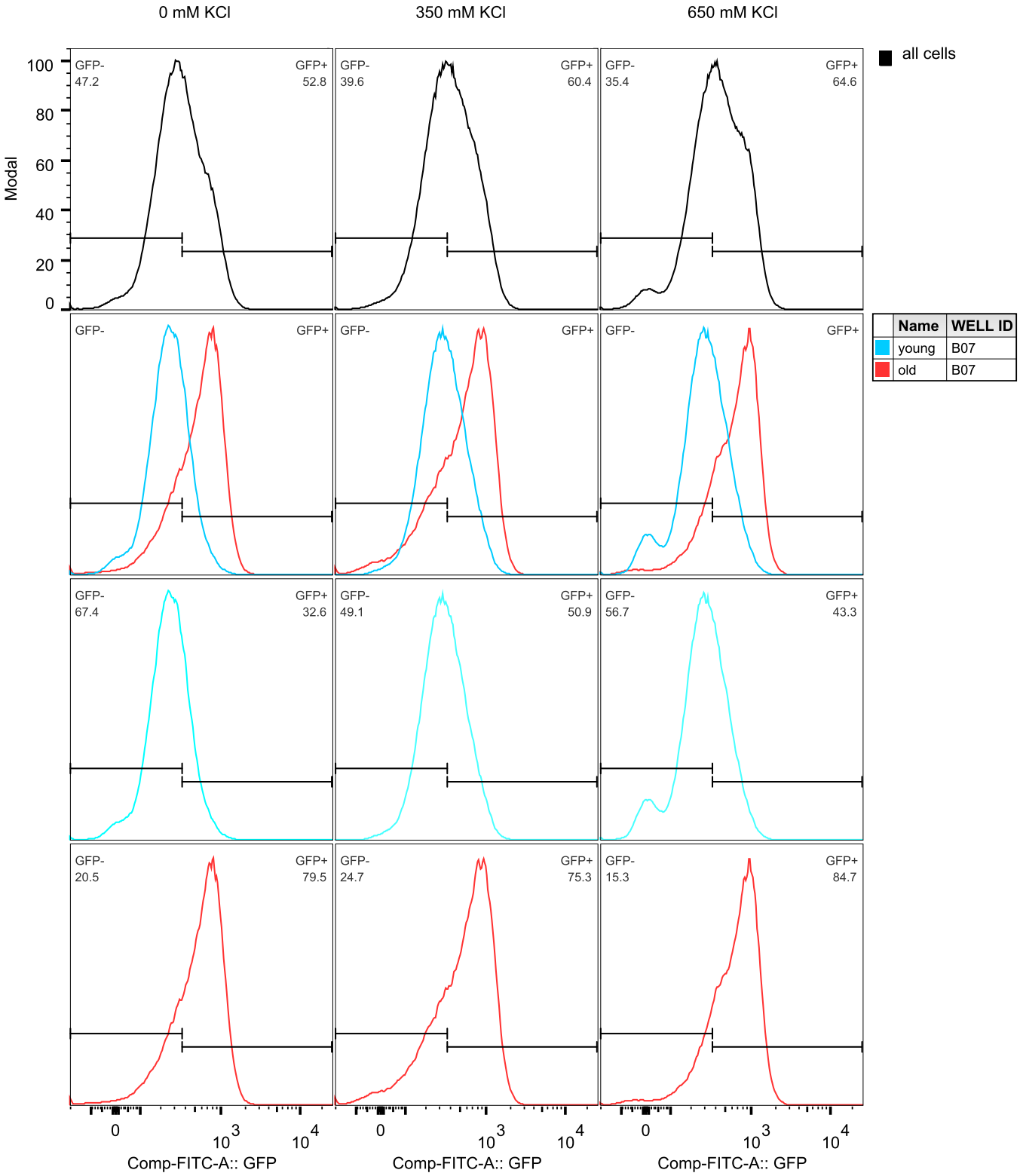

Figure 3.11. Age distribution analysis of yeast cell population. Y axis is a linear modal normalization of data. X axis is a biexponential scale of GFP fluorescence. Black, all cells. Cyan, young cells (low WGA signal). Red, old cells (high WGA signal). The GFP-tagged protein in this analysis is Gsy1.

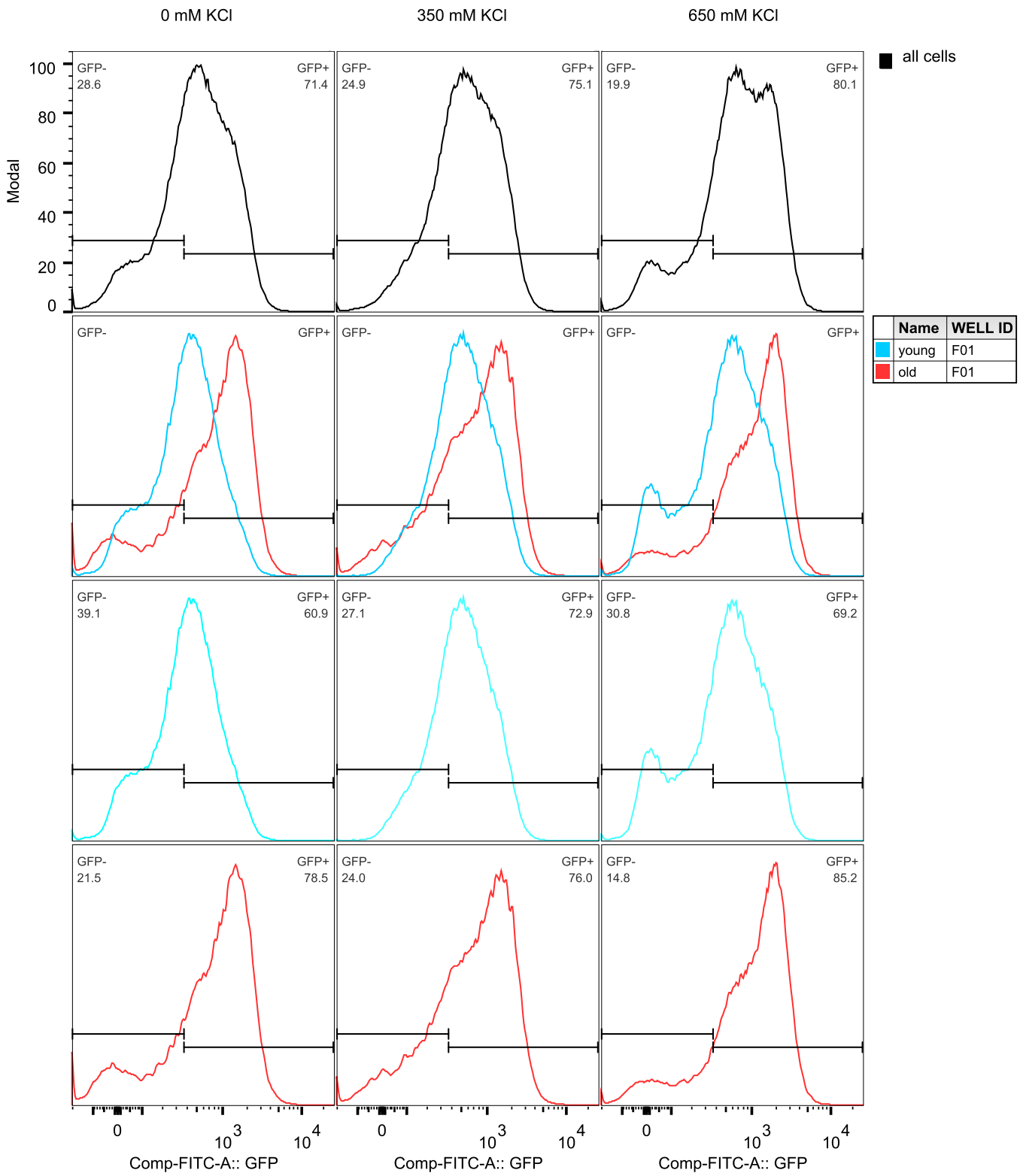

Figure 3.12. Age distribution analysis of yeast cell population. Y axis is a linear modal normalization of data. X axis is a biexponential scale of GFP fluorescence. Black, all cells. Cyan, young cells (low WGA signal). Red, old cells (high WGA signal). The GFP-tagged protein in this analysis is Gph1.

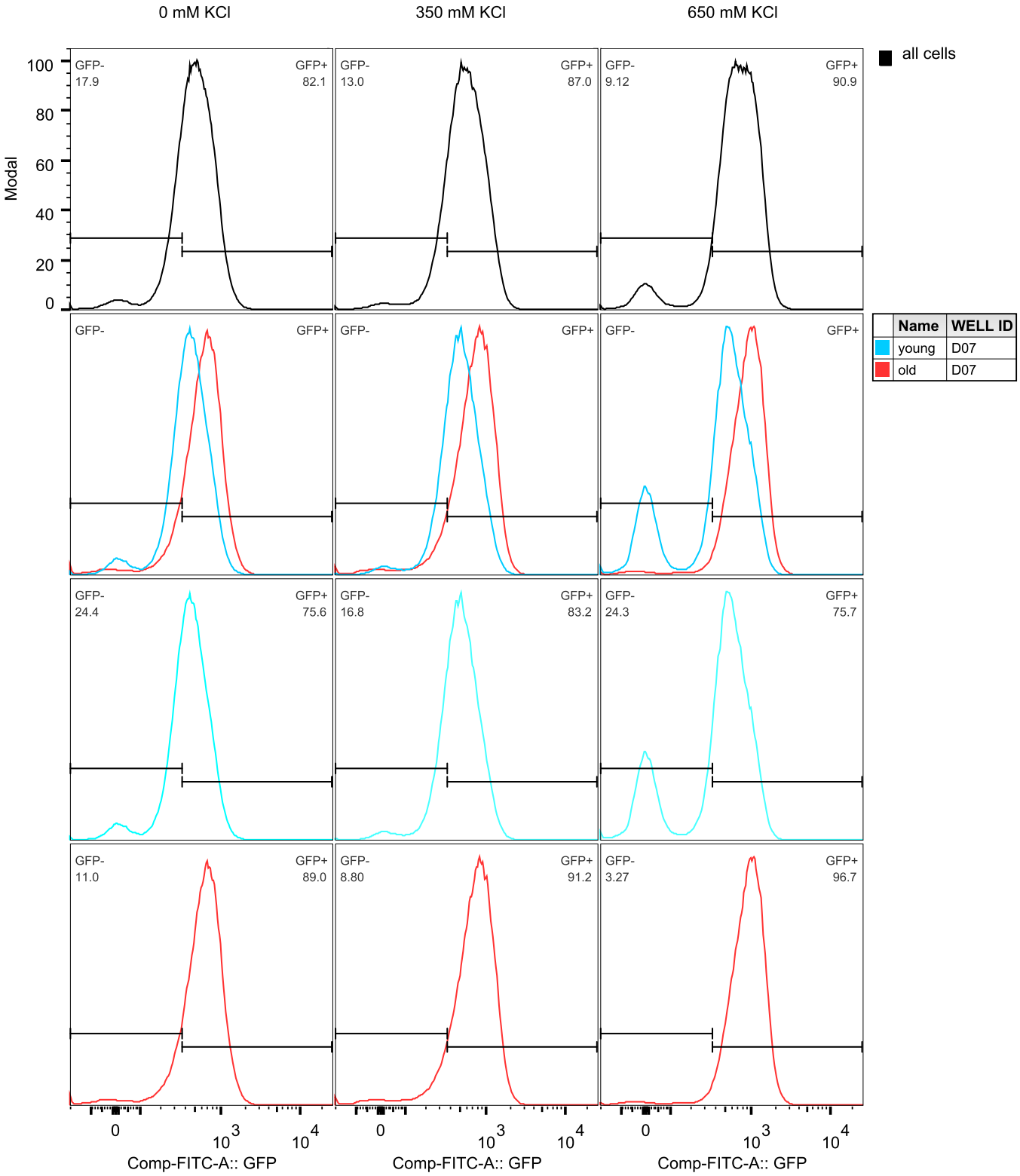

Figure 3.13. Age distribution analysis of yeast cell population. Y axis is a linear modal normalization of data. X axis is a biexponential scale of GFP fluorescence. Black, all cells. Cyan, young cells (low WGA signal). Red, old cells (high WGA signal). The GFP-tagged protein in this analysis is Dcs1.

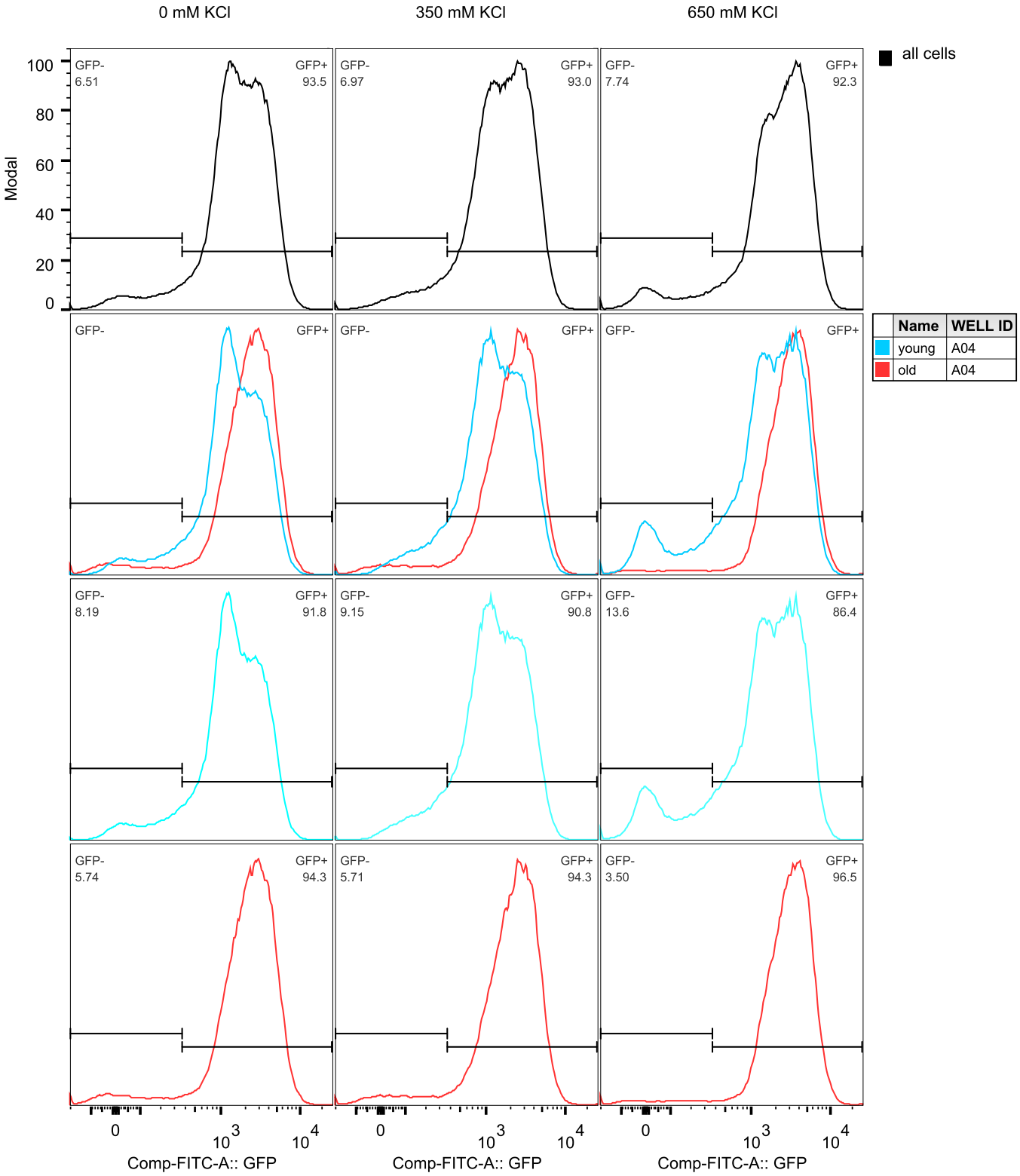

Figure 3.14. Age distribution analysis of yeast cell population. Y axis is a linear modal normalization of data. X axis is a biexponential scale of GFP fluorescence. Black, all cells. Cyan, young cells (low WGA signal). Red, old cells (high WGA signal). The GFP-tagged protein in this analysis is Hsp26.

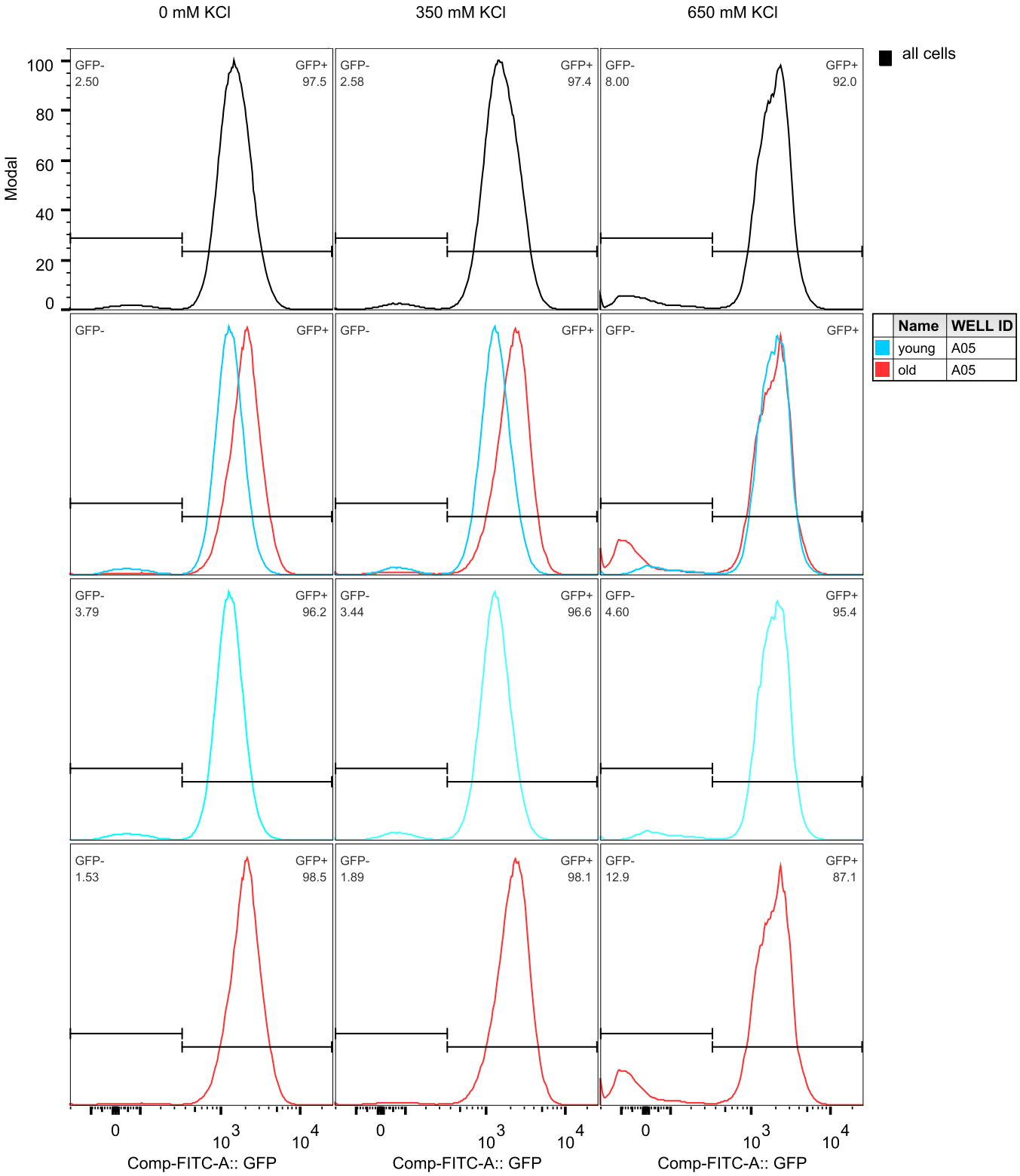

Figure 3.15. Age distribution analysis of yeast cell population. Y axis is a linear modal normalization of data. X axis is a biexponential scale of GFP fluorescence. Black, all cells. Cyan, young cells (low WGA signal). Red, old cells (high WGA signal). The GFP-tagged protein in this analysis is Tsl1.

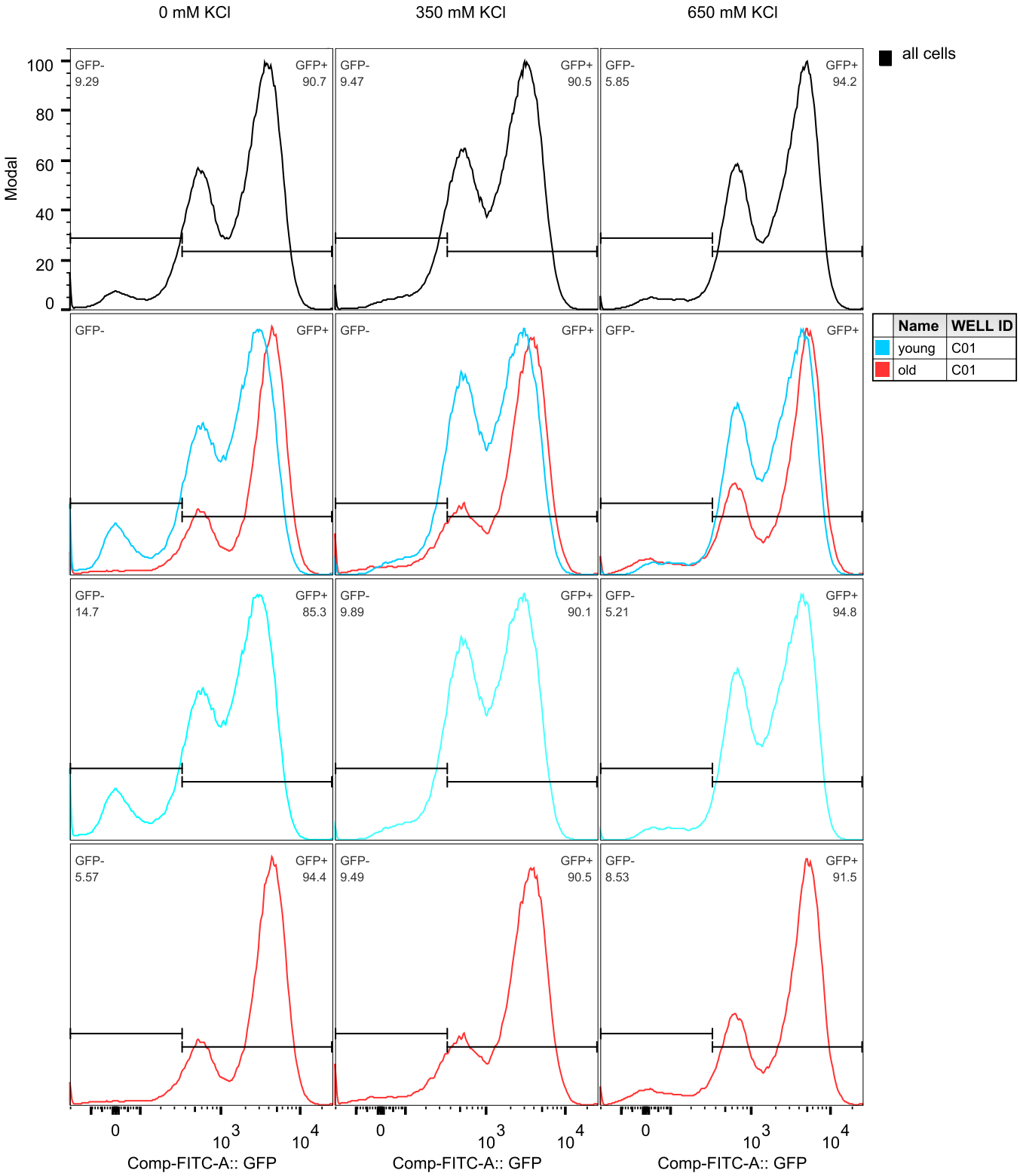

Figure 3.16. Age distribution analysis of yeast cell population. Y axis is a linear modal normalization of data. X axis is a biexponential scale of GFP fluorescence. Black, all cells. Cyan, young cells (low WGA signal). Red, old cells (high WGA signal). The GFP-tagged protein in this analysis is Hsp30.

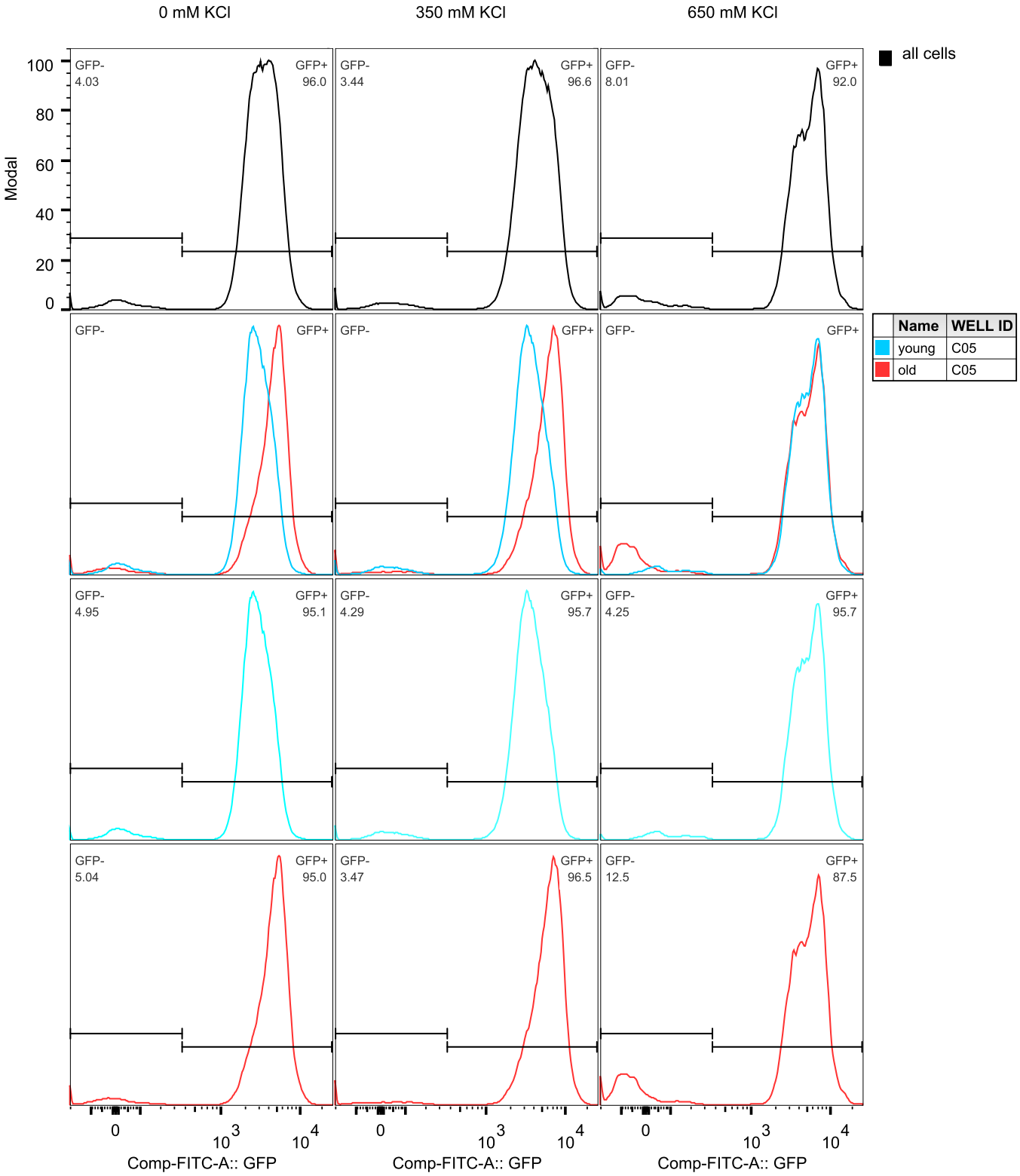

Figure 3.17. Age distribution analysis of yeast cell population. Y axis is a linear modal normalization of data. X axis is a biexponential scale of GFP fluorescence. Black, all cells. Cyan, young cells (low WGA signal). Red, old cells (high WGA signal). The GFP-tagged protein in this analysis is Mbf1.

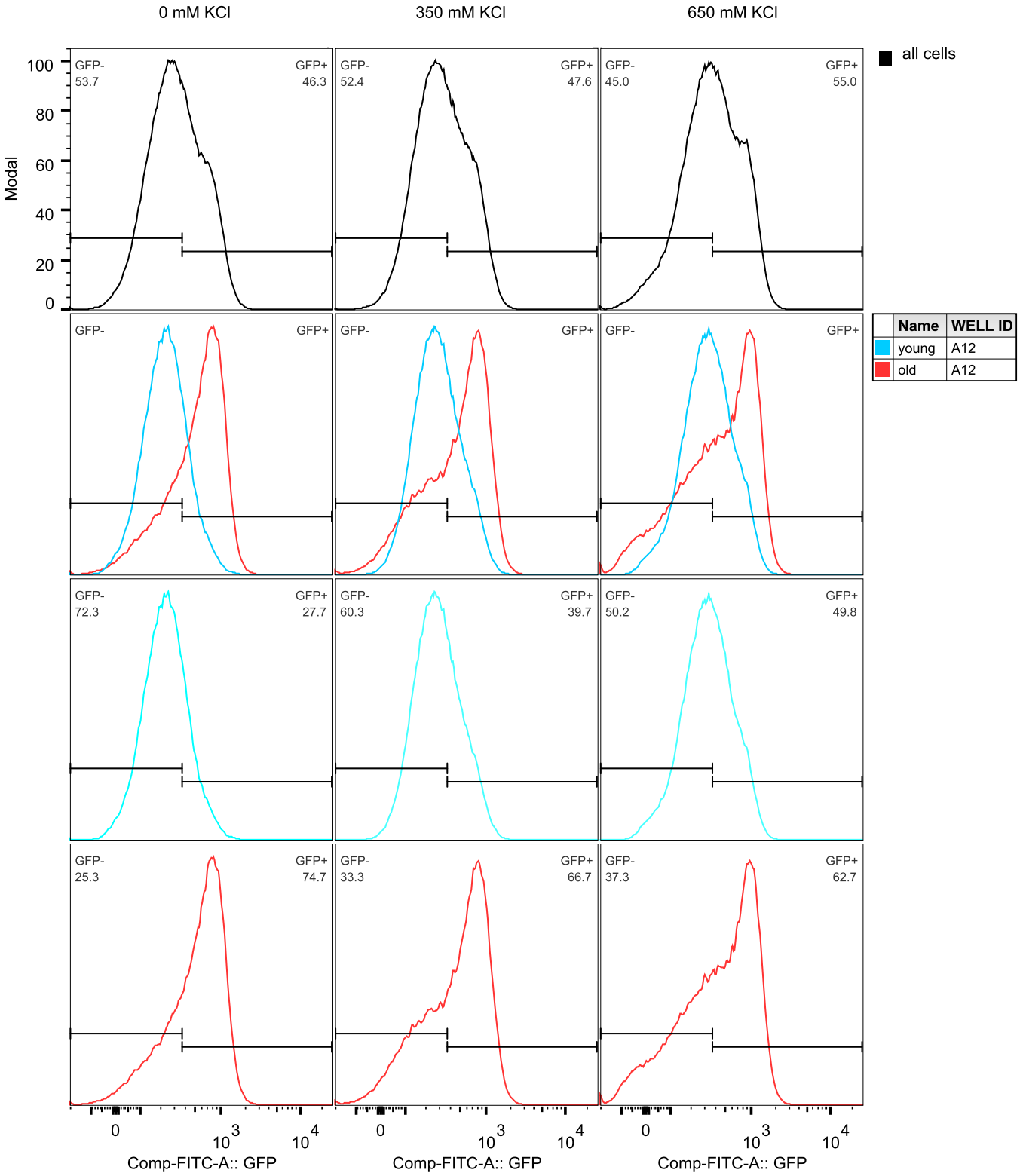

Figure 3.18. Age distribution analysis of yeast cell population. Y axis is a linear modal normalization of data. X axis is a biexponential scale of GFP fluorescence. Black, all cells. Cyan, young cells (low WGA signal). Red, old cells (high WGA signal). The GFP-tagged protein in this analysis is Glc3.

Hog1 signaling[159,160]. Tsl1 is an essential enzyme in the production of trehalose[161,162]. Mbf1 is a transcriptional coactivator that specifically mediates DNA damage[163,164]. Thus, in this expression pattern class, aged cells appear pre-prepared to mediate stress – expressing quantities of proteins at levels young cells must synthesize to achieve when stressed.

We also observed a single instance where osmostress caused older cells to take on the protein intensity distribution of the younger population (**Figure 3.18**). This protein is Glc3, a glycogen maturation enzyme. It may stand to reason that in this scenario, aged cells are producing more of the enzyme than is necessary under either of the stress conditions. In line with this observation, few young cells produce this molecule, even after high osmostress.

There were also multiple instances where both populations responded to osmostress, but the older population produced more of the gene product on average than the young population (**Figure 3.19 – 3.22**). In these examples the proteins in question are Fmp43, Rcn2, Sur1, and Gip2. These represent another set of glucose and glycogen synthesis enzymes, similar to those observed for the high basal expression populations. However, Rcn2 is a functional outlier, a regulator of calcineurin involved in the yeast mating response with unknown cellular function. Deletion of this gene makes yeast sensitive to treatment with salt.

The final categorical class are those where 350 mM osmostress produces a significantly different expression profile than either 0 or 650 mM. In these examples, a greater portion of old cells maintain a consistent expression profile at all doses, however both populations take on the same expression profile at high doses (**Figure 3.23 – 3.29**). In these examples the proteins in question are Arg1, Arg3, Arg4, Sed1, Bap2, Tmt1, and Aco2. Arg1, 3, 4, and Bap2 represent a core group of enzymes occupied with the synthesis of arginine, ornithine, and leucine; the precursor molecules to polyamine synthesis. Tmt1 and Aco2 are

both involved in the regulation of aconitate, a critical process for the progression of the Krebs cycle. Sed1 is a glycoprotein generated during extreme stress conditions.

Our observations suggest two possibilities for the stress-adaptive capacity of old cells. Aged cells may be weak or wise to the dangers of their environment. Both perspectives carry scientific and theoretical merit. Aged cells on average produce a greater number of stress-mediating enzymes. This behavior may underlie a chronic instance of stress for these cells, wherein the environment they share with young cells is perceived differently. Whereas the young cells demonstrate minimal adaptive output until a stress is observed, the aged cells are perpetually responding in a stressed manner. This chronic stress may slow the reproductive efficiency of older cells, reducing their evolutionary fitness relative to young cells. However, the inverse may also be true. Aged cells may be acting through experience. An aged cell has witnessed a greater diversity of environmental microenvironments and life stages than young cells. From this viewpoint, overexpression of stress adaptive proteins may represent the comfortable and safe equilibrium that the aged cell has established through trial and error. This theory is supported by the observation that young cells frequently rise to meet the expression levels of aged cells upon osmostress. The converse, old cells shifting expression to mirror that of young cells, was only observed to occur once, weakly, from 95 instances of protein expression measurements. In this way, aged cells may be better adapted to the variety of potential environments the cell may witness. While this work is insufficient to draw a definitive conclusion, the preponderance of evidence suggests old cells may act wisely, rather than weakly.

Through this analysis we have identified a number of unique, age dependent stress adaptive protein expression patterns. These patterns, while masked in a whole population

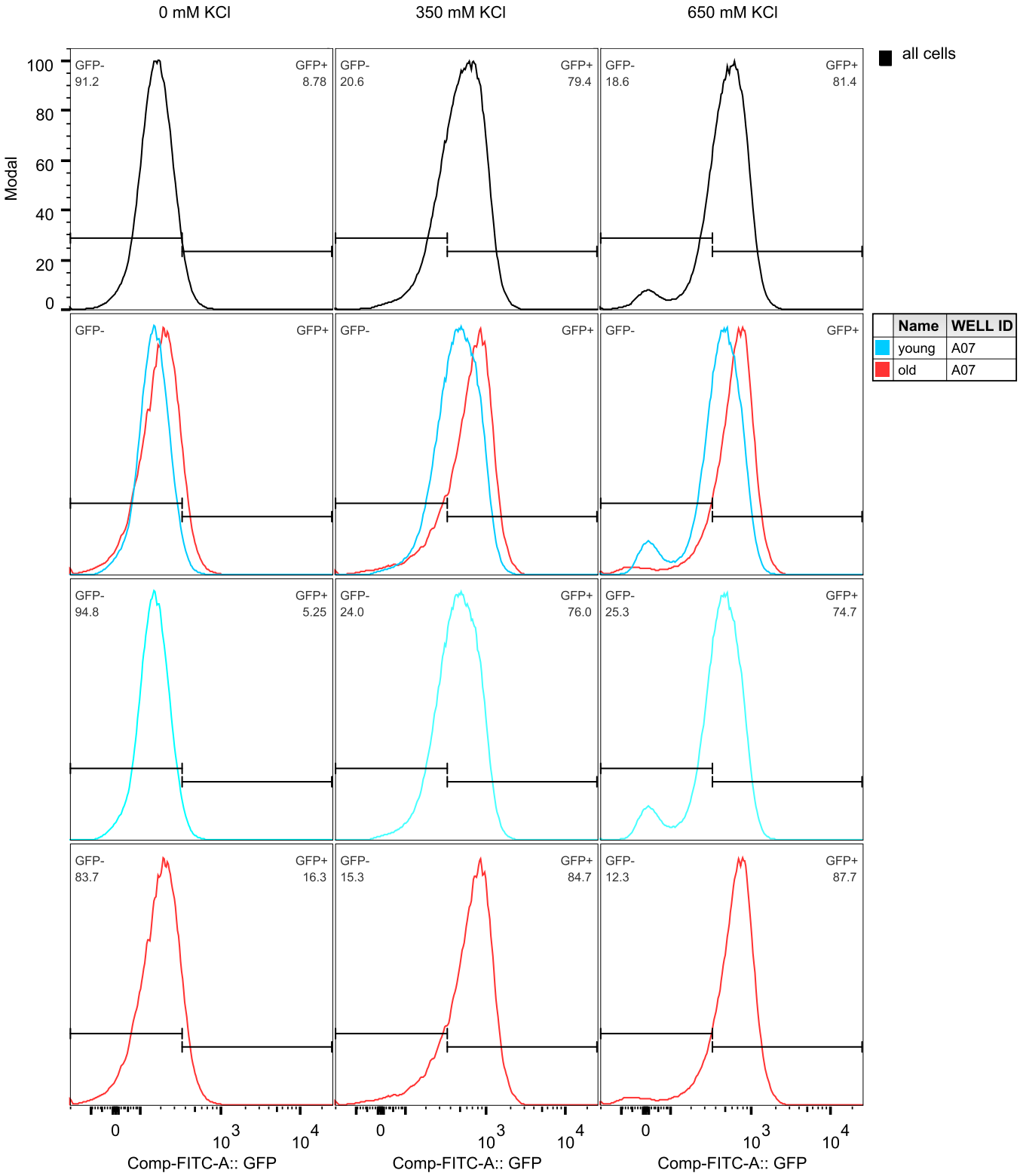

Figure 3.19. Age distribution analysis of yeast cell population. Y axis is a linear modal normalization of data. X axis is a biexponential scale of GFP fluorescence. Black, all cells. Cyan, young cells (low WGA signal). Red, old cells (high WGA signal). The GFP-tagged protein in this analysis is Fmp48.

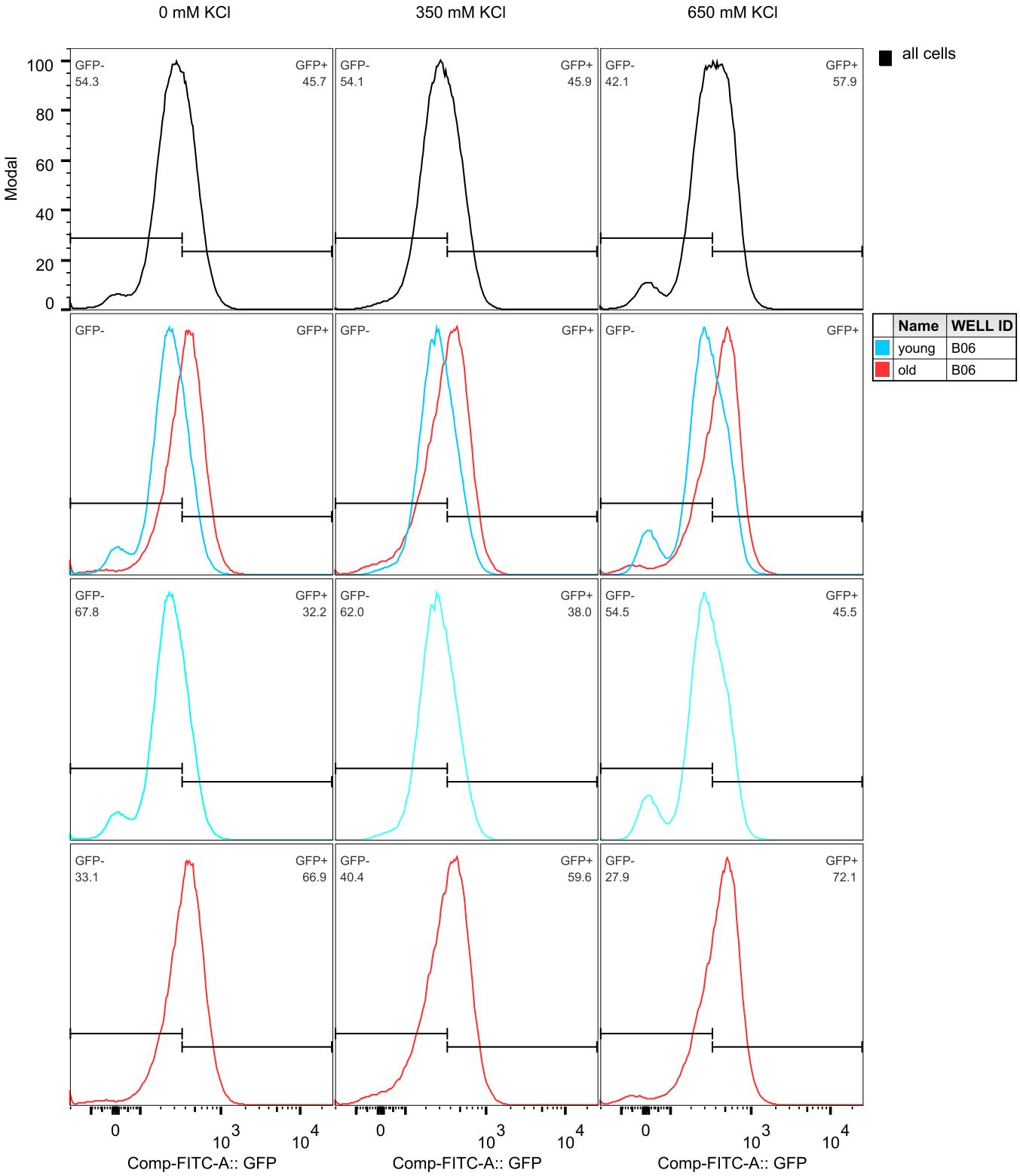

Figure 3.20. Age distribution analysis of yeast cell population. Y axis is a linear modal normalization of data. X axis is a biexponential scale of GFP fluorescence. Black, all cells. Cyan, young cells (low WGA signal). Red, old cells (high WGA signal). The GFP-tagged protein in this analysis is Rcn2.

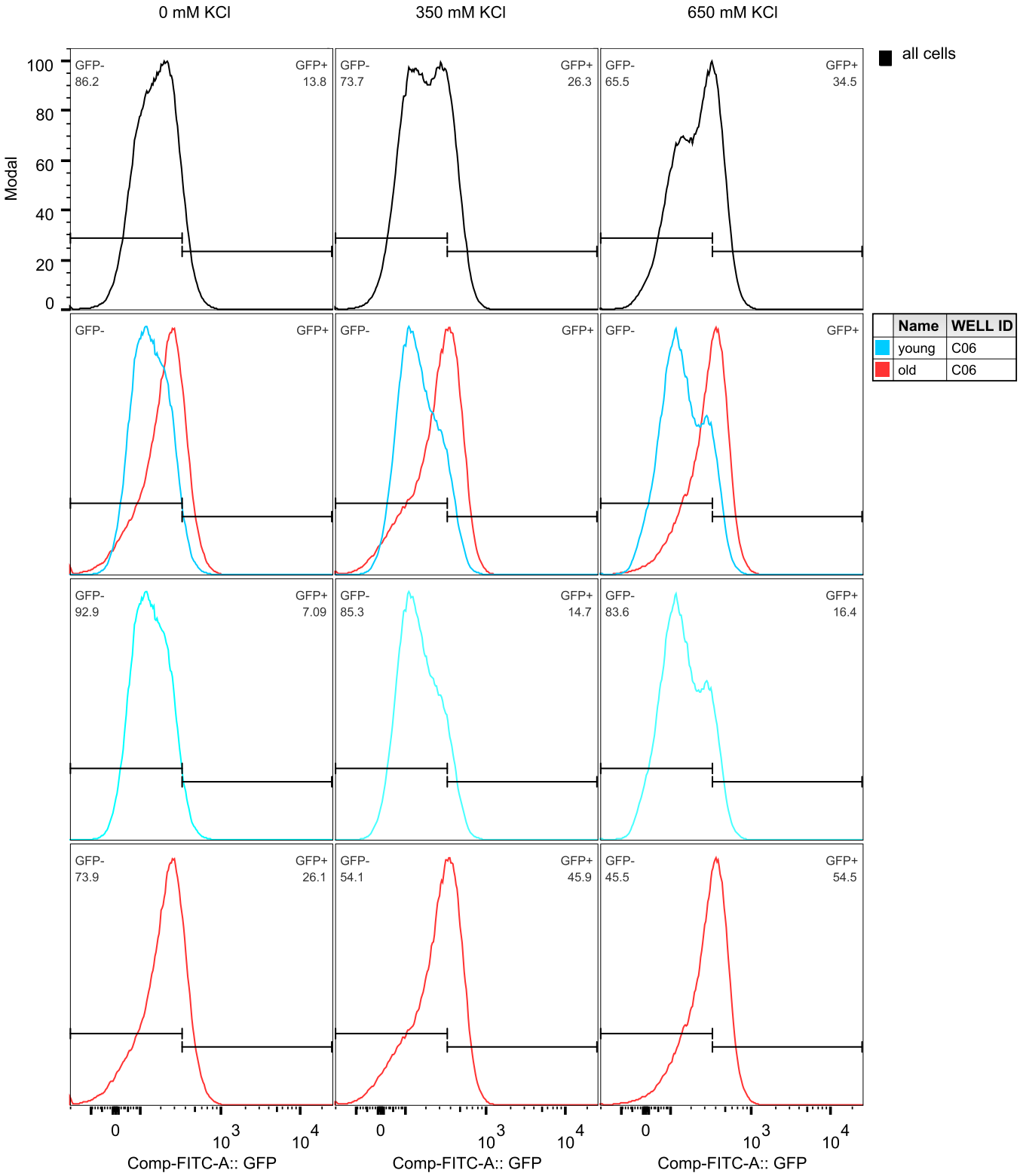

Figure 3.21. Age distribution analysis of yeast cell population. Y axis is a linear modal normalization of data. X axis is a biexponential scale of GFP fluorescence. Black, all cells. Cyan, young cells (low WGA signal). Red, old cells (high WGA signal). The GFP-tagged protein in this analysis is Sur1.

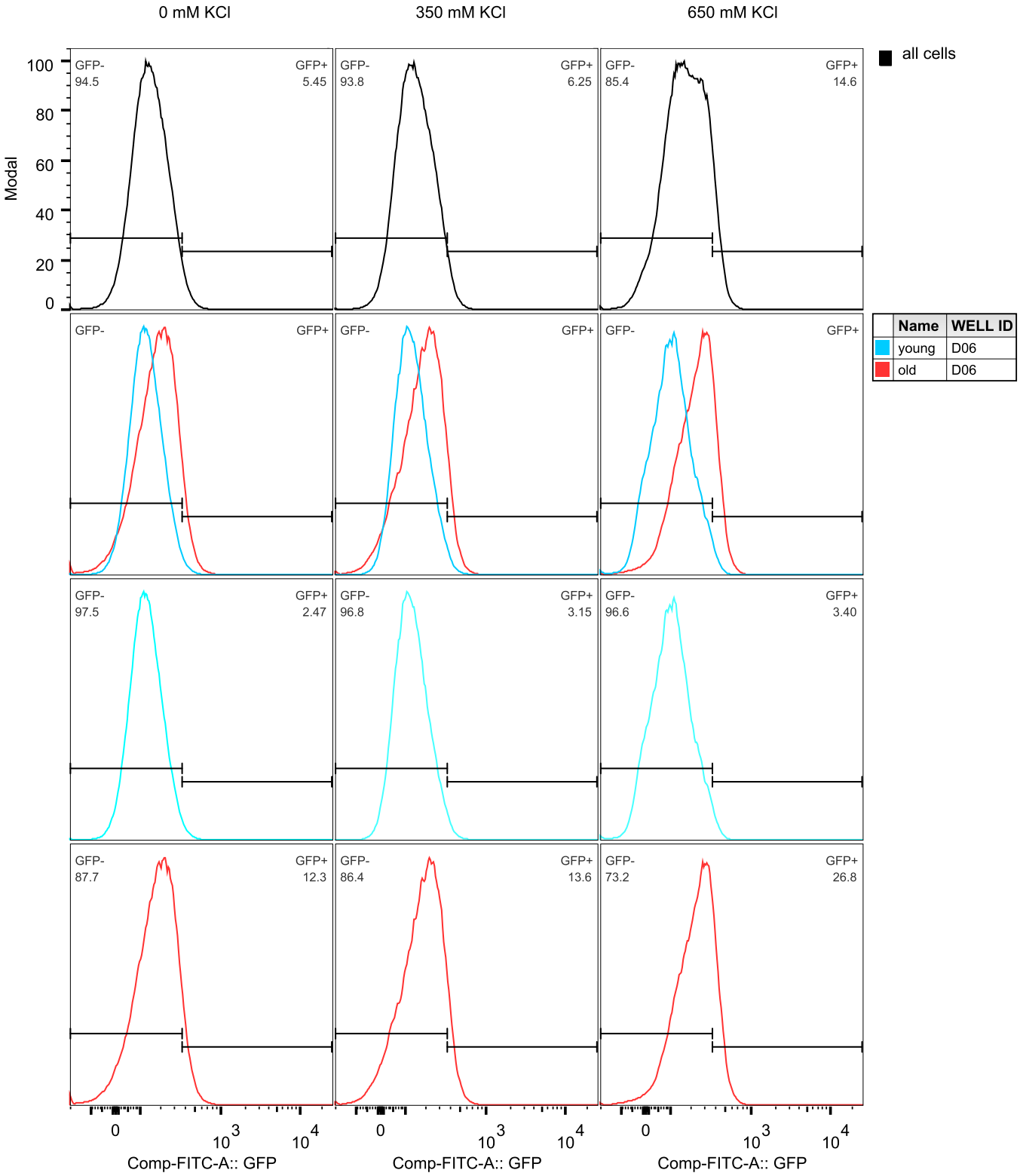

Figure 3.22. Age distribution analysis of yeast cell population. Y axis is a linear modal normalization of data. X axis is a biexponential scale of GFP fluorescence. Black, all cells. Cyan, young cells (low WGA signal). Red, old cells (high WGA signal). The GFP-tagged protein in this analysis is Gip2.

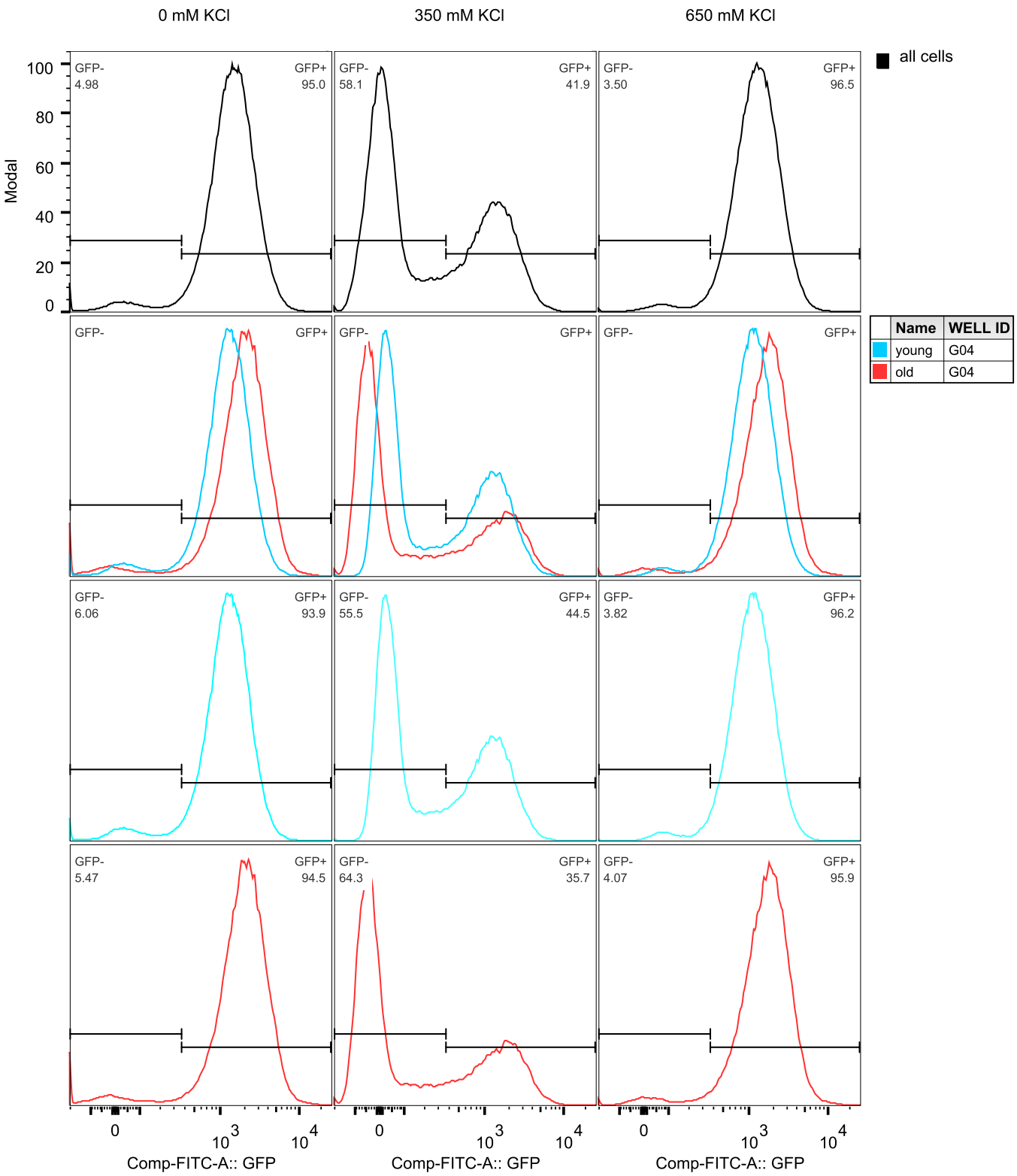

Figure 3.23. Age distribution analysis of yeast cell population. Y axis is a linear modal normalization of data. X axis is a biexponential scale of GFP fluorescence. Black, all cells. Cyan, young cells (low WGA signal). Red, old cells (high WGA signal). The GFP-tagged protein in this analysis is Arg1.

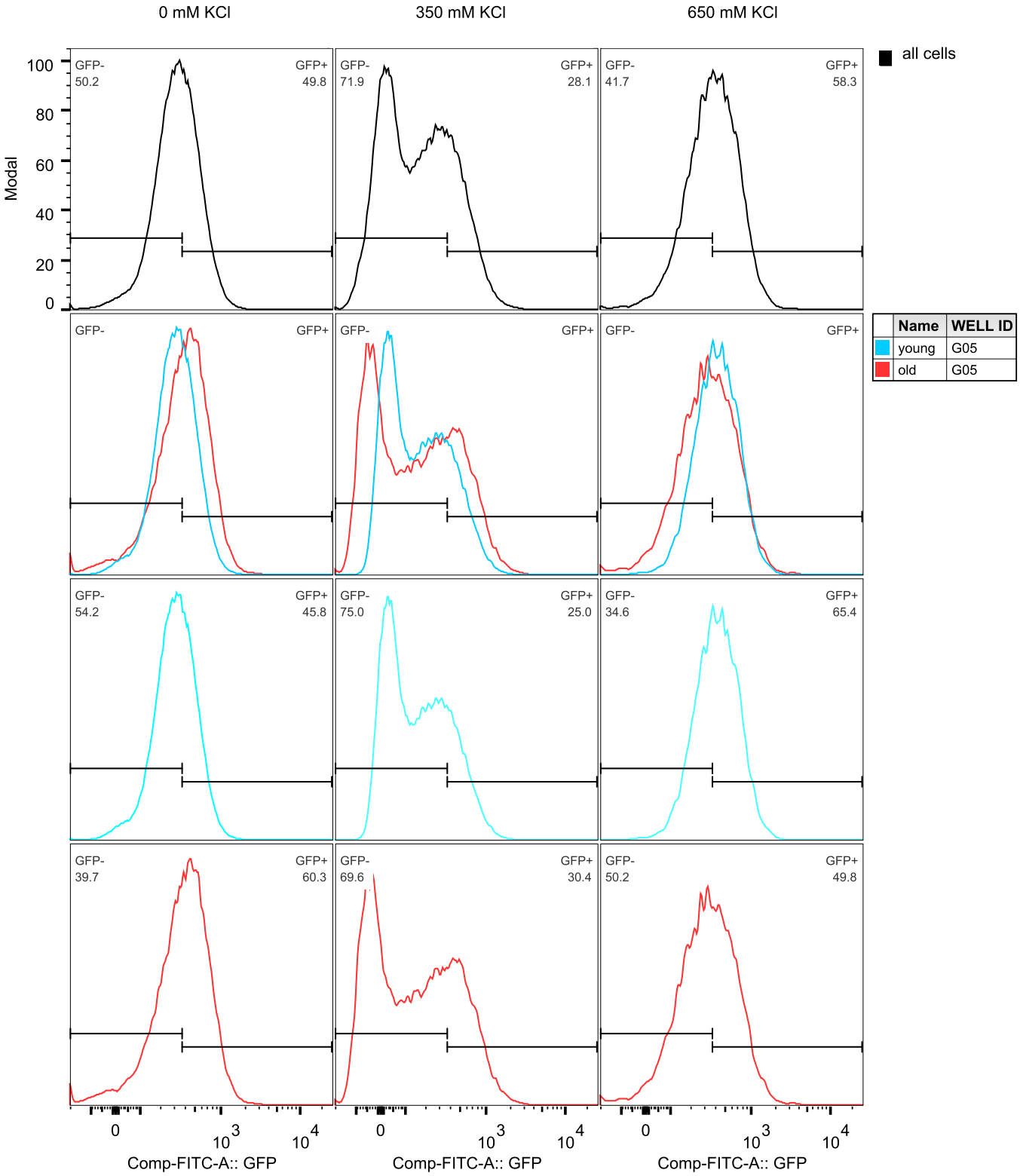

Figure 3.24. Age distribution analysis of yeast cell population. Y axis is a linear modal normalization of data. X axis is a biexponential scale of GFP fluorescence. Black, all cells. Cyan, young cells (low WGA signal). Red, old cells (high WGA signal). The GFP-tagged protein in this analysis is Arg3.

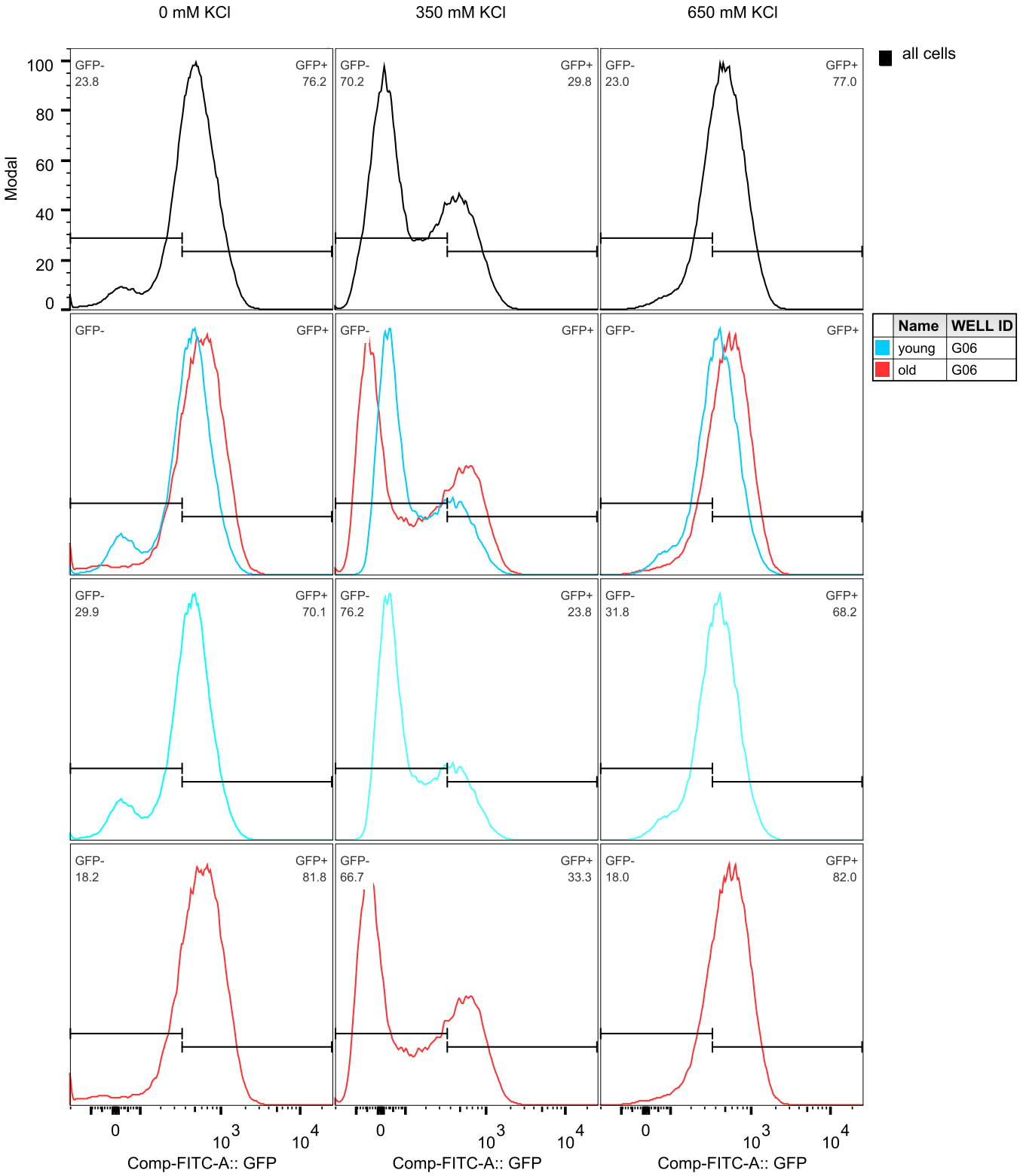

Figure 3.25. Age distribution analysis of yeast cell population. Y axis is a linear modal normalization of data. X axis is a biexponential scale of GFP fluorescence. Black, all cells. Cyan, young cells (low WGA signal). Red, old cells (high WGA signal). The GFP-tagged protein in this analysis is Arg4.

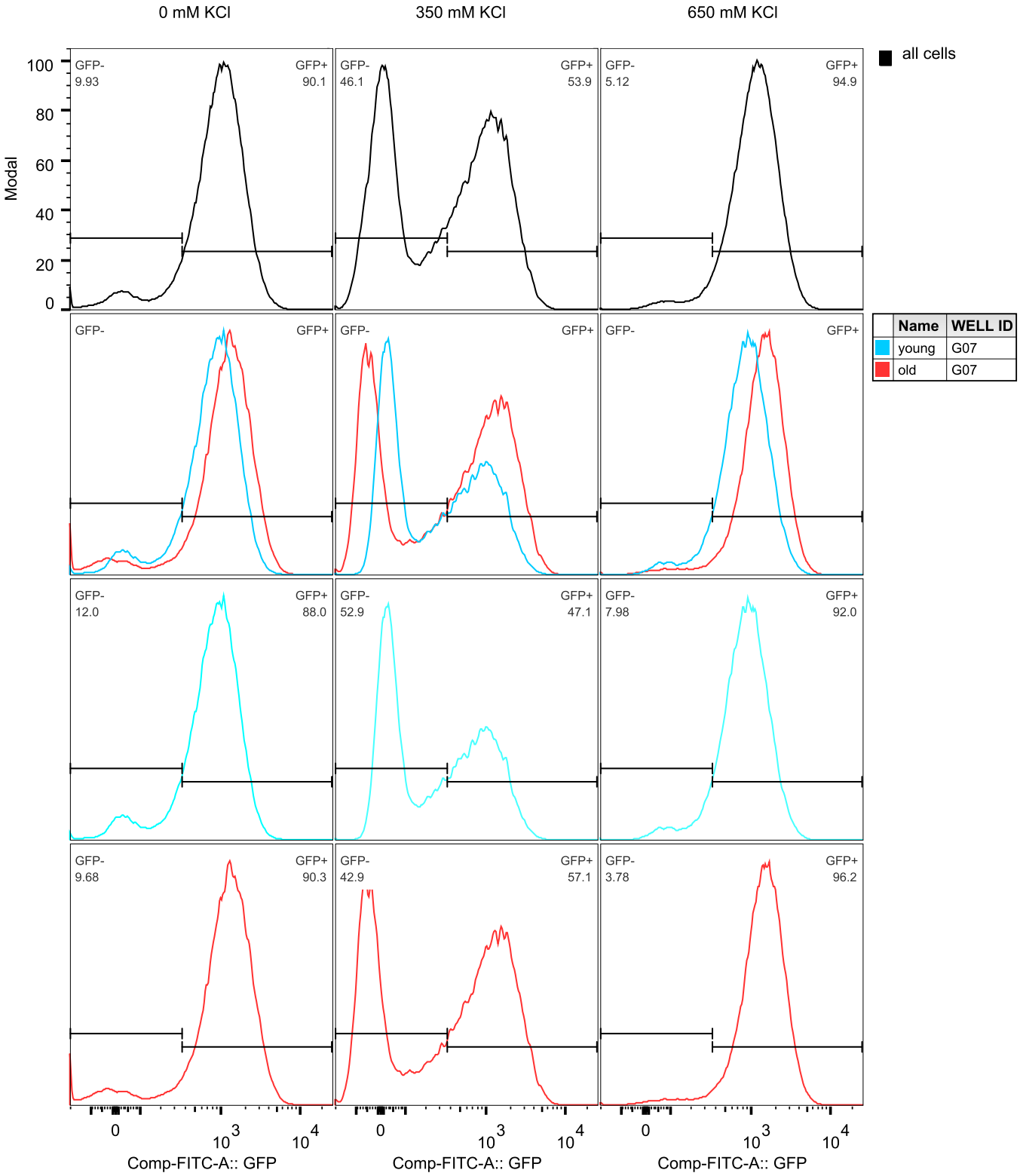

Figure 3.26. Age distribution analysis of yeast cell population. Y axis is a linear modal normalization of data. X axis is a biexponential scale of GFP fluorescence. Black, all cells. Cyan, young cells (low WGA signal). Red, old cells (high WGA signal). The GFP-tagged protein in this analysis is Sed1.

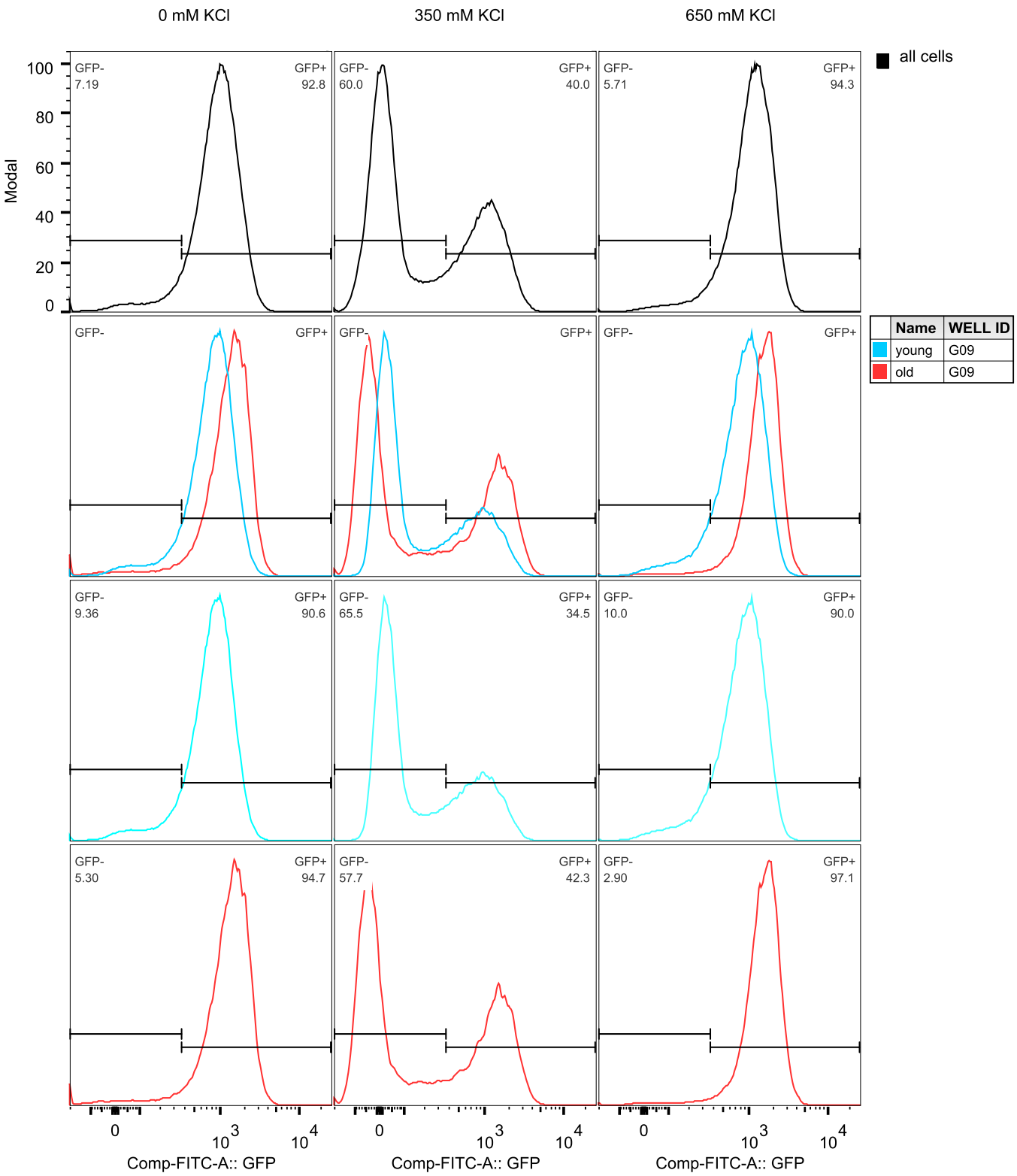

Figure 3.27. Age distribution analysis of yeast cell population. Y axis is a linear modal normalization of data. X axis is a biexponential scale of GFP fluorescence. Black, all cells. Cyan, young cells (low WGA signal). Red, old cells (high WGA signal). The GFP-tagged protein in this analysis is Bap2.

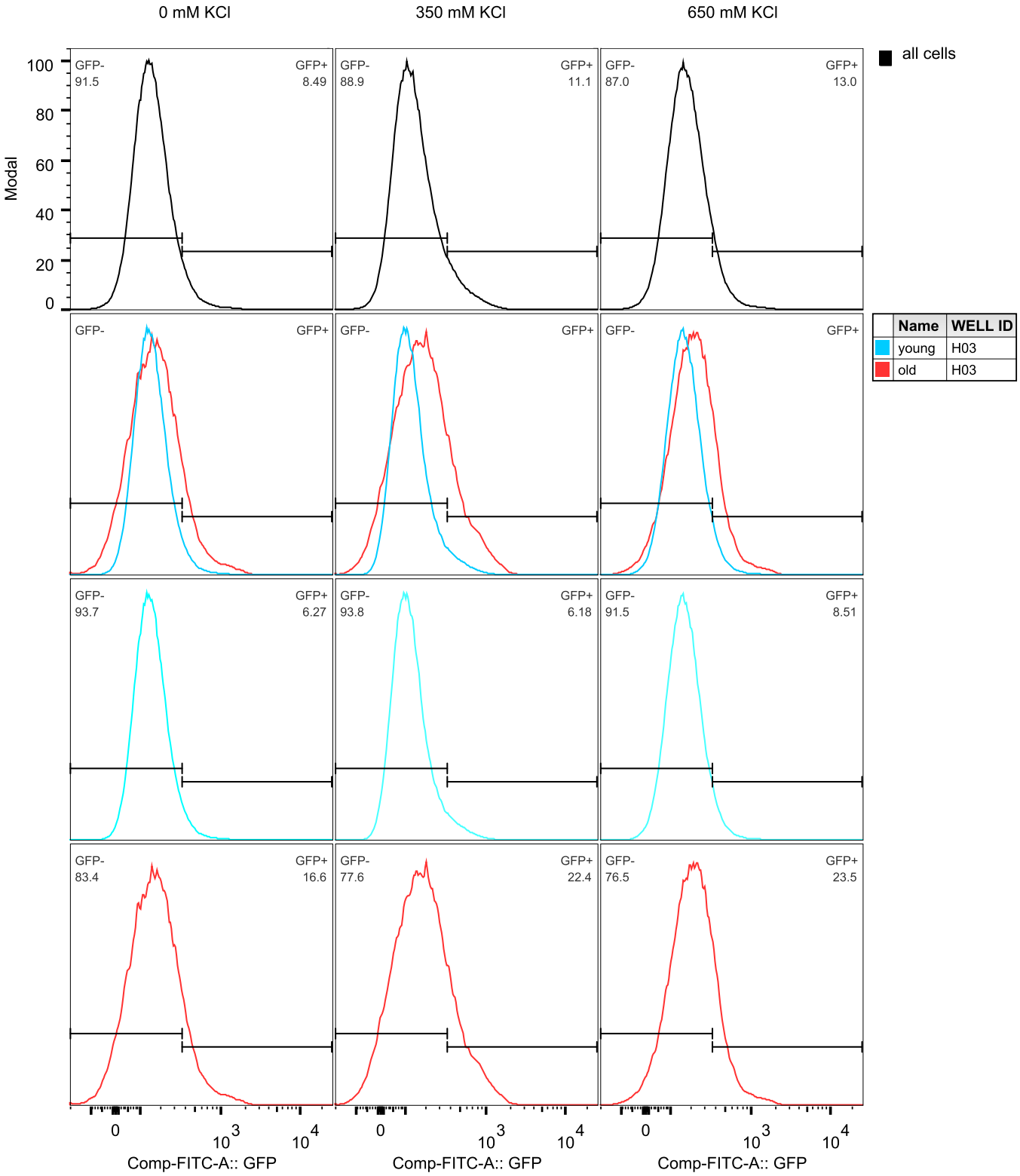

Figure 3.28. Age distribution analysis of yeast cell population. Y axis is a linear modal normalization of data. X axis is a biexponential scale of GFP fluorescence. Black, all cells. Cyan, young cells (low WGA signal). Red, old cells (high WGA signal). The GFP-tagged protein in this analysis is Tmt1.

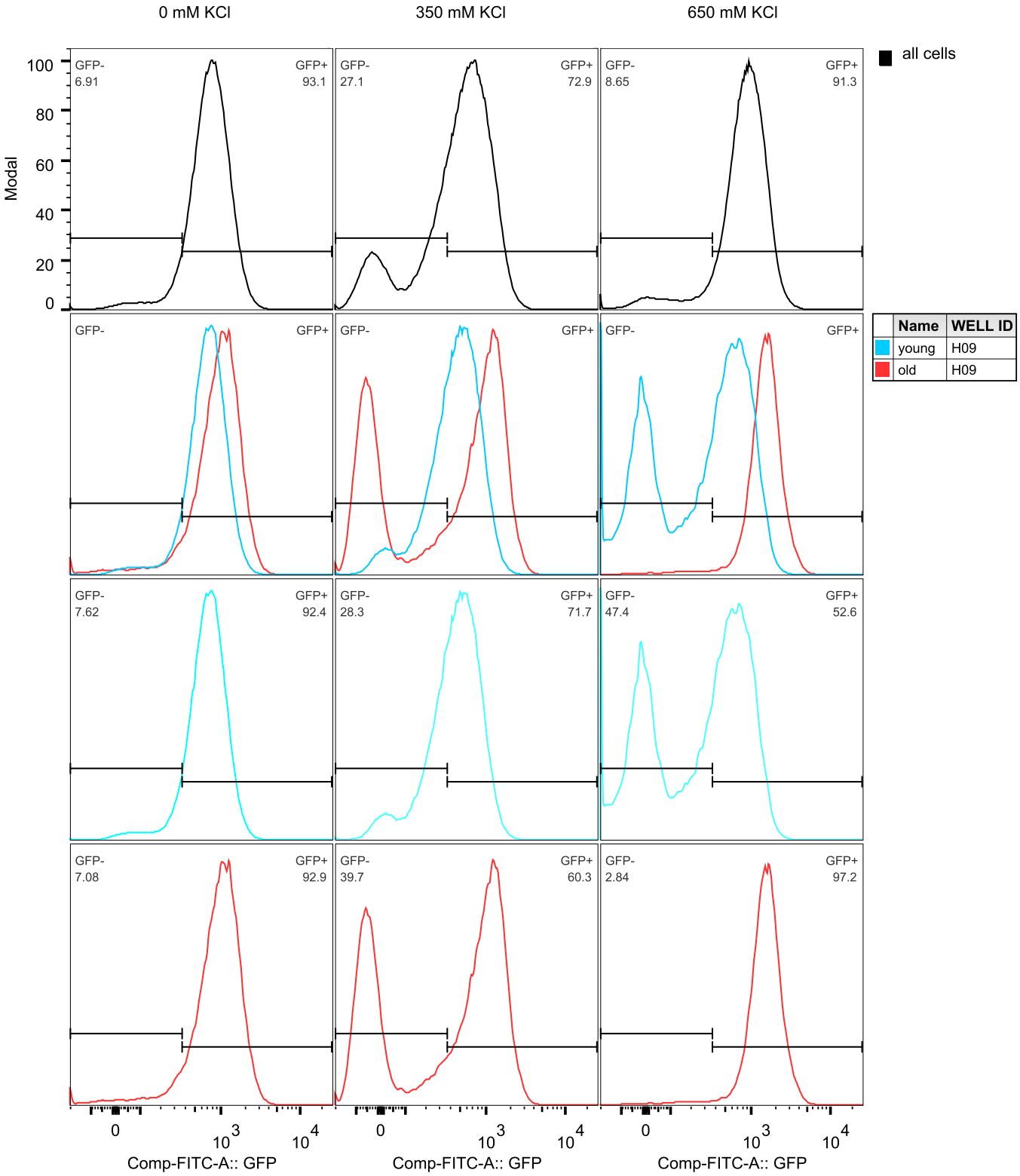

Figure 3.29. Age distribution analysis of yeast cell population. Y axis is a linear modal normalization of data. X axis is a biexponential scale of GFP fluorescence. Black, all cells. Cyan, young cells (low WGA signal). Red, old cells (high WGA signal). The GFP-tagged protein in this analysis is Aco2.

analysis, were easily discerned through addition of a single experimental variable. This analysis represents the tip of a cell population variability iceberg. We omitted from this analysis considerations such as cell cycle stage, volume, pH, and cytoplasmic glucose concentrations. All of these variables are measurable in the context of this experiment. It is likely that through a multi-dimensional approach a greater picture of the cells dynamic response program may be uncovered. For now, however, we must suffice with a conclusion that cell age results in a significant increase in the machinery necessary to respond to stress. Whether this difference represents weakness or wisdom, it is clear that no single expression pattern of the stress adaptive network exists for all cells.

Discussion

The analyses in this chapter represent panoramic snapshots of cell activity. Each describes a static point in a fluid response mechanism. By leveraging an integrated bioinformatic approach each picture comes together as a part of the whole, hinting at the intentions and actions of the cell after stress. This approach proved very informative. Through a combined analysis of metabolomic and proteomic data sets we have highlighted a previously unrecognized mechanism for synthesis of glycerol and energy from lipids during osmostress. This analysis also identified starch synthesis as the primary mechanism of yeast osmoadaptation. Additionally, it uncovered the previously unknown synthesis of polyamines as a potentially critical mechanism in osmostress recovery. Lastly, we demonstrate that the age of a cell dictates stress preparedness for the individual – a feature that may explain the stochastic variability observed in protein expression from the previous chapter.

The picture painted in this chapter highlights the value of combining functionally relevant -omics analyses. However, to understand the entire adaptive program we must push further. A coupled time and dose dependent analysis using multiple experimental platforms will be essential to transition from predictions to determinations. The tools, platforms, and analysis techniques are available. It requires only that we obtain the data and look carefully for the answers.

Experimental Procedures

Metabolomics Screen and Bioinformatic Mapping

Cells were cultured and stressed, or not, as outlined in Chapter II using 500 mM KCl for 10 minutes with James P. Shellhammer. Samples were then centrifuged at 3000 *x g* for 3 min, decanted, and snap frozen in liquid nitrogen. This experiment was repeated in triplicate. All frozen pellets were then delivered to Metabolon, Inc. for lysis and mass spectrometric analysis via LC-MS/MS (+ESI), LC-MS/MS (-ESI), and GC-MS. Individual flight counts for each metabolite were normalized to Bradford protein assay quantifications performed on each sample to account for cell number variability. These values were then normalized to metabolite standards run in parallel to our experimental set. An ANOVA statistical analysis was then applied to identify significant fold change between treated and untreated cell populations.

Statistically significant hits were isolated and applied to metabolomics pathway maps using the KEGG2 "Search&Color" pathway mapper[165,166]. Red nodes indicate a significant increase in fold induction, green nodes indicate a significant decrease in fold induction. Significant fold change of metabolic enzymes was annotated to these maps[128], with raw data

and statistics obtained through direct communication with the authors Tobias Walther and Florian Froehlich. Red lines or identification boxes indicate a significant increase in fold induction, green lines or identification boxes indicate a significant decrease in fold induction. Individual maps were pruned and linked together to highlight points of interest and do not represent complete metabolic pathways.

Fluorescence-based Flow Cytometry and Data Analysis

Cell culture, stress treatment, staining, and analysis were performed as outlined in Chapter II. Data were gated and analyzed using FlowJo v.10 analytic software as outlined in Chapter II. An additional gate was applied to isolate cells for low (young), medium (middle), or high (old) WGA staining as indicated in **Figure 3.30**. The medium population was excluded from further analysis for simplification, however we note that this population possessed significant heterogeneity in many of the age-related protein expression patterns. Unique behavioral classifications were first identified through statistical analysis of the median fluorescence intensity values between young and old cell populations, as outlined in Chapter II. Significant hits were then hand categorized through visual analysis and reported.

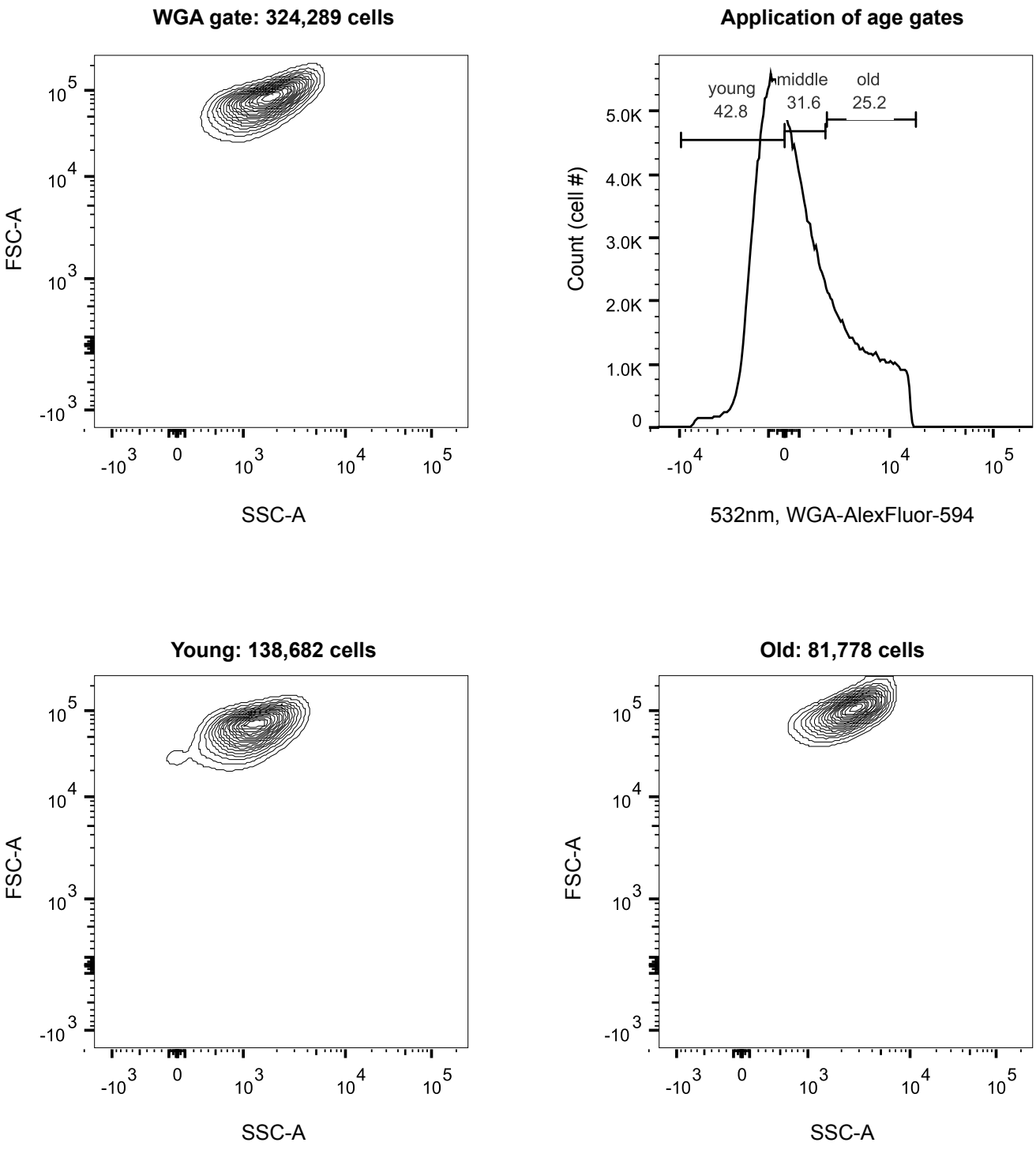

Figue 3.30. Gating parameters for flow cytometry data. Cells established from the gating in Figure 2.10 were further segegated by their relative age. This was determined by fluorscence intensity from wheat germ-agglutinin (WGA) conjugated to AlexFluor-594. Fluorescence minus one (FMO) experiments were performed to compensate for bleed-through on line. Data is compensated fluorescence values. FSC-A, forward scatter area; SSC-A, side scatter area.

CHAPTER IV

CONCLUSIONS AND FUTURE DIRECTIONS[1]

All cells adapt. The adaptive process underlies development and division as well as deterioration and disease. In deciding to adapt, a cell must determine whether to redefine its homeostatic balance or return to it. While many studies have focused on decoding the circuitry of the former, this thesis considers the later. Using a multifaceted approach we assessed the capacity of the cell to respond to environmental danger from the very beginning to the very end of this circuit. Chapter II defines how information is converted, amplified, and distributed to the cell to engage adaptation. Chapter III assessed how this transmitted information manifests in to the functional reorganization of the organism. In this chapter, I will consider how these observations can guide future investigations.

Functional Characterization of MAPK Signaling

In Chapter II the signaling profile of the Hog1 MAPK was elucidated through rigorous quantification and dissection of the signaling cascade over a range of inputs and times. This focused, comprehensive analysis resulted in the discovery of an unanticipated and consistent relationship between dose and signaling duration. Surprisingly, this signaling profile was orchestrated by a rarely observed switch-to-rheostat mechanism. To establish this

[1] All figures contributed by Justin G. English

mechanism the MAPK engages in signaling feedback, essential for the maintenance of a dose-to-duration relationship. Investigation of this mechanism uncovered a perplexing example of graded bit-state phosphorylation on the protein scaffold Ste50. The requirement of graded feedback on Ste50 for proper signal encodement is unlikely to be the only example in this pathway. Indeed, through uncoupling of Ste50 feedback we do not recapitulate the drastic disruption of the Hog1 signaling profile exhibited when Hog1 catalytic activity is impaired (**Figure 2.5**). Identification of other Hog1 feedback substrates, and their contributions to the Hog1 signaling profile will provide us with additional examples of how biological systems integrate and communicate environmental information. In this way, the studies of the simple signaling architecture paradigms in yeast can greatly inform how we approach studies of human health and disease.

In Chapter II we observed that the Sln1 and Sho1 branches function like a clutch and throttle. Hog1 is sluggish to activate without Sln1, but fails to amplify its signal without feedback toward, presumably, the Sho1 branch. It stood to reason then, that Pbs2 may be dynamically regulated over dose and time – disengaging the clutch for the throttle. In this analogy Ste11, observed as upregulated after osmostress in our mass spectral data analysis, may serve to goose the throttle. Under these circumstances Pbs2 would act as a gearbox. If this is true, is Pbs2 shifting? Through measurements of Pbs2 protein abundance and phosphorylation status it appears it may very well be (**Figure 4.1**). Both Pbs2 abundance and phosphorylation are highly dynamic with respect to both dose and time in these measurements. This data could represent the capacity of the Hog pathway to coordinate pathway activation power to establish dose-to-duration. Note that the low abundance of the Pbs2-TAP strain at time 0 is real and was isolated to the presence of the epitope tag. This

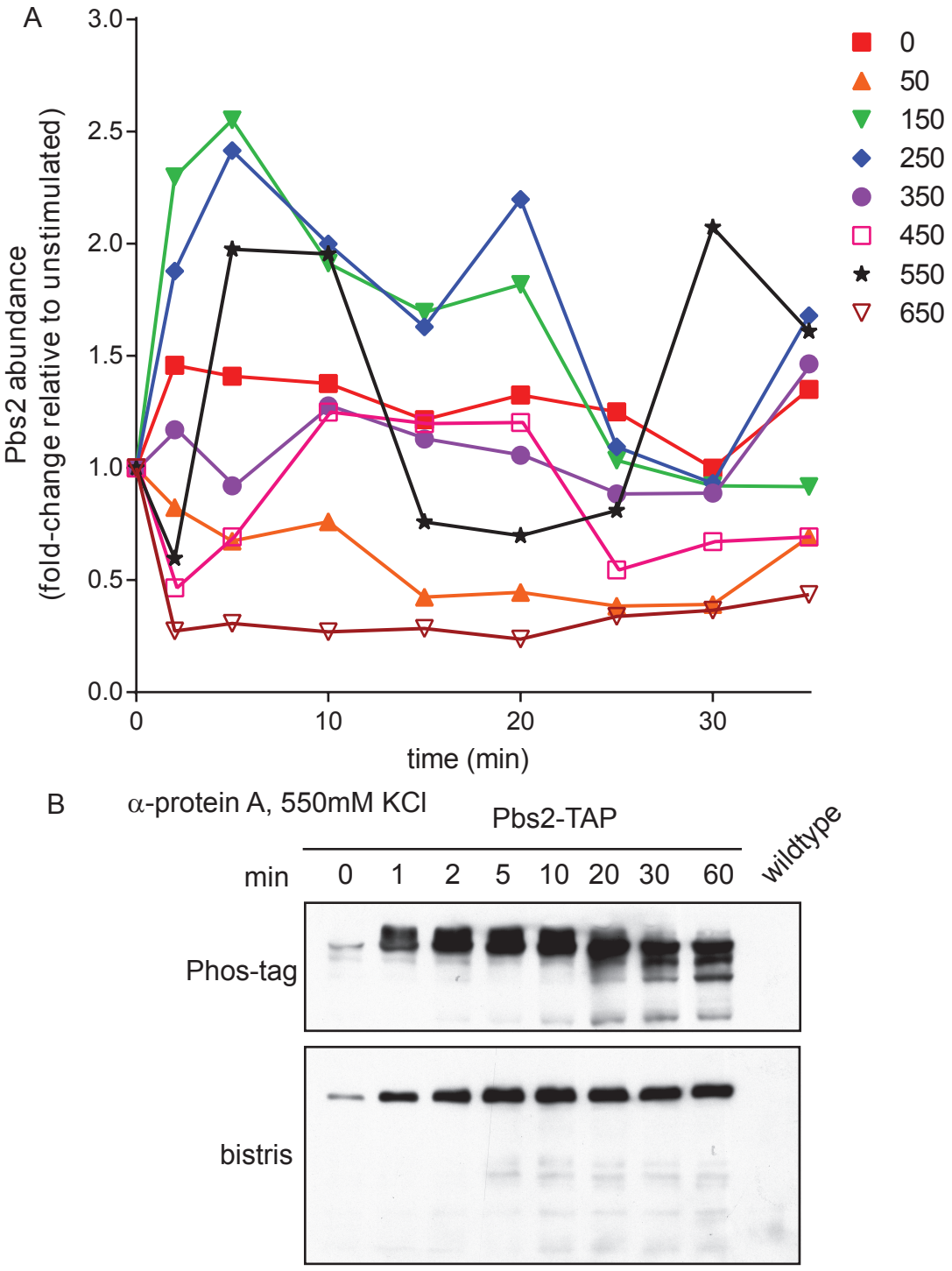

Figure 4.1. Adundance and phosphorylation dynamics of the MAP2K Pbs2.
A. Fold-change in Pbs2 abundance over time. Wildtype cells were treated with the indicated doses of KCl, lysed, and probed by immunoblotting with anti-Pbs2 (Santa Cruz, sc-6812). Data is relative to unstimulated cells (n=1).
B. Pbs2 phosphorylation over time. Pbs2-TAP tagged cells were treated with 550 mM KCl, lysed and probed by immunoblotting with anti-protein A antibodies. Top, Phos-tag Bis-Tris SDS PAGE. Bottom, identical samples in the absence of Phos-tag.

phenotype disappears when assessing Pbs2 in wildtype strains with protein specific antibodies, as seen in Figure 4.1a.

Our analysis of Pbs2 underscores the need to continually assess the dynamics of pathway components with respect to both dose and time. Pbs2 represents yet another potential point of regulation, alongside Ste50, for programming the Hog1 circuit. It stood to reason that feedback phosphorylation on Pbs2, represented by the phospho-dynamics of the molecule, could generate the observed shifting of Pbs2 abundance. However, substitution of 6 MAPK phosphorylation consensus sites on endogenous Pbs2 had no effect on Hog1 activity (**Figure 4.2**). However, I have not yet directly measured how Pbs2 abundance changes over time and dose in this mutant. Perhaps the gearbox regulates signaling properties outside the scope of Hog1 dose-to-duration. Or perhaps we have not yet stripped a sufficient number of regulatory sites from Pbs2, a protein possessing ~12 S/T/Y sites.

In an endeavor to identify further points of regulation we conducted a screen for dynamic abundance and phosphorylation accumulation on other pathway components. While several interesting phenotypes were observed. For example, the receptor Sho1 (**Figure 4.3**), exhibited dynamic abundance and phosphorylation dynamics. Both the relative abundance and phosphorylation ratio of this receptor increases with time after osmostress. This phenotype may represent a potential mechanism for mediating the duration of the Hog1 response to osmostress. Indeed, a previous study from our laboratory determined that a single amino acid substitution could uncouple Hog1 feedback phosphorylation to this receptor[50]. This mutant was sufficient to perturb the duration of Hog1 at a single dose of osmostress. Thus, further consideration of how the Hog1 dose-to-duration response may be encoded on

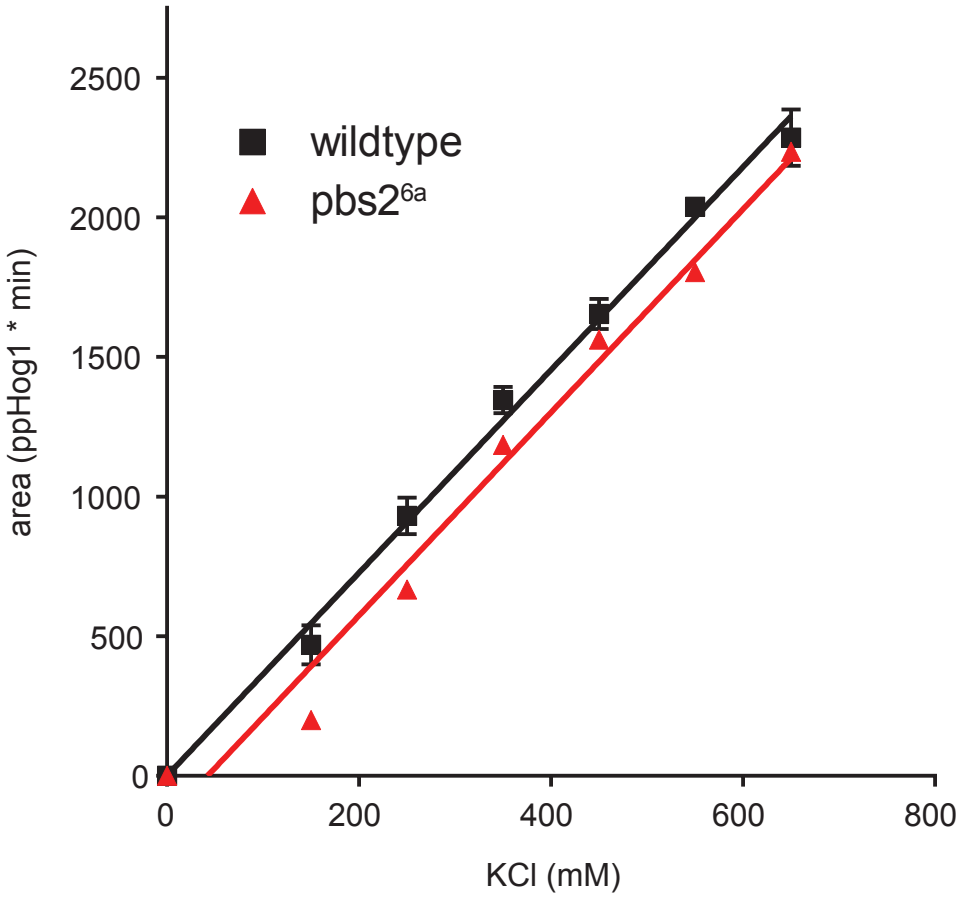

Figure 4.2. Integration of Hog1 signaling profiles for the Pbs2^{6A} strain. Wildtype is shown for reference (see Figure 2.1). (n = 1)

this molecule would be informative, and may reveal an inherent ability of the pathway to further tune input amplitude for the purposes of duration encodement.

But let's cast a wider net. A truly comprehensive analysis of the proteome will be necessary to unlock the complete network of regulatory mechanisms serving to encode the Hog1 signaling profile. The approach likely to achieve the greatest success, and stand to be most informative, would be a combination of proteomic analyses. The use of Phos-tag provides the next level of protein-state clustering necessary to understand communication networks. Mass spectrometry can identify the frequency of a phosphorylation or other post-translational modification among the total population of a given protein. However, mass spectrometry cannot determine the ratio of these posttranslational modifications, or their relationship, across whole peptides. Here I propose that sorting of whole cell lysate with Phos-tag gel electrophoresis prior to mass spectrometry would cluster whole proteins in to phospho-patterned sub-groups. The gel could be cut and dissolved to retrieve the peptides from these sub-groups. Each sub-group could be digested, isobaric tag for relative and absolute quantitation (iTRAQ) labeled, pooled, sorted by size, and analyzed via mass spectrometry. In this way not only the relative phosphorylation frequency, but the ratio and relationship of these phosphorylation events on the observed peptides could be assessed. This information could be used to understand how information is appended to these molecules as bits of patterned phosphorylation, providing clearer insights on how the cell system is regulated and information is communicated under normal signaling conditions. This process could then be repeated under a plethora of stimulus conditions. Each stimulus would generate its own protein network signature, and these could be overlayed to identify nodes of information transmission. This approach would have the added benefit of revealing the

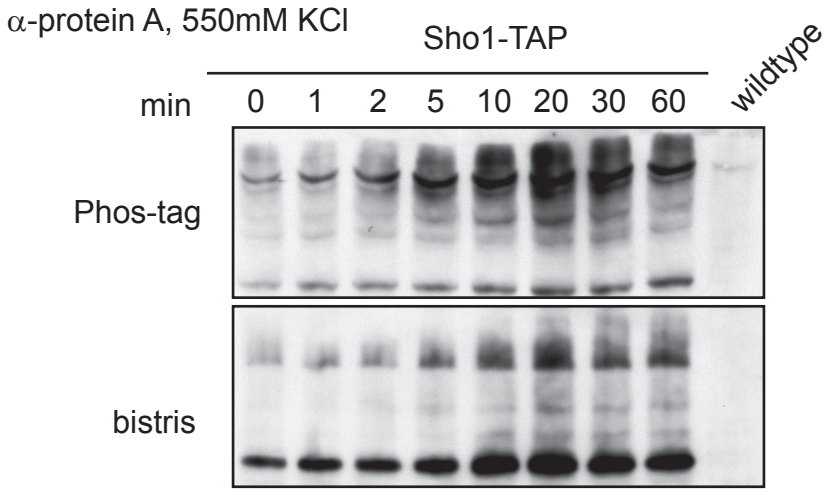

F**igure 4.3.** Sho1 phosphorylation over time. Sho1-TAP tagged cells were treated with 550 mM KCl, lysed and probed by immunoblotting with anti-protein A antibodies. Top, Phos-tag Bis-Tris SDS PAGE. Bottom, identical samples in the absence of Phos-tag.

downstream components, enzymes, and adaptive machinery Hog1 is specifically responsible for regulating. In this way the above experiments would address two considerations at once. How Hog1 programs its own activity, and how this program then facilitates downstream adaptive reprogramming.

Regulatory hits from the above analysis would represent high priority targets for in-depth analysis of phosphorylation, abundance, and localization dynamics. By decoupling the regulatory mechanisms controlling these targets a toolbox of encoding components for the Hog1 circuit can be compiled. Once this toolbox is established combinations of regulatory components can be synthetically controlled, removed, induced, or otherwise impinged upon to exert exacting control over the cells adaptive machinery. The ultimate goal would be to generate sufficient control over the system to program desired outputs for any given input to the system. This thesis work has demonstrated that such control is possible through mutation of Ste50 and deletion of pathway components. However, the dynamic range of this system can be greatly improved through identification and control of additional regulatory components.

Age, Adaptation, and Polyamines

In Chapter III it was determined that the replicative age of yeast has a pronounced effect on the readiness of the cell for stress adaptation. Unclear from this analysis is an understanding of whether this readiness underlies the weakness or wisdom of that particular cell toward stress. Metabolomic analysis after stress indicated that polyamine levels rise substantially, and previous reports have demonstrated that polyamine levels are in decline within older yeast. One would perhaps assume then that older yeast, containing less of a

strongly stress induced metabolite, may be weakened toward future stress. Indeed, the elderly often fail to heal or fully recover from serious insult or injury. Perhaps then the metabolites that are over-expressed in aged yeast are compensatory, the minimum unit necessary for survival if stress were to befall them. However, the converse is also possible. Yeast are not human tissues, and it may hold that old yeast accumulate sufficient experience and environmental considerations to tune their adaptive and metabolic networks to an optimally safe level. Several experiments could be conducted to address this uncertainty. Specifically, to determine the duration of Hog1 activity in cells based on age and polyamine levels.

Addressing how age and Hog1 activity duration correlate can be approached in two ways. Yeast stressed and fixed over time could be simultaneously stained with WGA as well as fluorescently conjugated anti-ppHog1 and Hog1 antibodies. Analysis of these cells by fluorescent cytometry would provide a ratio of active Hog1 in individual cells, the age of those cells, and perpetuity of Hog1 activity over time in these individual cells. This experiment could then be repeated with direct application of polyamines to yeast, as described previously[148], to assess whether cell age, polyamine content, or both factors increase Hog1 activity duration in individual cells.

Alternatively, live cell imaging in a flow chamber may be appropriate for this analysis. Hog1 shuttles to the nuclease after activation and remains there for a period of time. This observation is commensurate with our duration observations in Chapter II. An exact correlative analysis would need to be conducted to ensure that the durations for various doses over time were identical; or at the very least proportional. With this information in hand it would be possible to monitor Hog1-GFP in individual cells stained with WGA in real-time after stress exposure. Considerations would need to be made for how WGA staining may

increase the Hog1 response, as WGA itself is a yeast specific cytotoxin. However, this analysis could provide information unattainable through flow cytometry, such as the relative variability of the response duration in individual cells or whether cells of differing ages localize Hog1 differently over time. This experimental platform could also be coupled with a fluorescently-tagged version of an induced protein product to specifically monitor the time between Hog1 activation and protein production. It stands to reason that the timing of this event may also be altered by cell age, as it is by reprogramming of the cells signaling circuitry (**Figure 2.3e)**.

Synthesizing the above ideas, on could apply Phos-tag and mass spectrometry to cell populations that have been sorted relative to their age range. In this way discrete, similar cell populations could be analyzed. Through this analysis proteins with dynamic but opposing regulatory influences could be revealed. This analysis could also provide clear mechanisms for how old and young cells alternatively address the task of adapting to stress.

REFERENCES

1. Williams, K. J. & Tabas, I. The Response-to-Retention Hypothesis of Early Atherogenesis. *Arterioscler. Thromb. Vasc. Biol.* **15,** 551–561 (1995).

2. Tousoulis, D. *et al.* Innate and adaptiveinflammation as a therapeutic target in vascular disease: The emerging role of statins. *J. Am. Coll. Cardiol.* (2014).

3. Schwartz, M. W. *et al.* Cooperation between brain and islet in glucose homeostasis and diabetes. *Nature* **503,** 59–66 (2013).

4. Wynn, T. A., Chawla, A. & Pollard, J. W. Macrophage biology in development, homeostasis and disease. *Nature* **496,** 445–455 (2013).

5. Gurtner, G. C., Werner, S., Barrandon, Y. & Longaker, M. T. Wound repair and regeneration. *Nature* **453,** 314–321 (2008).

6. Firestein, G. S. Evolving concepts of rheumatoid arthritis. *Nature* **423,** 356–361 (2003).
7. Xiong, Z.-G. *et al.* Neuroprotection in ischemia: blocking calcium-permeable acid-sensing ion channels. *Cell* **118,** 687–698 (2004).

8. Lu, A. *et al.* Unified Polymerization Mechanism for the Assembly of ASC-Dependent Inflammasomes. *Cell* **156,** 1193–1206 (2014).

9. Hamilton, A. J. & Baulcombe, D. C. A Species of Small Antisense RNA in Posttranscriptional Gene Silencing in Plants. *Science* **286,** 950–952 (1999).

10. Pennisi, E. The CRISPR Craze. *Science* **341,** 833–836 (2013).

11. Garske, A. L., Peters, U., Cortesi, A. T., Perez, J. L. & Shokat, K. M. Chemical genetic strategy for targeting protein kinases based on covalent complementarity. *Proc. Natl. Acad. Sci.* **108,** 15046–15052 (2011).

12. Dar, A. C., Das, T. K., Shokat, K. M. & Cagan, R. L. Chemical genetic discovery of targets and anti-targets for cancer polypharmacology. *Nature* **486,** 80–84 (2012).

13. Duncan, J. S. *et al.* Dynamic reprogramming of the kinome in response to targeted MEK inhibition in triple-negative breast cancer. *Cell* **149,** 307–321 (2012).

14. Graves, L. M., Duncan, J. S., Whittle, M. C. & Johnson, G. L. The dynamic nature of the kinome. *Biochem. J.* **450,** 1–8 (2013).

15. Winter, G. E. *et al.* Systems-pharmacology dissection of a drug synergy in imatinib-resistant CML. *Nat. Chem. Biol.* **8,** 905–912 (2012).

16. Milenkovic, O. *et al.* Introduction to the Special Issue on Information Theory in Molecular Biology and Neuroscience. *IEEE Trans. Inf. Theory* **56,** 649–652 (2010).

17. Waltermann, C. & Klipp, E. Information theory based approaches to cellular signaling. *Biochim. Biophys. Acta BBA - Gen. Subj.* **1810,** 924–932 (2011).

18. Shannon, C. E. A mathematical theory of communication. *ACM SIGMOBILE Mob. Comput. Commun. Rev.* **5,** 3–55 (2001).

19. Schneider, T. D. A brief review of molecular information theory. *Nano Commun. Netw.* **1,** 173–180 (2010).

20. Komarova, N. L., Zou, X., Nie, Q. & Bardwell, L. A theoretical framework for specificity in cell signaling. *Mol. Syst. Biol.* **1,** E1–E5 (2005).

21. Galas, D. J., Nykter, M., Carter, G. W., Price, N. D. & Shmulevich, I. Biological Information as Set-Based Complexity. *IEEE Trans. Inf. Theory* **56,** 667–677 (2010).

22. Brennan, M. D., Cheong, R. & Levchenko, A. How Information Theory Handles Cell Signaling and Uncertainty. *Science* **338,** 334–335 (2012).

23. Isom, D. G. *et al.* Protons as second messenger regulators of G protein signaling. *Mol. Cell* **51,** 531–538 (2013).

24. Uhlik, M. T. *et al.* Rac-MEKK3-MKK3 scaffolding for p38 MAPK activation during hyperosmotic shock. *Nat. Cell Biol.* **5,** 1104–1110 (2003).

25. Zawistowski, J. S. *et al.* CCM1 and CCM2 protein interactions in cell signaling: implications for cerebral cavernous malformations pathogenesis. *Hum. Mol. Genet.* **14,** 2521–2531 (2005).

26. Garrington, T. P. & Johnson, G. L. Organization and regulation of mitogen-activated protein kinase signaling pathways. *Curr. Opin. Cell Biol.* **11,** 211–218 (1999).

27. Chang, L. & Karin, M. Mammalian MAP kinase signalling cascades. *Nature* **410,** 37–40 (2001).
28. Seger, R. & Krebs, E. G. The MAPK signaling cascade. *FASEB J. Off. Publ. Fed. Am. Soc. Exp. Biol.* **9,** 726–735 (1995).

29. Goldbeter, A. Zero-order switches and developmental thresholds. *Mol. Syst. Biol.* **1,** (2005).

30. Goldbeter, A. & Koshland, D. E. An amplified sensitivity arising from covalent modification in biological systems. *Proc. Natl. Acad. Sci.* **78,** 6840–6844 (1981).

31. O'Shaughnessy, E. C., Palani, S., Collins, J. J. & Sarkar, C. A. Tunable Signal Processing in Synthetic MAP Kinase Cascades. *Cell* **144,** 119–131 (2011).

32. Bandyopadhyay, S. *et al.* A Human MAP Kinase Interactome. *Nat. Methods* **7,** 801–805 (2010).

33. Courcelles, M. *et al.* Phosphoproteome dynamics reveal novel ERK1/2 MAP kinase substrates with broad spectrum of functions. *Mol. Syst. Biol.* **9,** 669 (2013).

34. Cargnello, M. & Roux, P. P. Activation and Function of the MAPKs and Their Substrates, the MAPK-Activated Protein Kinases. *Microbiol. Mol. Biol. Rev.* **75,** 50–83 (2011).

35. Hazzalin, C. A. & Mahadevan, L. C. MAPK-regulated transcription: a continuously variable gene switch? *Nat. Rev. Mol. Cell Biol.* **3,** 30–40 (2002).

36. Topisirovic, I. & Sonenberg, N. mRNA Translation and Energy Metabolism in Cancer: The Role of the MAPK and mTORC1 Pathways. *Cold Spring Harb. Symp. Quant. Biol.* **76,** 355–367 (2011).

37. Gehart, H., Kumpf, S., Ittner, A. & Ricci, R. MAPK signalling in cellular metabolism: stress or wellness? *EMBO Rep.* **11,** 834–840 (2010).

38. Huff, K., End, D. & Guroff, G. Nerve growth factor-induced alteration in the response of PC12 pheochromocytoma cells to epidermal growth factor. *J. Cell Biol.* **88,** 189–198 (1981).

39. Johnson, G. L. & Lapadat, R. Mitogen-activated protein kinase pathways mediated by ERK, JNK, and p38 protein kinases. *Science* **298,** 1911–1912 (2002).

40. Santos, S. D. M., Verveer, P. J. & Bastiaens, P. I. H. Growth factor-induced MAPK network topology shapes Erk response determining PC-12 cell fate. *Nat. Cell Biol.* **9,** 324–330 (2007).

41. Purvis, J. E. & Lahav, G. Encoding and Decoding Cellular Information through Signaling Dynamics. *Cell* **152,** 945–956 (2013).

42. Hao, N. *et al.* Regulation of cell signaling dynamics by the protein kinase-scaffold Ste5. *Mol. Cell* **30,** 649–656 (2008).

43. Mattison, C. P. & Ota, I. M. Two protein tyrosine phosphatases, Ptp2 and Ptp3, modulate the subcellular localization of the Hog1 MAP kinase in yeast. *Genes Dev.* **14,** 1229–1235 (2000).

44. Barford, D. Molecular mechanisms of theprotein serine/threonine phosphatases. *Trends Biochem. Sci.* **21,** 407–412 (1996).

45. Caunt, C. J. & Keyse, S. M. Dual-specificity MAP kinase phosphatases (MKPs): shaping the outcome of MAP kinase signalling. *FEBS J.* **280,** 489–504 (2013).

46. Farooq, A. & Zhou, M.-M. Structure and regulation of MAPK phosphatases. *Cell. Signal.* **16,** 769–779 (2004).

47. Ferrell, J. E., Jr. Self-perpetuating states in signal transduction: positive feedback, double-negative feedback and bistability. *Curr. Opin. Cell Biol.* **14,** 140–148 (2002).

48. Justman, Q. A., Serber, Z., Ferrell, J. E., El-Samad, H. & Shokat, K. M. Tuning the Activation Threshold of a Kinase Network by Nested Feedback Loops. *Science* **324,** 509–512 (2009).

49. Hao, N., Zeng, Y., Elston, T. C. & Dohlman, H. G. Control of MAPK Specificity by Feedback Phosphorylation of Shared Adaptor Protein Ste50. *J. Biol. Chem.* **283,** 33798–33802 (2008).

50. Hao, N. *et al.* A Systems-Biology Analysis of Feedback Inhibition in the Sho1 Osmotic-Stress-Response Pathway. *Curr. Biol.* **17,** 659–667 (2007).

51. Flotho, A., Simpson, D. M., Qi, M. & Elion, E. A. Localized feedback phosphorylation of Ste5p scaffold by associated MAPK cascade. *J. Biol. Chem.* **279,** 47391–47401 (2004).

52. Hao, N. & O'Shea, E. K. Signal-dependent dynamics of transcription factor translocation controls gene expression. *Nat. Struct. Mol. Biol.* **19,** 31–39 (2012).

53. Albeck, J. G., Mills, G. B. & Brugge, J. S. Frequency-Modulated Pulses of ERK Activity Transmit Quantitative Proliferation Signals. *Mol. Cell* **49,** 249–261 (2013).

54. Purvis, J. E. *et al.* p53 Dynamics Control Cell Fate. *Science* **336,** 1440–1444 (2012).

55. Brandman, O., Ferrell, J. E., Li, R. & Meyer, T. Interlinked Fast and Slow Positive Feedback Loops Drive Reliable Cell Decisions. *Science* **310,** 496–498 (2005).

56. Brewster, J. L., de Valoir, T., Dwyer, N. D., Winter, E. & Gustin, M. C. An osmosensing signal transduction pathway in yeast. *Science* **259,** 1760–1763 (1993).

57. Westfall, P. J., Ballon, D. R. & Thorner, J. When the stress of your environment makes you go HOG wild. *Science* **306,** 1511–1512 (2004).

58. Saito, H. & Posas, F. Response to Hyperosmotic Stress. *Genetics* **192,** 289–318 (2012).

59. Gasch, A. P. *et al.* Genomic Expression Programs in the Response of Yeast Cells to Environmental Changes. *Mol. Biol. Cell* **11,** 4241–4257 (2000).

60. Guan, Q., Haroon, S., Bravo, D. G., Will, J. L. & Gasch, A. P. Cellular Memory of Acquired Stress Resistance in Saccharomyces cerevisiae. *Genetics* **192,** 495–505 (2012).

61. Tanaka, K. *et al.* Yeast Osmosensors Hkr1 and Msb2 Activate the Hog1 MAPK Cascade by Different Mechanisms. *Sci. Signal.* **7,** ra21 (2014).

62. Neuert, G. *et al.* Systematic Identification of Signal-Activated Stochastic Gene Regulation. *Science* **339,** 584–587 (2013).

63. Muzzey, D., Gomez-Uribe, C. A., Mettetal, J. T. & van Oudenaarden, A. A systems-level analysis of perfect adaptation in yeast osmoregulation. *Cell* **138,** 160–171 (2009).

64. Hersen, P., McClean, M. N., Mahadevan, L. & Ramanathan, S. Signal processing by the HOG MAP kinase pathway. *Proc. Natl. Acad. Sci.* **105,** 7165–7170 (2008).

65. Schaber, J., Baltanas, R., Bush, A., Klipp, E. & Colman-Lerner, A. Modelling reveals novel roles of two parallel signalling pathways and homeostatic feedbacks in yeast. *Mol. Syst. Biol.* **8,** (2012).

66. Nagiec, M. J. & Dohlman, H. G. Checkpoints in a Yeast Differentiation Pathway Coordinate Signaling during Hyperosmotic Stress. *PLoS Genet* **8,** e1002437 (2012).

67. Wagner, E. F. & Nebreda, Á. R. Signal integration by JNK and p38 MAPK pathways in cancer development. *Nat. Rev. Cancer* **9,** 537–549 (2009).

68. Webber, J. L. & Tooze, S. A. Coordinated regulation of autophagy by p38α MAPK through mAtg9 and p38IP. *EMBO J.* **29,** 27–40 (2010).

69. Rouse, J. *et al.* A novel kinase cascade triggered by stress and heat shock that stimulates MAPKAP kinase-2 and phosphorylation of the small heat shock proteins. *Cell* **78,** 1027–1037 (1994).

70. Galcheva-Gargova, Z., Dérijard, B., Wu, I. H. & Davis, R. J. An osmosensing signal transduction pathway in mammalian cells. *Science* **265,** 806–808 (1994).

71. Nelson, D. E. *et al.* Oscillations in NF-κB Signaling Control the Dynamics of Gene Expression. *Science* **306,** 704–708 (2004).

72. Ferrell, J. E. & Machleder, E. M. The Biochemical Basis of an All-or-None Cell Fate Switch in Xenopus Oocytes. *Science* **280,** 895–898 (1998).

73. Malleshaiah, M. K., Shahrezaei, V., Swain, P. S. & Michnick, S. W. The scaffold protein Ste5 directly controls a switch-like mating decision in yeast. *Nature* **465,** 101–105 (2010).

74. Takahashi, S. & Pryciak, P. M. Membrane localization of scaffold proteins promotes graded signaling in the yeast MAP kinase cascade. *Curr. Biol. CB* **18,** 1184–1191 (2008).

75. Behar, M., Hao, N., Dohlman, H. G. & Elston, T. C. Dose-to-Duration Encoding and Signaling beyond Saturation in Intracellular Signaling Networks. *PLoS Comput Biol* **4,** e1000197 (2008).

76. Bell, M. & Engelberg, D. Phosphorylation of Tyr-176 of the Yeast MAPK Hog1/p38 Is Not Vital for Hog1 Biological Activity ,. *J. Biol. Chem.* **278,** 14603–14606 (2003).

77. Mao, K., Wang, K., Zhao, M., Xu, T. & Klionsky, D. J. Two MAPK-signaling pathways are required for mitophagy in Saccharomyces cerevisiae. *J. Cell Biol.* **193,** 755–767 (2011).

78. Westfall, P. J., Patterson, J. C., Chen, R. E. & Thorner, J. Stress resistance and signal fidelity independent of nuclear MAPK function. *Proc. Natl. Acad. Sci.* **105,** 12212–12217 (2008).

79. Kinoshita, E., Kinoshita-Kikuta, E., Takiyama, K. & Koike, T. Phosphate-binding Tag, a New Tool to Visualize Phosphorylated Proteins. *Mol. Cell. Proteomics* **5,** 749–757 (2006).

80. Miermont, A. *et al.* Severe osmotic compression triggers a slowdown of intracellular signaling, which can be explained by molecular crowding. *Proc. Natl. Acad. Sci.* **110,** 5725–5730 (2013).

81. Findlay, G. M. *et al.* Interaction Domains of Sos1/Grb2 Are Finely Tuned for Cooperative Control of Embryonic Stem Cell Fate. *Cell* **152,** 1008–1020 (2013).

82. Zalatan, J. G., Coyle, S. M., Rajan, S., Sidhu, S. S. & Lim, W. A. Conformational control of the Ste5 scaffold protein insulates against MAP kinase misactivation. *Science* **337,** 1218–1222 (2012).

83. Coyle, S. M., Flores, J. & Lim, W. A. Exploitation of latent allostery enables the evolution of new modes of MAP kinase regulation. *Cell* **154,** 875–887 (2013).

84. Smith, G. R., Givan, S. A., Cullen, P. & Jr, G. F. S. GTPase-Activating Proteins for Cdc42. *Eukaryot. Cell* **1,** 469–480 (2002).

85. Zheng, Y., Cerione, R. & Bender, A. Control of the yeast bud-site assembly GTPase Cdc42. Catalysis of guanine nucleotide exchange by Cdc24 and stimulation of GTPase activity by Bem3. *J. Biol. Chem.* **269,** 2369–2372 (1994).

86. Raitt, D. C., Posas, F. & Saito, H. Yeast Cdc42 GTPase and Ste20 PAK-like kinase regulate Sho1-dependent activation of the Hog1 MAPK pathway. *EMBO J.* **19,** 4623–4631 (2000).

87. Macia, J. *et al.* Dynamic Signaling in the Hog1 MAPK Pathway Relies on High Basal Signal Transduction. *Sci. Signal.* **2,** ra13 (2009).

88. Tyson, J. J., Chen, K. C. & Novak, B. Sniffers, buzzers, toggles and blinkers: dynamics of regulatory and signaling pathways in the cell. *Curr. Opin. Cell Biol.* **15,** 221–231 (2003).

89. Westfall, P. J. & Thorner, J. Analysis of Mitogen-Activated Protein Kinase Signaling Specificity in Response to Hyperosmotic Stress: Use of an Analog-Sensitive HOG1 Allele. *Eukaryot. Cell* **5,** 1215–1228 (2006).

90. Kung, C., Kenski, D. M., Krukenberg, K., Madhani, H. D. & Shokat, K. M. Selective Kinase Inhibition by Exploiting Differential Pathway Sensitivity. *Chem. Biol.* **13,** 399–407 (2006).

91. Thomson, M. & Gunawardena, J. Unlimited multistability in multisite phosphorylation systems. *Nature* **460,** 274–277 (2009).

92. Yamamoto, K., Tatebayashi, K., Tanaka, K. & Saito, H. Dynamic Control of Yeast MAP Kinase Network by Induced Association and Dissociation between the Ste50 Scaffold and the Opy2 Membrane Anchor. *Mol. Cell* **40,** 87–98 (2010).

93. Santos, S. D. M. & Ferrell, J. E. Systems biology: On the cell cycle and its switches. *Nature* **454,** 288–289 (2008).

94. Bradshaw, J. M., Kubota, Y., Meyer, T. & Schulman, H. An ultrasensitive Ca2+/calmodulin-dependent protein kinase II-protein phosphatase 1 switch facilitates specificity in postsynaptic calcium signaling. *Proc. Natl. Acad. Sci.* **100,** 10512–10517 (2003).

95. Harnett, M. T., Makara, J. K., Spruston, N., Kath, W. L. & Magee, J. C. Synaptic amplification by dendritic spines enhances input cooperativity. *Nature* **491,** 599–602 (2012).

96. Goldbeter, A. & Wolpert, L. Covalent modification of proteins as a threshold mechanism in development. *J. Theor. Biol.* **142,** 243–250 (1990).

97. Melen, G. J., Levy, S., Barkai, N. & Shilo, B.-Z. Threshold responses to morphogen gradients by zero-order ultrasensitivity. *Mol. Syst. Biol.* **1,** (2005).

98. Ni, L. *et al.* Dynamic and complex transcription factor binding during an inducible response in yeast. *Genes Dev.* **23,** 1351–1363 (2009).

99. Bardwell, L. Signal Transduction: Turning a Switch into a Rheostat. *Curr. Biol. CB* **18,** R910–R912 (2008).

100. Trunnell, N. B., Poon, A. C., Kim, S. Y. & Ferrell, J. E. Ultrasensitivity in the Regulation of Cdc25C by Cdk1. *Mol. Cell* **41,** 263–274 (2011).

101. Dohlman, H. G. A Scaffold Makes the Switch. *Sci. Signal.* **1,** pe46 (2008).

102. Whitehurst, A., Cobb, M. H. & White, M. A. Stimulus-Coupled Spatial Restriction of Extracellular Signal-Regulated Kinase 1/2 Activity Contributes to the Specificity of Signal-Response Pathways. *Mol. Cell. Biol.* **24,** 10145–10150 (2004).

103. Pawson, T. & Nash, P. Assembly of Cell Regulatory Systems Through Protein Interaction Domains. *Science* **300,** 445–452 (2003).

104. Baker, R. *et al.* Site-specific monoubiquitination activates Ras by impeding GTPase-activating protein function. *Nat. Struct. Mol. Biol.* **20,** 46–52 (2013).

105. Hurst, J. H. & Dohlman, H. G. Dynamic Ubiquitination of the Mitogen-activated Protein Kinase Kinase (MAPKK) Ste7 Determines Mitogen-activated Protein Kinase (MAPK) Specificity. *J. Biol. Chem.* **288,** 18660–18671 (2013).

106. Mittal, R., Peak-Chew, S.-Y. & McMahon, H. T. Acetylation of MEK2 and IκB kinase (IKK) activation loop residues by YopJ inhibits signaling. *Proc. Natl. Acad. Sci.* **103,** 18574–18579 (2006).

107. Pillai, V. B. *et al.* Acetylation of a Conserved Lysine Residue in the ATP Binding Pocket of p38 Augments Its Kinase Activity during Hypertrophy of Cardiomyocytes ▿ . *Mol. Cell. Biol.* **31,** 2349–2363 (2011).

108. Andreu-Perez, P. *et al.* Protein Arginine Methyltransferase 5 Regulates ERK1/2 Signal Transduction Amplitude and Cell Fate Through CRAF. *Sci. Signal.* **4,** ra58 (2011).

109. Huang, T. T., Wuerzberger-Davis, S. M., Wu, Z.-H. & Miyamoto, S. Sequential Modification of NEMO/IKKγ by SUMO-1 and Ubiquitin Mediates NF-κB Activation by Genotoxic Stress. *Cell* **115,** 565–576 (2003).

110. Merbl, Y., Refour, P., Patel, H., Springer, M. & Kirschner, M. W. Profiling of Ubiquitin-like Modifications Reveals Features of Mitotic Control. *Cell* **152,** 1160–1172 (2013).

111. Tang, X. *et al.* Composite low affinity interactions dictate recognition of the cyclin-dependent kinase inhibitor Sic1 by the SCFCdc4 ubiquitin ligase. *Proc. Natl. Acad. Sci.* **109,** 3287–3292 (2012).

112. Kinoshita, E. & Kinoshita-Kikuta, E. Improved Phos-tag SDS-PAGE under neutral pH conditions for advanced protein phosphorylation profiling. *PROTEOMICS* **11,** 319–323 (2011).

113. Schindelin, J. *et al.* Fiji: an open-source platform for biological-image analysis. *Nat. Methods* **9,** 676–682 (2012).

114. Abdulrehman, D. *et al.* YEASTRACT: providing a programmatic access to curated transcriptional regulatory associations in Saccharomyces cerevisiae through a web services interface. *Nucleic Acids Res.* **39,** D136–D140 (2011).

115. Huang, D. W., Sherman, B. T. & Lempicki, R. A. Systematic and integrative analysis of large gene lists using DAVID bioinformatics resources. *Nat. Protoc.* **4,** 44–57 (2008).

116. Huang, D. W., Sherman, B. T. & Lempicki, R. A. Bioinformatics enrichment tools: paths toward the comprehensive functional analysis of large gene lists. *Nucleic Acids Res.* **37,** 1–13 (2009).

117. Kuvrec, M. *et al.* Flow cytometry for age assessment of a yeast population and its application in beer fermentations. *J. Inst. Brew.* **115,** 253–258 (2009).

118. Tatebayashi, K. *et al.* Adaptor functions of Cdc42, Ste50, and Sho1 in the yeast osmoregulatory HOG MAPK pathway. *EMBO J.* **25,** 3033–3044 (2006).

119. Cappell, S. D., Baker, R., Skowyra, D. & Dohlman, H. G. Systematic analysis of essential genes reveals important regulators of G protein signaling. *Mol. Cell* **38,** 746–757 (2010).

120. Albertyn, J., Hohmann, S., Thevelein, J. M. & Prior, B. A. GPD1, which encodes glycerol-3-phosphate dehydrogenase, is essential for growth under osmotic stress in Saccharomyces cerevisiae, and its expression is regulated by the high-osmolarity glycerol response pathway. *Mol. Cell. Biol.* **14,** 4135–4144 (1994).

121. Capaldi, A. P. *et al.* Structure and Function of a Transcriptional Network Activated by the MAPK Hog1. *Nat. Genet.* **40,** 1300–1306 (2008).

122. Vogel, C. *et al.* Sequence signatures and mRNA concentration can explain two-thirds of protein abundance variation in a human cell line. *Mol. Syst. Biol.* **6,** 400 (2010).

123. Vogel, C. & Marcotte, E. M. Insights into the regulation of protein abundance from proteomic and transcriptomic analyses. *Nat. Rev. Genet.* **13,** 227–232 (2012).

124. Tian, Q. *et al.* Integrated genomic and proteomic analyses of gene expression in Mammalian cells. *Mol. Cell. Proteomics MCP* **3,** 960–969 (2004).

125. Schwanhäusser, B. *et al.* Global quantification of mammalian gene expression control. *Nature* **473,** 337–342 (2011).

126. Knowles, J. R. Enzyme-Catalyzed Phosphoryl Transfer Reactions. *Annu. Rev. Biochem.* **49,** 877–919 (1980).

127. Törnroth-Horsefield, S. & Neutze, R. Opening and closing the metabolite gate. *Proc. Natl. Acad. Sci.* **105,** 19565–19566 (2008).

128. Fröhlich, F., Christiano, R. & Walther, T. C. Native SILAC: Metabolic Labeling of Proteins in Prototroph Microorganisms Based on Lysine Synthesis Regulation. *Mol. Cell. Proteomics* **12,** 1995–2005 (2013).

129. Babazadeh, R. *et al.* Osmostress-induced cell volume loss delays yeast Hog1 signaling by limiting diffusion processes and by Hog1-specific effects. *PloS One* **8,** e80901 (2013).

130. Kaserer, A. O., Andi, B., Cook, P. F. & West, A. H. Effects of osmolytes on the SLN1-YPD1-SSK1 phosphorelay system from Saccharomyces cerevisiae. *Biochemistry (Mosc.)* **48,** 8044–8050 (2009).

131. Petelenz-Kurdziel, E. *et al.* Quantitative analysis of glycerol accumulation, glycolysis and growth under hyper osmotic stress. *PLoS Comput. Biol.* **9,** e1003084 (2013).

132. Thauer, R. K. Citric-acid cycle, 50 years on. *Eur. J. Biochem.* **176,** 497–508 (1988).

133. Ruggles, K. V., Turkish, A. & Sturley, S. L. Making, Baking, and Breaking: the Synthesis, Storage, and Hydrolysis of Neutral Lipids. *Annu. Rev. Nutr.* **33,** 413–451 (2013).

134. Cronwright, G. R., Rohwer, J. M. & Prior, B. A. Metabolic Control Analysis of Glycerol Synthesis in Saccharomyces cerevisiae. *Appl. Environ. Microbiol.* **68,** 4448–4456 (2002).

135. Elbein, A. D., Pan, Y. T., Pastuszak, I. & Carroll, D. New insights on trehalose: a multifunctional molecule. *Glycobiology* **13,** 17R–27R (2003).

136. Higashiyama, T. Novel functions and applications of trehalose. *Pure Appl. Chem.* **74,** 1263–1269 (2002).

137. Sarkar, S., Davies, J. E., Huang, Z., Tunnacliffe, A. & Rubinsztein, D. C. Trehalose, a Novel mTOR-independent Autophagy Enhancer, Accelerates the Clearance of Mutant Huntingtin and α-Synuclein. *J. Biol. Chem.* **282,** 5641–5652 (2007).

138. Sola-Penna, M. & Meyer-Fernandes, J. R. Stabilization against thermal inactivation promoted by sugars on enzyme structure and function: why is trehalose more effective than other sugars? *Arch. Biochem. Biophys.* **360,** 10–14 (1998).

139. Tillequin, F. [Trehala, a meeting point between zoology, botany, chemistry, and biochemistry]. *Rev. Hist. Pharm.* **57,** 163–172 (2009).

140. Young, F. G. Claude Bernard and the Discovery of Glycogen. *Br. Med. J.* **1,** 1431 (1957).

141. Lawrence, S. A. *Amines: Synthesis, Properties and Applications*. (Cambridge University Press, 2004).

142. Bauer, M. A. *et al.* Spermidine promotes mating and fertilization efficiency in model organisms. *Cell Cycle Georget. Tex* **12,** 346–352 (2013).

143. Zhao, T., Goh, K. J., Ng, H. H. & Vardy, L. A. A role for polyamine regulators in ESC self-renewal. *Cell Cycle Georget. Tex* **11,** 4517–4523 (2012).

144. Ioannidis, N. E. & Kotzabasis, K. Polyamines in chemiosmosis in vivo: A cunning mechanism for the regulation of ATP synthesis during growth and stress. *Front. Plant Sci.* **5,** 71 (2014).

145. Holen, E. *et al.* A co culture approach show that polyamine turnover is affected during inflammation in Atlantic salmon immune and liver cells and that arginine and LPS exerts opposite effects on p38MAPK signaling. *Fish Shellfish Immunol.* **37,** 286–298 (2014).

146. Lin, D.-W., Chung, B. P. & Kaiser, P. S-adenosylmethionine limitation induces p38 mitogen-activated protein kinase and triggers cell cycle arrest in G1. *J. Cell Sci.* **127,** 50–59 (2014).

147. Rato, C., Amirova, S. R., Bates, D. G., Stansfield, I. & Wallace, H. M. Translational recoding as a feedback controller: systems approaches reveal polyamine-specific effects on the antizyme ribosomal frameshift. *Nucleic Acids Res.* **39,** 4587–4597 (2011).

148. Eisenberg, T. *et al.* Induction of autophagy by spermidine promotes longevity. *Nat. Cell Biol.* **11,** 1305–1314 (2009).

149. Madeo, F., Eisenberg, T., Büttner, S., Ruckenstuhl, C. & Kroemer, G. Spermidine: a novel autophagy inducer and longevity elixir. *Autophagy* **6,** 160–162 (2010).

150. Madeo, F., Tavernarakis, N. & Kroemer, G. Can autophagy promote longevity? *Nat. Cell Biol.* **12,** 842–846 (2010).

151. Tiburcio, A. F., Altabella, T., Bitrián, M. & Alcázar, R. The roles of polyamines during the lifespan of plants: from development to stress. *Planta* (2014).

152. Chen, C. & Contreras, R. The bud scar-based screening system for hunting human genes extending life span. *Ann. N. Y. Acad. Sci.* **1019,** 355–359 (2004).

153. Rodrigues, M. L., Alvarez, M., Fonseca, F. L. & Casadevall, A. Binding of the Wheat Germ Lectin to Cryptococcus neoformans Suggests an Association of Chitinlike Structures with Yeast Budding and Capsular Glucuronoxylomannan. *Eukaryot. Cell* **7,** 602–609 (2008).

154. Clifton, D., Walsh, R. B. & Fraenkel, D. G. Functional studies of yeast glucokinase. *J. Bacteriol.* **175,** 3289–3294 (1993).

155. Farkas, I., Hardy, T. A., DePaoli-Roach, A. A. & Roach, P. J. Isolation of the GSY1 gene encoding yeast glycogen synthase and evidence for the existence of a second gene. *J. Biol. Chem.* **265,** 20879–20886 (1990).

156. Hwang, P. K., Tugendreich, S. & Fletterick, R. J. Molecular analysis of GPH1, the gene encoding glycogen phosphorylase in Saccharomyces cerevisiae. *Mol. Cell. Biol.* **9,** 1659–1666 (1989).

157. Schepers, W., Van Zeebroeck, G., Pinkse, M., Verhaert, P. & Thevelein, J. M. In vivo phosphorylation of Ser21 and Ser83 during nutrient-induced activation of the yeast protein kinase A (PKA) target trehalase. *J. Biol. Chem.* **287,** 44130–44142 (2012).

158. Haslbeck, M. *et al.* Hsp26: a temperature-regulated chaperone. *EMBO J.* **18,** 6744–6751 (1999).

159. Panaretou, B. & Piper, P. W. The plasma membrane of yeast acquires a novel heat-shock protein (hsp30) and displays a decline in proton-pumping ATPase levels in response to both heat shock and the entry to stationary phase. *Eur. J. Biochem. FEBS* **206,** 635–640 (1992).

160. Piper, P. W., Ortiz-Calderon, C., Holyoak, C., Coote, P. & Cole, M. Hsp30, the integral plasma membrane heat shock protein of Saccharomyces cerevisiae, is a stress-inducible regulator of plasma membrane H(+)-ATPase. *Cell Stress Chaperones* **2,** 12–24 (1997).

161. Hohmann, S., Bell, W., Neves, M. J., Valckx, D. & Thevelein, J. M. Evidence for trehalose-6-phosphate-dependent and -independent mechanisms in the control of sugar influx into yeast glycolysis. *Mol. Microbiol.* **20,** 981–991 (1996).

162. Vuorio, O. E., Kalkkinen, N. & Londesborough, J. Cloning of two related genes encoding the 56-kDa and 123-kDa subunits of trehalose synthase from the yeast Saccharomyces cerevisiae. *Eur. J. Biochem. FEBS* **216,** 849–861 (1993).

163. Takemaru, K. i, Li, F. Q., Ueda, H. & Hirose, S. Multiprotein bridging factor 1 (MBF1) is an evolutionarily conserved transcriptional coactivator that connects a regulatory factor and TATA element-binding protein. *Proc. Natl. Acad. Sci. U. S. A.* **94,** 7251–7256 (1997).

164. Tkach, J. M. *et al.* Dissecting DNA damage response pathways by analysing protein localization and abundance changes during DNA replication stress. *Nat. Cell Biol.* **14,** 966–976 (2012).

165. Kanehisa, M. & Goto, S. KEGG: kyoto encyclopedia of genes and genomes. *Nucleic Acids Res.* **28,** 27–30 (2000).

166. Kanehisa, M. *et al.* Data, information, knowledge and principle: back to metabolism in KEGG. *Nucleic Acids Res.* **42,** D199–205 (2014).